3D-UHR Survey Results Report WPD

Energinet Denmark Hesselø 3D-UHR Survey | Denmark, Inner Danish Sea, *Kattegat*

F172145-REP-UHR-001 02 | 18 August 2021
Final

Energinet Eltransmission A/S

Document Control

Document Information

Project Title	Energinet Denmark Hesselø 3D-UHR Survey
Document Title	3D-UHR Survey Results Report WPD
Fugro Project No.	F172145
Fugro Document No.	F172145-REP-UHR-001
Issue Number	02
Issue Status	Final

Client Information

Client	Energinet Eltransmission A/S
Client Address	Tonne Kjærsvej 65, DK-7000 Fredericia, Denmark
Client Contact	Stricker Mathiasen, Søren
Client Document No.	N/A

Document History

Issue	Date	Status	Comments on Content	Prepared By	Checked By	Approved By
01	2 July 2021	Complete		MH/PSC	WVK/CIW	AP
02	18 Aug 2021	Final		MH/PSC	WVK/CIW	AP

Project Team

Initials	Name	Role
AP	A. Padwalkar	Project Manager
MH	Menno Hofstra	Geologist
PSC	Peter Schilder	Geologist
WVK	Wessel van Kesteren	Principal Geologist
CIW	Chris Wright	Project Reporting and Deliverables Manager

FUGRO
Fugro Netherlands Marine Limited
Prismastraat 4
Nootdorp
2631 RT
The Netherlands

Energinet Eltransmission A/S

Tonne Kjærsvej 65
DK-7000 Fredericia
Denmark Bldg

18 August 2021

Dear Sir/Madam,

We have the pleasure of submitting the '3D-UHR Survey Results Report WPD for the 'Energinet Denmark Hesselø Geophysical Survey'. This report presents the results of WPD (3D-UHR scope).

This report was prepared by Menno Hofstra and Peter Schilder under the supervision of Wessel van Kesteren (Principal Geologist) and Chris Wright (Project Reporting and Deliverables Manager).

We hope that you find this report to your satisfaction; should you have any queries, please do not hesitate to contact us.

Yours faithfully,

Chris Wright
Project Reporting and Deliverables Manager

Executive Summary

Interpretative Site Investigation - Hesselø OWF	
Survey Dates	28 February until 10 March 2021
Equipment	3D-UHR seismic
Coordinate System	Datum: European Terrestrial Reference System 1989 (ETRS89) Projection: UTM Zone 32N, CM 3°E
Potential Site-Specific Hazards	
Boulders, cobbles and gravel	A total of 576 positive point anomalies were observed in Unit D, Unit E and Unit H at the OSS1 site, interpreted as cobbles and/or boulders. No positive point anomalies were observed at the OSS2 site.
Postglacial anomalies	Postglacial anomalies were observed in Holocene units, sporadically at the OSS1 site and abundantly at the OSS2 site.
Buried channels	Buried channels were observed internally in Unit D at the OSS1 site.
Mass Transport Deposits (MTDs)	MTDs are present in the upper part of Unit D at the OSS1 site.
Glacial deformation	Locally, Unit D and Unit E show indications of glacial deformation at both OSS1 and OSS2 sites.
Shallow Geology	
Holocene (Units A, B and C)	Holocene deposits (Units A, B and C) are present in the OSS1 and OSS2 sites. These units consist of Postglacial SAND and CLAY.
Unit D	Unit D is present across the entire OSS1 site and locally at the OSS2 site. The seismic character of Unit D is in general defined by low to medium-amplitude parallel reflectors. In the OSS1 site, three internal horizons were discriminated between different acoustic facies. The unit comprises Late Glacial CLAY deposited in a glaciomarine and/or glaciolacustrine environment.
Unit E	Unit E is present across the OSS1 and OSS2 sites. The seismic character of Unit E is semi-transparent to chaotic. The unit comprises glacially deformed glaciomarine and glaciolacustrine CLAY.
Unit F	Unit F is absent in the OSS1 and OSS2 sites.
Unit G	Unit is absent at the OSS2 site and in the top 60 m at the OSS1 site.
Unit H	Unit H is present across the entire OSS2 site and locally at the OSS1 site. The seismic character is variable. At the OSS1 site, the unit is acoustically semi-transparent to chaotic, while at the OSS2 site it is (semi-)transparent with some medium-amplitude parallel reflectors. The unit comprises glacial, periglacial and/or glaciomarine TILL of Early Pleistocene age.
Unit I	Unit I is present at the OSS1 and OSS2 sites. The seismic character shows low to medium-amplitude, low-frequency parallel reflectors. Locally the seismic character is acoustically (semi-)transparent. The unit is interpreted as pre-Quaternary bedrock and comprises Jurassic sandy MUDSTONE to Lower Cretaceous LIMESTONE and glauconitic SANDSTONE, deposited in a marine environment.

Document Arrangement

Document Number	Document Title
F172145-REP-MOB-001	Mobilisation Report - Pioneer
F172145-REP-MOB-002	Mobilisation Report - Frontier
F172145-REP-OPS-001	Operations Report - Pioneer
F172145-REP-OPS-002	Operations Report - Frontier
F172145-REP-GEOP-001	Geophysical Survey Report (WPA scope)
F172145-REP-HYD-001	Hydrographical Report (WPB scope)
F172145-REP-MAG-001	Magnetometer Box Survey Report (WPC scope)
F172145-REP-UHR-001	**3D-UHR Survey Results Report (WPD scope)**

Contents

Appendices

Figures in the Main Text

Tables in the Main Text

Abbreviations

ADRS	Altitude and Heading Reference System
ALARP	As low as reasonably practicable
APOS	Acoustic positioning operating station
BR	Bedrock
BSF	Below seafloor
CM	Central meridian
COG	Centre of gravity
COVID	Coronavirus disease
CRP	Common reference point
CTD	Conductivity, Temperature and Density
DGPS	Differential global positioning system
DP	Dynamic positioning
DTM	Digital terrain model
DTU	Technical University of Denmark
ERP	Emergency response plan
FMGT	Fledermaus geocoder toolbox
FNLM	Fugro Netherlands Marine
GEUS	Danmarks Og Grønlands Geologiske Undersøgelse (Denmark's and Greenland's Geological Survey)
GL	Glacial
GNSS	Global navigation satellite system
GPS	Global positioning system
HB	Head buoy
HF	High frequency
HOC	Hazard observation card
HOWF	Hesselø Offshore Wind Farm
HSE/HSSE	Health, safety and environment / Health, safety, security and environment
HV	High voltage
IHO	International Hydrographic Organization
IMU	Inertial measurement unit
INS	Inertial navigation sensor
IODP	International Ocean Discovery Program
ISO	International Standards Organisation
LAT	Lowest Astronomical Tide
LF	Low frequency
LG	Late Glacial
MBES	Multibeam echosounder
MCS	Multi-channel Seismic

MDAC	Methane-derived authigenic carbonates
MLSS	Multi-level stacked sparker
MOB	Mobilisation
MRU	Motion reference unit
MSL	Mean sea level
MTD	Mass transport deposits
NG	Next generation
OCP	Offshore converter platform
OCR	Offshore client representative
OHSAS	Occupational Health and Safety Assessment Series
OPS	Operations
OSS	Offshore substation
OWF	Offshore wind farm
PBP	Precise buoy positioning
PEP	Project execution plan
PG	Postglacial
PPE	Personal protective equipment
PPP	Precise point positioning
QA	Quality assurance
REP	Representative
RMS	Root-mean-square
RTK	Realtime kinematic
SBES	Single beam echosounder
SBP	Sub-bottom profiler
SPRK	Sparker
SVP	Sound velocity profile
TB	Tail buoy
TP	Tow point
UHR	Ultra-high resolution
UHRS	Ultra-high resolution seismic
UTM	Universal transverse mercator
VRF	Vertical reference frame
WG	Weichselian Glacial
WIFI	Wireless Fidelity
WPA	Work Package A
WPD	Work Package D

1. Introduction

1.1 General

Energinet Eltransmission A/S (Energinet) is developing a new offshore wind farm in the inner Danish Sea, Kattegat, the Hesselø Offshore Wind Farm (HOWF). The project survey site is located between Denmark and Sweden approximately 30 km North of Sjælland. Figure 1.1 presents the location of the site.

This report provides information relating to the acquisition and operations in respect to WPD (3D-UHR scope). The 3D-UHR seismic data acquisition took place in an approximately 1700 m by 500 m area centred on two offshore sub-station (OSS) locations (Figure 1.2, Figure 1.3 and Figure 1.4). These survey areas are referred to as 'OSS1 site' and 'OSS2 site' or 'the OSS sites'.

Guidelines on the use of this report are provided in Appendix A.

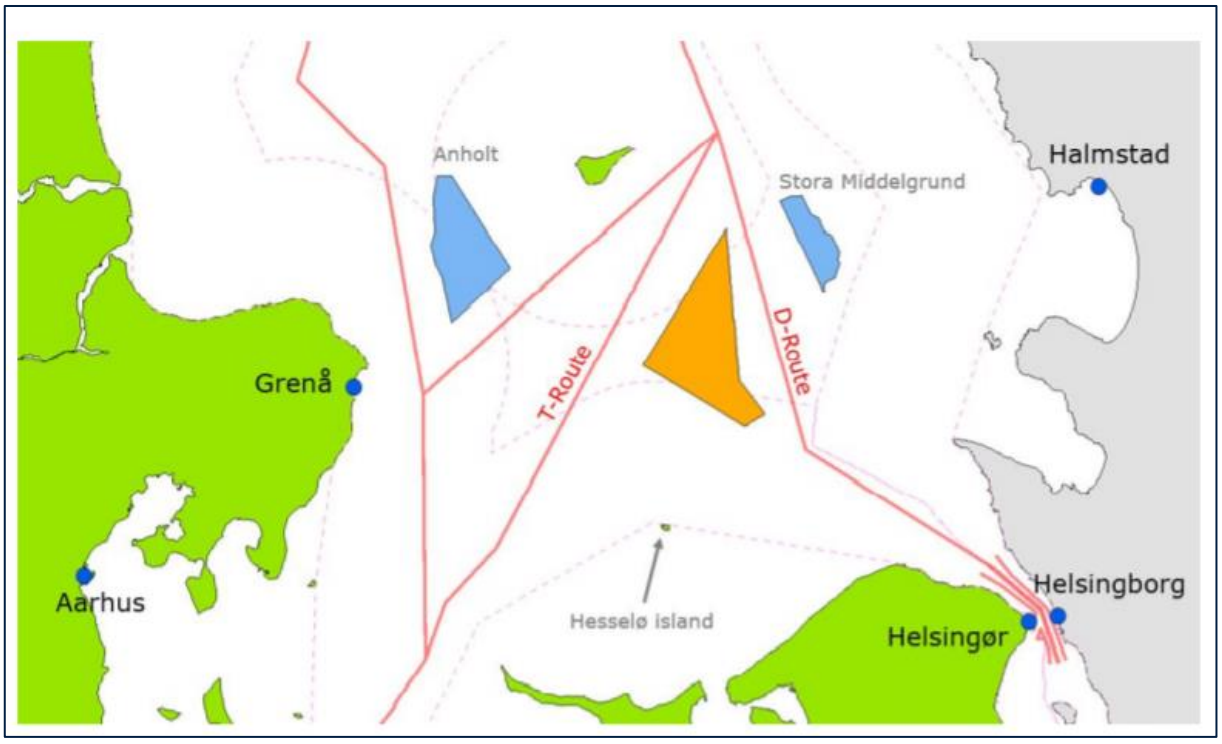

Figure 1.1: Location of the HOWF site (marked in orange).

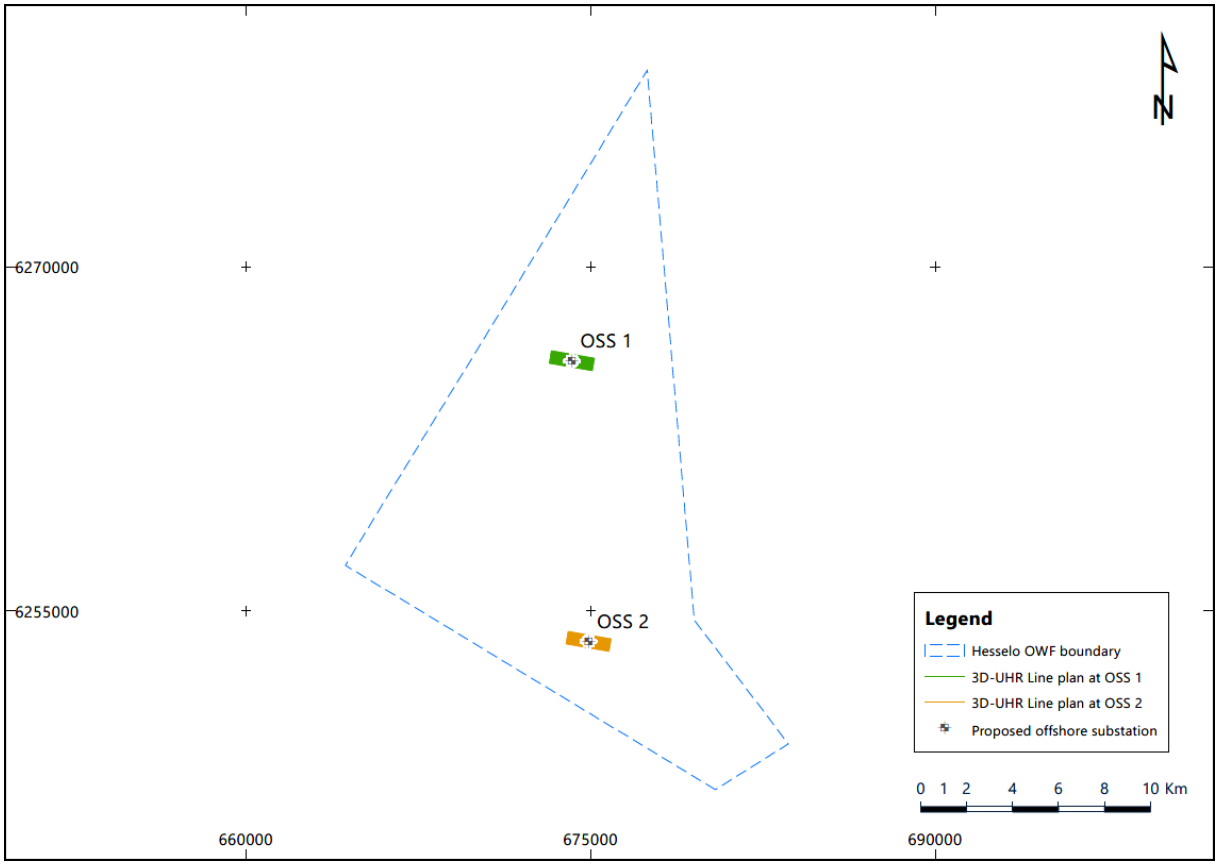

Figure 1.2: Location of the OSS1 and OSS2 sites in the HOWF site.

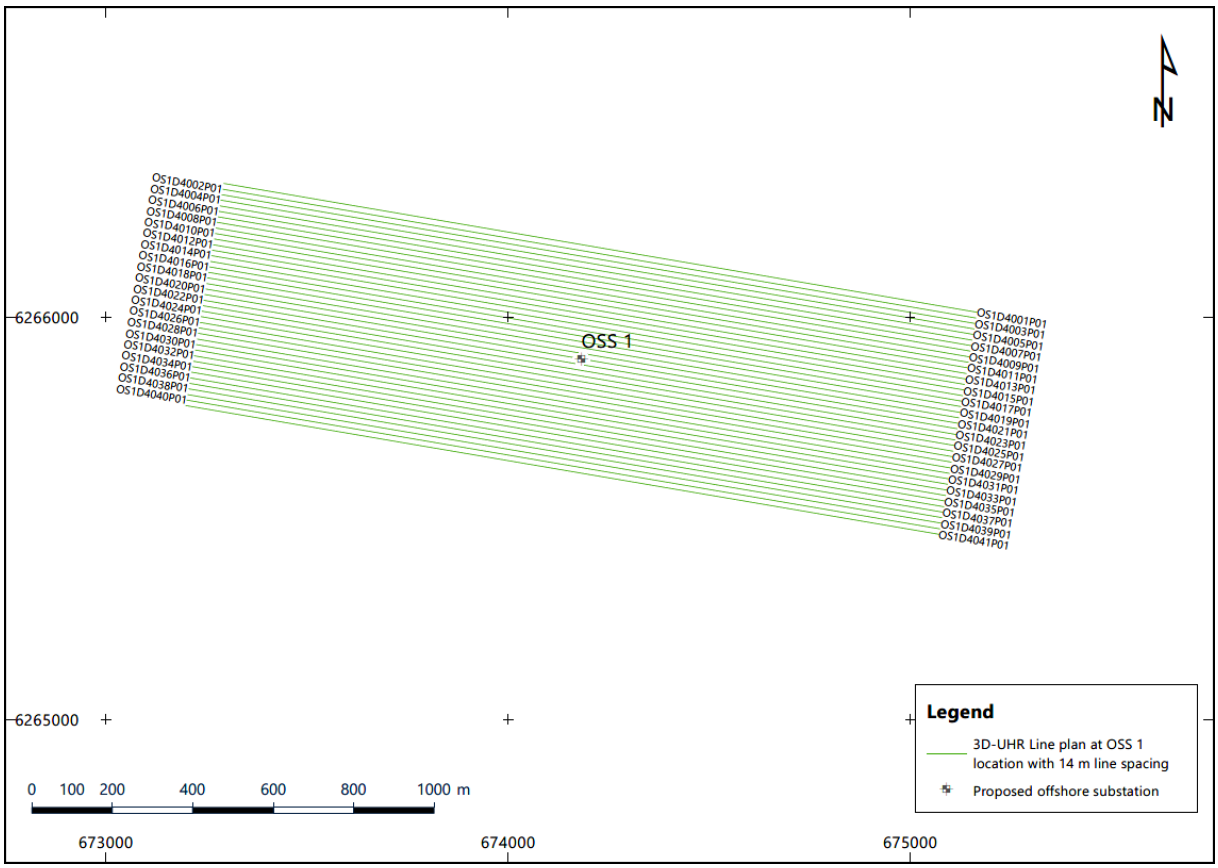

Figure 1.3: 3D-UHR seismic line plan for the OSS1 site in the HOWF site.

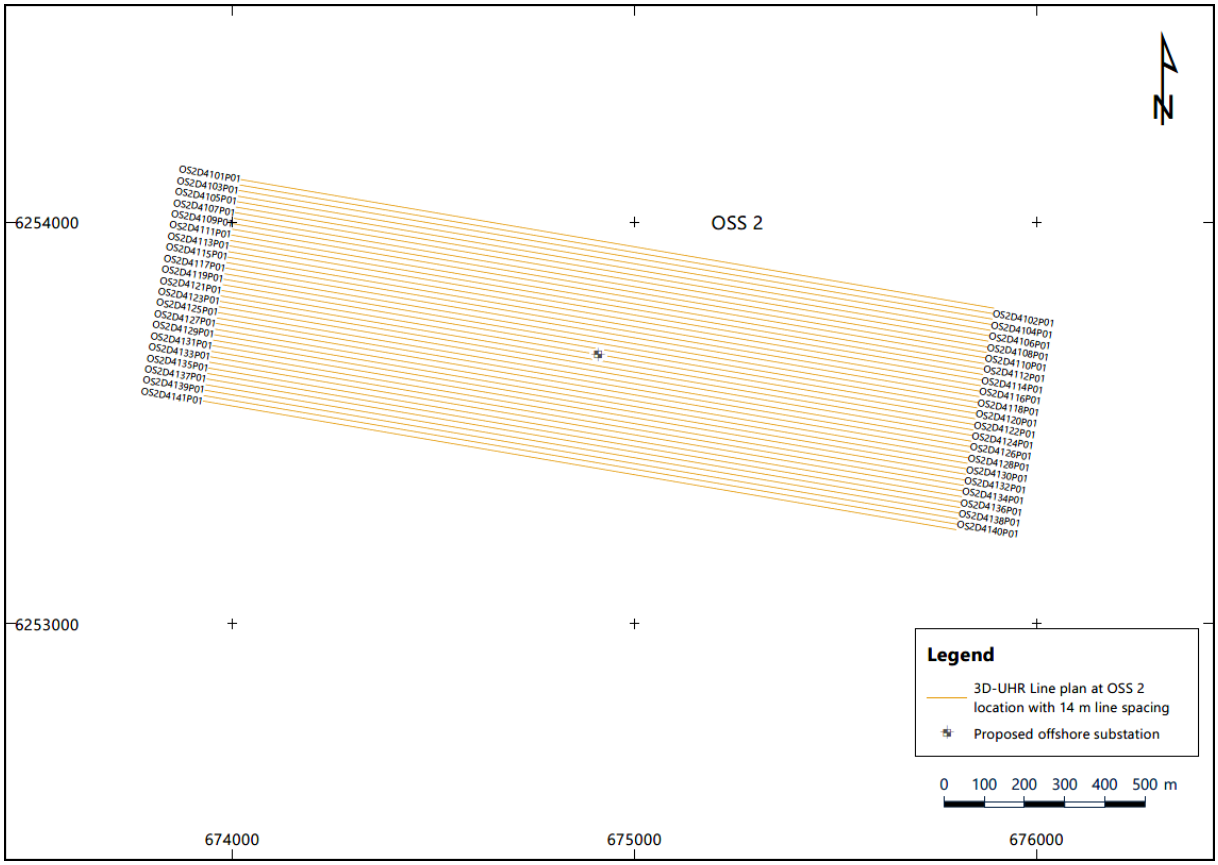

Figure 1.4: 3D-UHR seismic line plan for the OSS2 site in the HOWF site.

1.2 Survey Aims and Overview

The following sub-sections provide details about the main survey requirements and the scope of work for the Client's Work Package D (WPD); the Energinet Denmark Hesselø Geophysical Survey.

1.2.1 Survey Aims

The aim of the 3D-UHR seismic survey is to carry out high-resolution mapping of the sub-surface geology to at least 60 m below seafloor (BSF) at the OSS sites, in order to identify and map:

- Stratigraphic horizons in high detail;
- Subsurface structures that could represent changes in soil properties;
- Geohazards and any boulders with dimensions larger than 1 m.

To achieve these objectives Fugro:

- Acquired 3D-UHR (ultra high resolution) seismic data to 60 m BSF to determine sub-surface soil conditions that may influence foundation design below the effective penetration of the SBP;
- Utilised existing bathymetric data and other available sub-seafloor data (WPA and historical geotechnical data) to assist in the interpretation at the OSS locations.

1.2.2 Survey Overview

A summary of the main survey requirements for the geophysical survey operations is presented in Table 1.1.

Table 1.1: Survey requirements overview –3D-UHR operations.

Equipment Method	Survey Requirements
Vessel	■ Fugro Pioneer
OSS1/OSS2 Area Line spacing	■ 14 m for 3D-UHR seismic
Survey Priority	■ 3D-UHR seismic
Surface Positioning	■ 2 Independent systems ■ Horizontal Positioning accuracy: 0.2 m (2σ, 95%); ■ Vertical Positioning accuracy: 0.2 m (2σ, 95%);
Multibeam Echosounder (To locate dropped objects).	■ To be recorded.
Multibeam Backscatter	■ To be recorded.
SVP	■ The speed of sound in water shall be measured in the survey area once per 12 hour shift (as a minimum)

1.3 Geodetic Parameters

The project geodetic and projection parameters are summarised in Figure 1.5.

Name: ETRS89 / UTM zone 32N [ETRF2000-ITRF2014]		
EPSG Code	EPSG:25832	
Global Navigation Satellite System (GNSS) Geodetic Parameters*		
Datum	International Terrestrial Reference Frame 2014	EPSG:1165
Ellipsoid	GRS 1980	
Semi major axis	a = 6 378 137.00 m	
Inverse flattening	1/f = 298.257222101	
Local Geodetic Datum Parameters		
Datum	European Terrestrial Reference System 1989	EPSG:6258
Ellipsoid	GRS 1980	
Semi major axis	a = 6 378 137.00 m	
Inverse flattening	1/f = 298.257222101	
Datum Transformation Parameters from ITRF2014 to ETRS89		
X-axis translation 0.05582 m	X-axis rotation -0.0026051"	Scale difference 0.00334778 ppm
Y-axis translation 0.05332 m	Y-axis rotation -0.0157592"	Coordinate Frame rotation
Z-axis translation -0.09531 m	Z-axis rotation 0.025472"	FUGRO:41366
Local Projection Parameters		
Map projection	Transverse Mercator	
Grid system	UTM zone 32N	EPSG:16032
Latitude origin	00° 00' 00.000" N	
Central meridian	009° 00' 00.000" E	
Scale factor on central meridian	0.9996	
False easting	500 000 m	
False northing	0 m	
Notes * The geodetic datum of Fugro's global GNSS correction data is ITRF2014, epoch 2021.162 (01/03/2021)		

Figure 1.5: Project geodetic and projection parameters.

1.4 Vertical Datum

The vertical datum for the Energinet Hesselø project is reduced to Mean Sea Level (MSL) utilising the DTU18 MSL Tide Model as a vertical offshore reference frame supplied by the Technical University of Denmark (DTU).

2. Mobilisation and Operations

The data was acquired using the survey vessel Fugro Pioneer.

Vessel mobilisation and verifications for the 3D-UHR seismic scope of the survey were undertaken between 20 February and 28 February 2021 alongside in the port of IJmuiden, the Netherlands, and at a calibration site within the survey area (see report F172145-REP-MOB-003).

Operations on the Fugro Pioneer occurred between 28 February and 10 March 2021. Details are provided in report F172145-REP-OPS-003.

3. Vessel Details and Instrument Spread

3.1 Vessel Details Fugro Pioneer

The Fugro Pioneer (Figure 3.1) is a 53 m vessel built at Damen Shipyards in 2014. Being purpose designed for the demanding environments in which Fugro's coastal fleet operate, the Fugro Pioneer has excellent weather capabilities and is an ideal platform for 2D UHRS and geophysical surveys.

Figure 3.1: Fugro Pioneer

The Fugro Pioneer is equipped for 24-hour operations with space for a maximum of 31 persons.

3.2 Instrument Spread Fugro Pioneer

The equipment used for the survey is presented in Table 3.1.

Table 3.1: Equipment List

Requirement	Equipment
Primary GNSS	Fugro StarPack GNSS receiver with StarFix.G2+ corrections
Secondary GNSS	Fugro StarPack GNSS receiver with StarFix.G2+ corrections
MRU and heading sensor	IXSEA Hydrins, IXBLUE Octans
Multibeam echosounder	Dual Head Kongsberg EM2040
Sound velocity probe	2x SAIV CTD
Sound velocity sensor	1x Valeport Mini SVS installed near MBES head with 1x spare
Tidal heights	Fugro StarPack GNSS receiver with Starfix.G2+ corrections
3D-UHR Seismic Source	2 x Fugro MLSS (700 J, 360 Tips [160, 120, 80] @ 0.52 m, 0.67 m, 1.12 m)

Requirement	Equipment
3D-UHR Seismic Receiver	4 x Geometrics 48 Channel, 1 m Group Interval Multi-Channel Streamer

For full details of the Fugro Pioneer including weather limitations, vessel offsets and field procedures refer to Fugro report F145225-REP-OPS-003.

4. Results

4.1 Regional Geological Setting

The geological record at the HOWF site has been heavily influenced by the Sorgenfrei–Tornquist Zone. This is a fault system with a south-east to north-west orientation, located between Skåne in southern Sweden, the Kattegat and northern Jutland (Figure 4.1). It forms the south-western boundary of the Baltic Shield (Erlström and Sivhed, 2001). The fault system has been active since the Palaeozoic and has been re-activated multiple times, most recently during the Quaternary (Jensen et al., 2002), as result of isostatic (re)adjustments following ice sheet advances and retreats. One of the major faults of the Sorgenfrei–Tornquist Zone, the Børglum Fault, is located in the northern part of the HOWF site, and has a south-east to north-west orientation (Figure 4.1). The Børglum Fault is associated with a large pre-Quaternary depression, which influenced the depositional patterns during the Quaternary.

The bedrock at the HOWF site consists of Jurassic sandy mudstone and Upper Cretaceous limestones and glauconitic sandstones (Figure 4.2; Erlström and Sivhed, 2001).

During the Pleistocene, the Scandinavian Ice Sheet advanced and retreated several times in northern Jutland and the Kattegat. This resulted in the accumulation of a series of glacial tills and interglacial lacustrine and marine deposits (Jensen et al., 2002; Larsen et al., 2009). In addition, the repeated ice-sheet advance and retreat also formed a complex series of ice-terminal ridges (terminal moraines or push-moraines). These can still be recognised in the geomorphology of the islands and bathymetry of the southern Kattegat. During the relative sea level rise in the Late Glacial period (Late Weichselian; 16.0 to 12.6 ka BP), a thick package of glaciomarine clay was deposited (Jensen et al., 2002; Houmark-Nielsen and Kjær, 2003). Figure 4.3 illustrates paleogeography and depositional environments during the Weichselian in the wider Kattegat area.

In the early Holocene or Postglacial period (~10.5 to 12.6 ka BP) the relative sea level dropped due to isostatic rebound. This resulted in erosion of Late Weichselian deposits and is evidenced by an unconformity in the larger Hesselø area (Jensen et al., 2002; Bendixen et al., 2015, 2017; GEUS, 2020). Due to the ongoing eustatic sea-level rise, the area was once again inundated, and sediment was deposited in a transgressive, shallow marine environment between 11.7 to 10.8 ka BP. During this time a freshwater lake (Ancylus Lake) was present in the Baltic Sea. Between 11.9 and 9.1 ka BP, the Ancylus Lake drained via the Dana river system through the Storebælt in the south-east, into the Kattegat and resulted in the deposition of coastal sediments in the Hesselø area. From 9.1 ka BP the Holocene marine

transgression continued, and a thin layer of marine sediment was deposited (Bendixen et al., 2015, 2017).

Figure 4.4 presents interpretative profiles of the shallow geology at and in close proximity of the HOWF site, based on information available in public domain (Jensen et al., 2002; Bendixen et al., 2015).

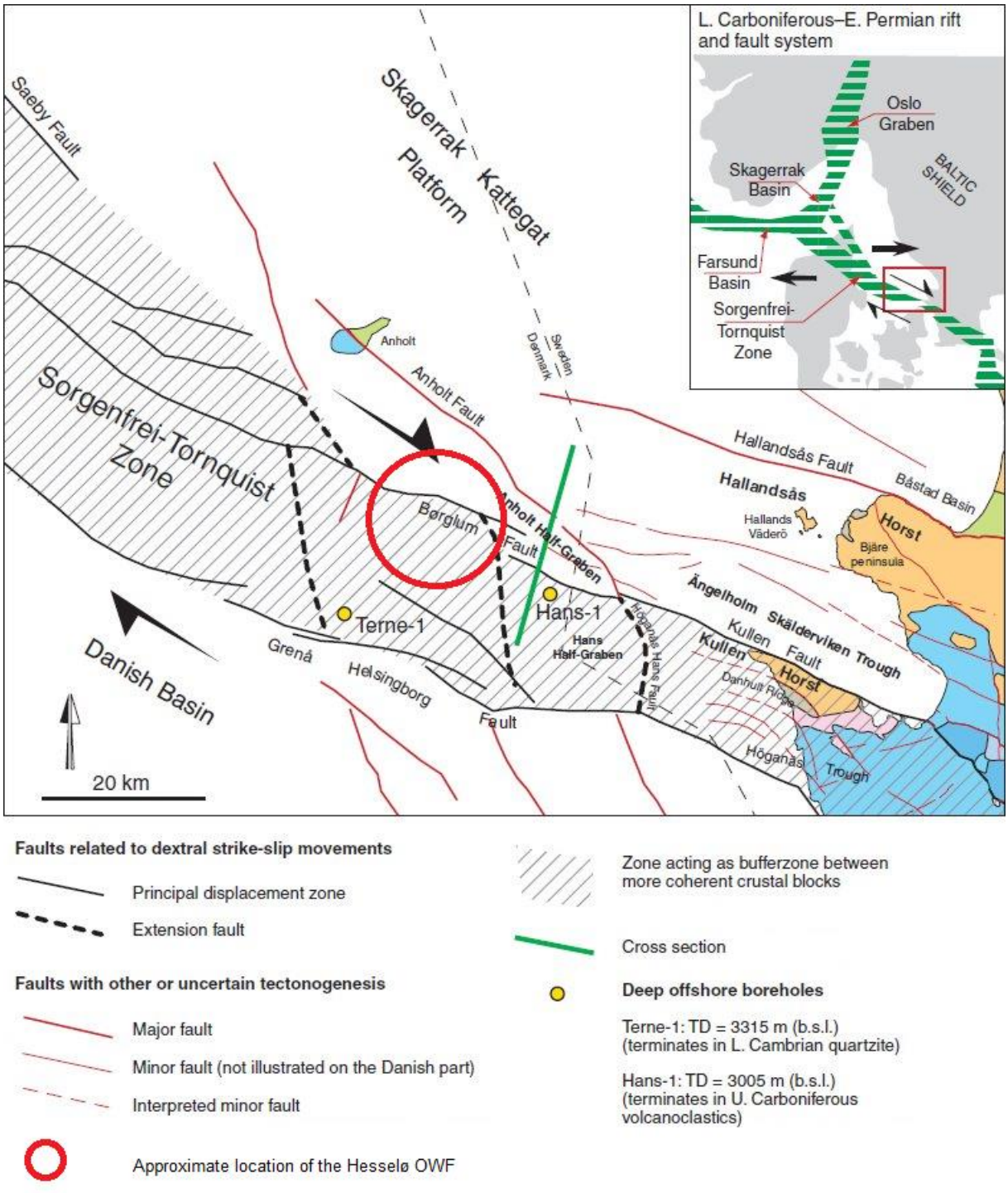

Figure 4.1: Structural setting of the southern Kattegat and the Sorgenfrei–Tornquist Zone (after GEUS, 2020).

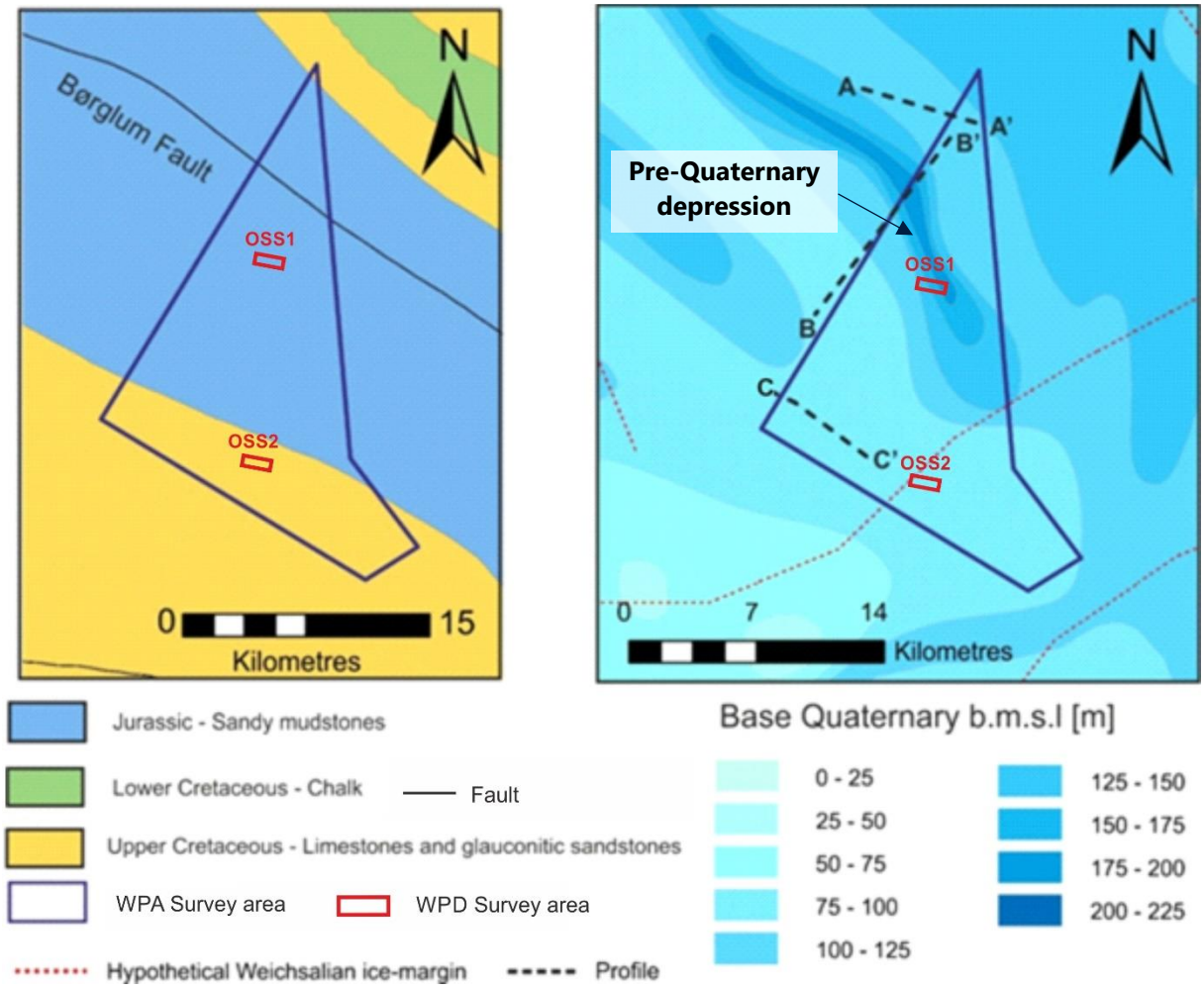

Figure 4.2: Bedrock geology (left image) and depth to the base of Quaternary (right image) at the HOWF site (modified after GEUS, 2020). Profiles are presented in Figure 4.4.

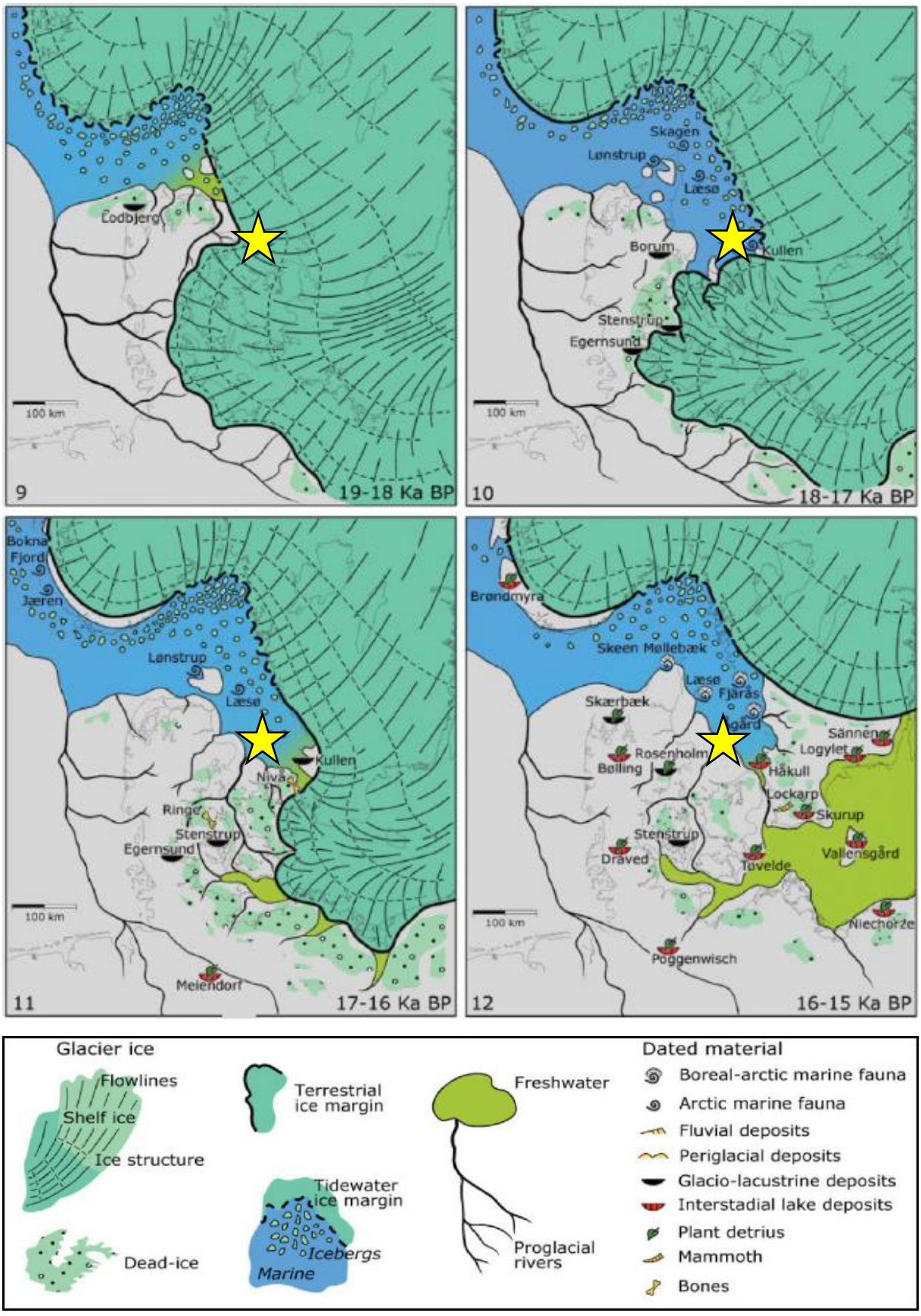

Figure 4.3: Palaeogeographies during the Weichselian in the Kattegat area (after Houmark-Nielsen and Kjær, 2003). The yellow star indicates the approximate location of the HOWF site

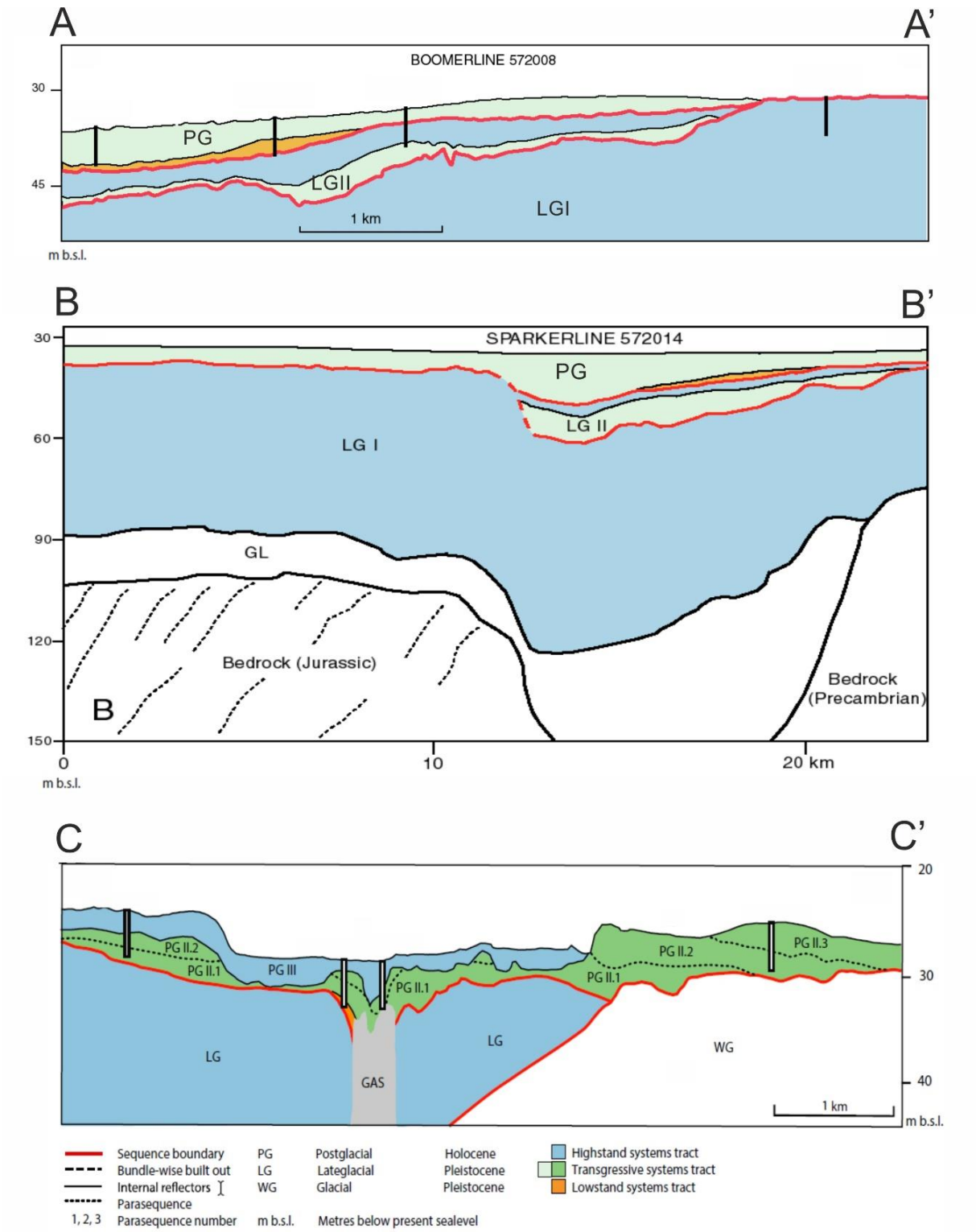

Figure 4.4: Interpretative profiles of the shallow geology at/near the HOWF site; profiles A–A' and B–B' from Jensen et al. (2002) and profile C–C' from Bendixen et al. (2015). See Figure 4.2 for the location of the profiles.

4.2 Seismostratigraphic Framework

Table 4.1 presents an overview of the interpreted seismostratigraphic units and associated horizons. Figure 4.5 and Figure 4.6 present seismic profiles across the OSS1 and OSS2 sites to give an overview of the spatial distribution of the seismostratigraphic units.

In the OSS sites, five seismostratigraphic units were interpreted in the 3D-UHR data in the top 60 m BSF. Seven different horizons represent unit boundaries, except for Horizons H11, H12 and H15, which are interpreted as internal surfaces separating different seismic facies within Unit D.

All horizons correspond to the horizons interpreted in the 2D-UUHR data (refer to Geophysical Survey Report (WPA scope): F172145-REP-GEOP-001).

Horizon H30 and H35, which were interpreted in the 2D-UUHR dataset as the base of Unit F and Unit G, respectively, were not interpreted in the OSS sites. Horizon H30 was not observed in both OSS sites. Horizon H35 was observed in the eastern part of the OSS1 site at a depth greater than 60 m BSF (i.e. below the interpretation window specified in the scope of work for WPD). This means that Unit F and Unit G are not present in the top 60 m BSF in the OSS sites.

The OSS1 site is located at the western margin of the large pre-Quaternary depression. The north-eastern part of the OSS1 site is influenced by the presence of this depression, and the thickness of the Holocene and Weichselian units (Units A to E) increase towards the north-east.

The OSS2 site, which is located 12 km to the south of the OSS1 site, has endured more glaciotectonism during the Weichselian. This is supported by the limited thickness of the undisturbed glaciomarine and glaciolacustrine deposits of Unit D and the increased thickness and shallow depth of glaciotectonised deposits of Unit E.

Table 4.1: Overview of seismostratigraphic units at the OSS sites.

Unit	Horizon [Colour]		Seismic Character	Expected Soil Type[1)]	Age	Depositional Environment	Previous Studies[2)]	
	Top	Base					Jensen et al. (2002)	Bendixen et al. (2015, 2017)
Holocene	H00 [seafloor]	H10	Acoustically transparent or low to medium-amplitude stratified reflectors	CLAY to clayey medium SAND or sandy GYTTJA; interlaminated to interbedded CLAY and SILT or medium SAND with shells and shell fragments	Holocene	Marine, deltaic to shallow marine	H	PG
D	H10	H20 H11 (internal) H12 (internal) H15 (internal)	Dominantly, low to high-amplitude parallel reflectors. Locally in the upper part, channel-like features with infill characterised by high-amplitude reflectors (base reflector H11). Locally, acoustically transparent to chaotic (base reflector H12). Generally, more chaotic below internal reflector H15.	CLAY with occasional laminae of SILT and/or SAND, locally sandy	Weichselian	Glaciomarine, glaciolacustrine to fluvial	LG I & LG II (16 to 13.5 ka BP)	LG I & LG II (16 to 12.6 ka BP)
E	H20	H25	Acoustically semi-transparent to chaotic with locally steeply inclined internal reflectors	CLAY, locally with sand beds	Weichselian	Glaciomarine and/or glacial deposits	GL	WG II
F	Unit is not present in the OSS1 and OSS2 sites							
G	Unit is not present in top 60 m in the OSS1 site and not present in the OSS2 site							
H	H20? H25	H50	Variable, either medium-amplitude parallel reflectors, or acoustically semi-transparent, or a chaotic (structureless) seismic character	SAND, CLAY, CLAY TILL and/or SAND TILL	Pleistocene	Glacial, periglacial and/or glaciomarine	-	-
I	H25 H50	N/A	Low to medium-amplitude low-frequency parallel reflectors; Locally acoustically (semi-)transparent	Sandy MUDSTONE, LIMESTONE and glauconitic SANDSTONE	Jurassic to Cretaceous	Marine	BR	-

Notes:

1) Based on historic geotechnical data:
   Units A, B, C and D and I from GEUS (2020)
   Units E and H from Jensen (2002); Bendixen et al. (2015; 2017); Andrén et al. (2015a; 2015b)
2) The units were correlated to seismostratigraphic units and age dating provided in previous studies of the southern Kattegat Figure 4.4 - Jensen et al., 2002; Bendixen et al., 2015, 2017), where: H = Holocene, PG = Postglacial, LG = Late Glacial, GL = Glacial, WG = Weichselian Glacial, BR = Bedrock

An overview of the interpreted horizons and their depth range is provided in Table 4.2.

Table 4.2: Depth range of the interpreted horizons at the OSS sites.

Horizon	Description	Depth Range in OSS1		Depth Range in OSS2	
		MSL [m]	BSF [m]	MSL [m]	BSF [m]
H10	Base Holocene	-33 to -38	1 to 5	-32 to -34	1 to 5
H11	Internal horizon in Unit D	-34 to -46	2 to 14	-	-
H12	Internal horizon in Unit D	-34 to -64	2 to 32	-	-
H15	Internal horizon in Unit D	-51 to -72	19 to 39	-	-
H20	Base of Unit D	-55 to -81	23 to 49	-33 to -47	23 to 48
H25	Base of Unit E	-59 to -134	27 to 101	-56 to -69	27 to 101
H50	Base of Unit H	-100 to -113	68 to 81	-87 to -99	68 to 81

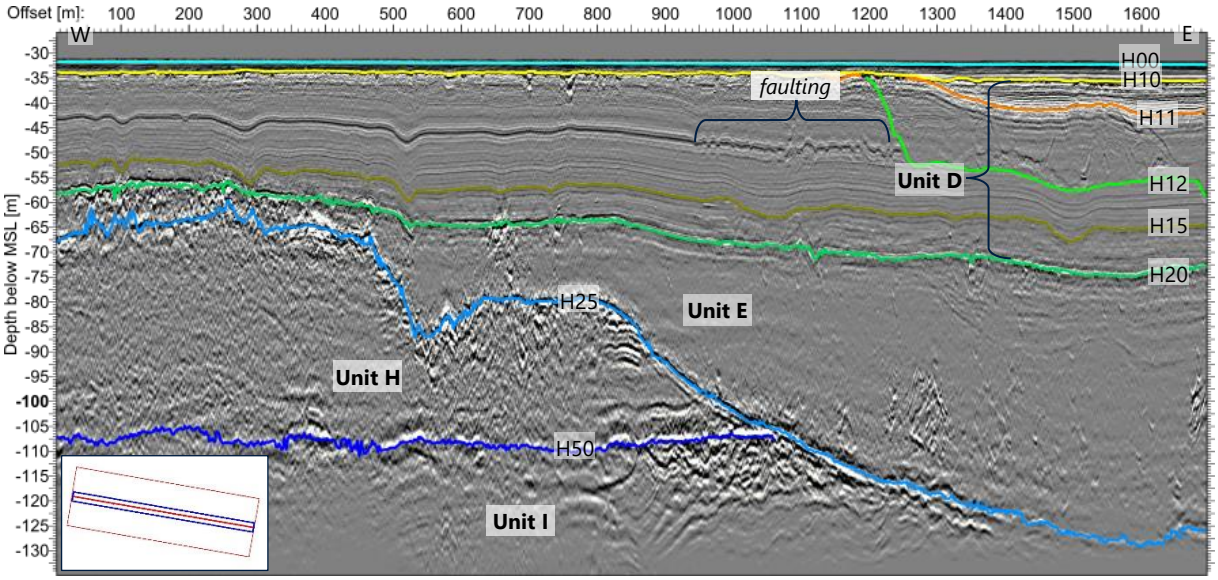

Figure 4.5: Inline 485. Overview of the seismostratigraphic units in OSS1.

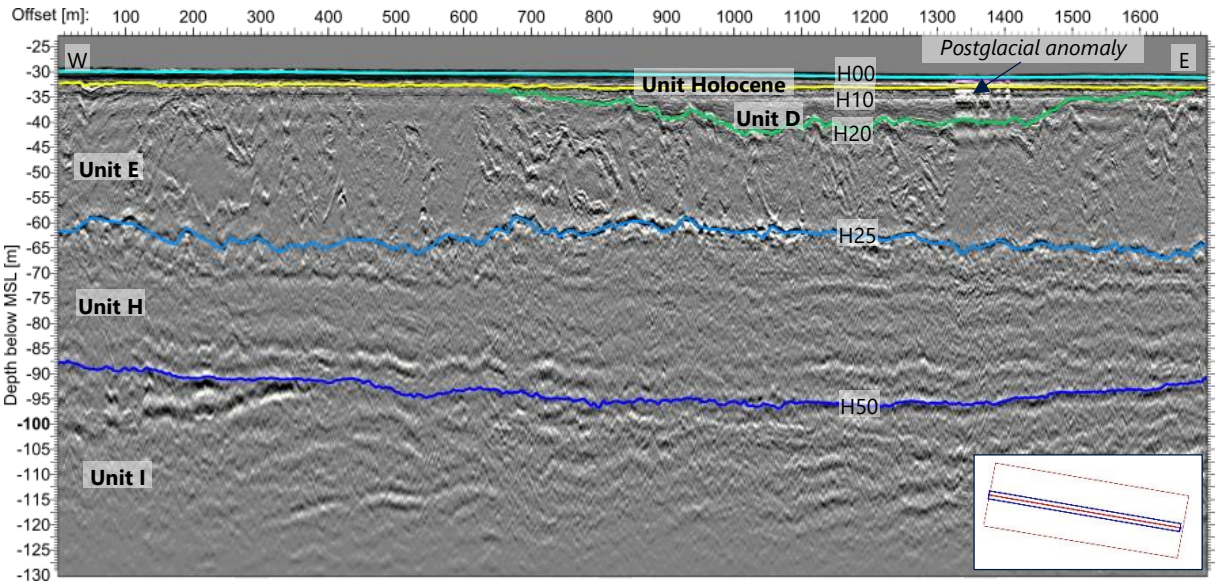

Figure 4.6: Inline 12405. Overview of the seismostratigraphic units in OSS2.

4.3 Seismostratigraphic Units

4.3.1 Unit Holocene

Unit Holocene represents the combination of all the Holocene units as defined in WPA (Unit A, Unit B and Unit C). The individual Holocene units are not seismically resolved in the 3D-UHR data and are therefore combined into one Unit Holocene.

Unit Holocene is present across the entire OSS1 and OSS2 sites. In the OSS1 site, Unit Holocene varies in thickness between 1 m and 5 m, showing an increase in thickness towards the north-eastern corner (Figure 4.7). Within OSS2 the unit varies in thickness between 1 m and 2 m in the east and between 2.5 m and 3 m in the west (Figure 4.8).

The internal seismic character of Unit Holocene varies from transparent to low to medium-amplitude internal reflectors (Figure 4.9).

Unit Holocene is interpreted to represent deposits varying from marine, deltaic to shallow-marine environments.

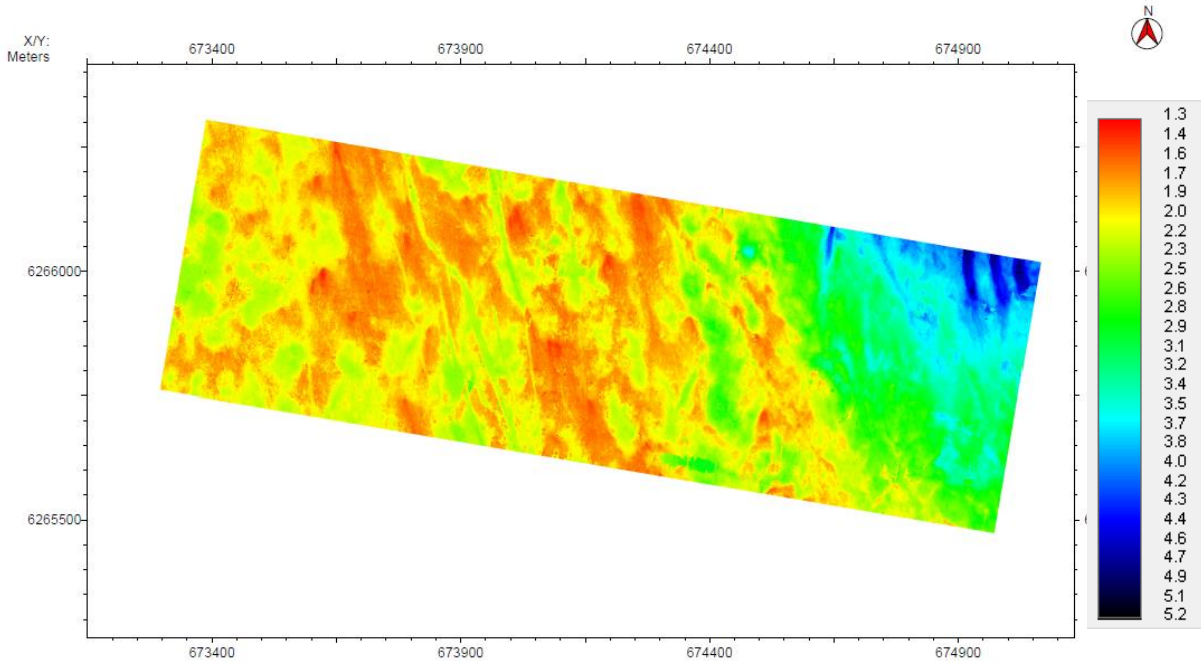

Figure 4.7: Thickness map of Unit Holocene in metres at the OSS1 site.

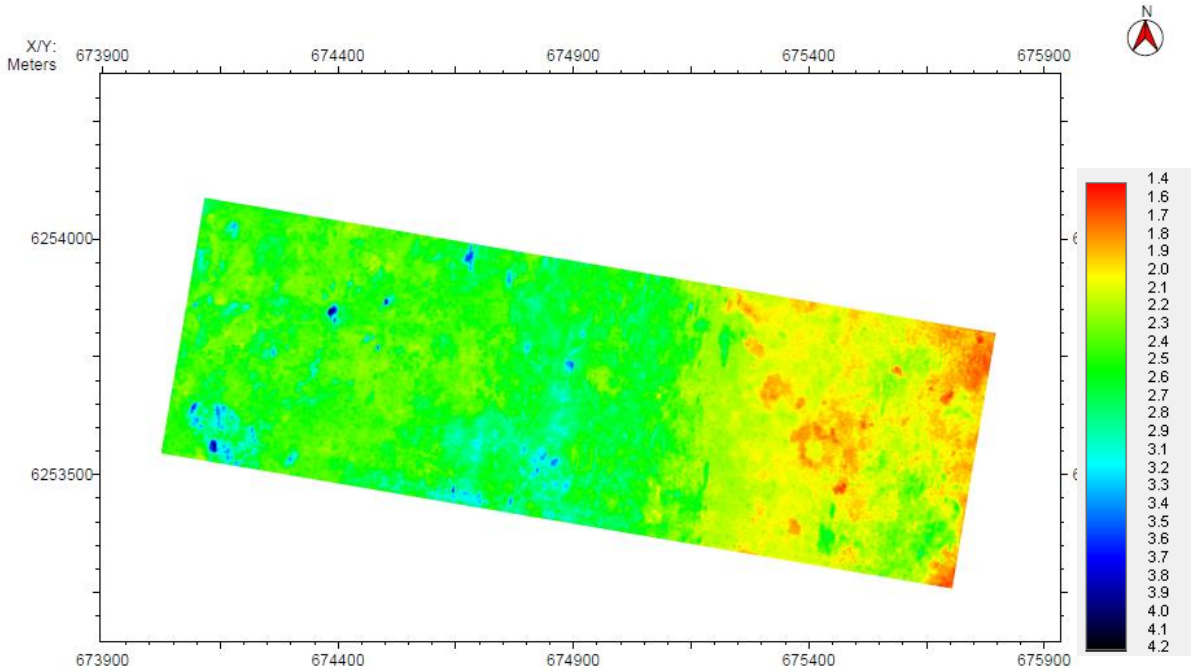

Figure 4.8: Thickness map of Unit Holocene in metres at the OSS2 site.

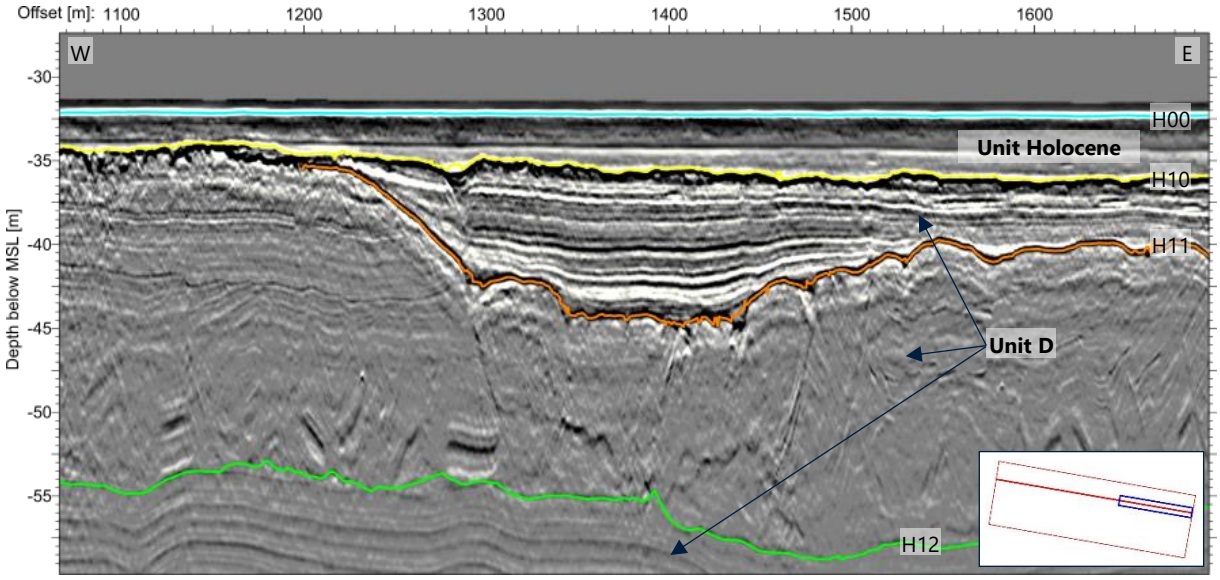

Figure 4.9: Inline 367 (OSS1). Data example of Unit Holocene and Unit D.

4.3.2 Unit D

Unit D is present across the entire OSS1 site with thickness varying between 21 m and 45 m (Figure 4.10). The thickness increases towards the east. At the OSS2 site, Unit D is only locally present in the eastern part, and reaches a maximum thickness of approximately 13 m (Figure 4.11).

Within Unit D three internal horizons (H11, H12 and H15) were interpreted at the OSS1 site. Within the OSS2 site, these internal horizons are not present. The general seismic character of Unit D is defined by low to medium amplitude parallel reflectors (Figure 4.12, Figure 4.13).

In Unit D, high amplitude positive anomalies are common in the OSS1 site, interpreted as possible gravel, cobbles and/or boulders (see Section 4.4.2).

Horizon H11 is characterised as a negative reflector with an erosional character and represents the base of a large channel, which infill is stratified, characterised by high amplitude parallel reflectors. It is predominantly present in the eastern part of the OSS1 site (Figure 4.13; Figure 4.14).

Horizon H12 also represents a negative reflector and denotes the base of channel-like features, whose infill has a transparent seismic character. Occasionally some vague parallel reflectors can be observed within the transparent facies. It is predominantly present in the eastern part of the OSS1 site.

Horizon H15 is a flat to undulating high amplitude positive reflector. The seismic character of Unit D below Horizon H15 is generally more chaotic compared to that above Horizon H15.

In the OSS2 site, the low to medium amplitude parallel reflectors are slightly more distorted compared to the OSS1 site.

Unit D is due to its seismic character, stratigraphic position and geotechnical properties interpreted as predominantly Late Glacial clays deposited in a glaciomarine and glaciolacustrine environment. The infill of channels underlain by Horizon H11 are interpreted to be deposited in a fluvial and/or tidal environment and the transparent facies underlain by Horizon H12 are interpreted as mass transport deposits (see Section 4.4.6).

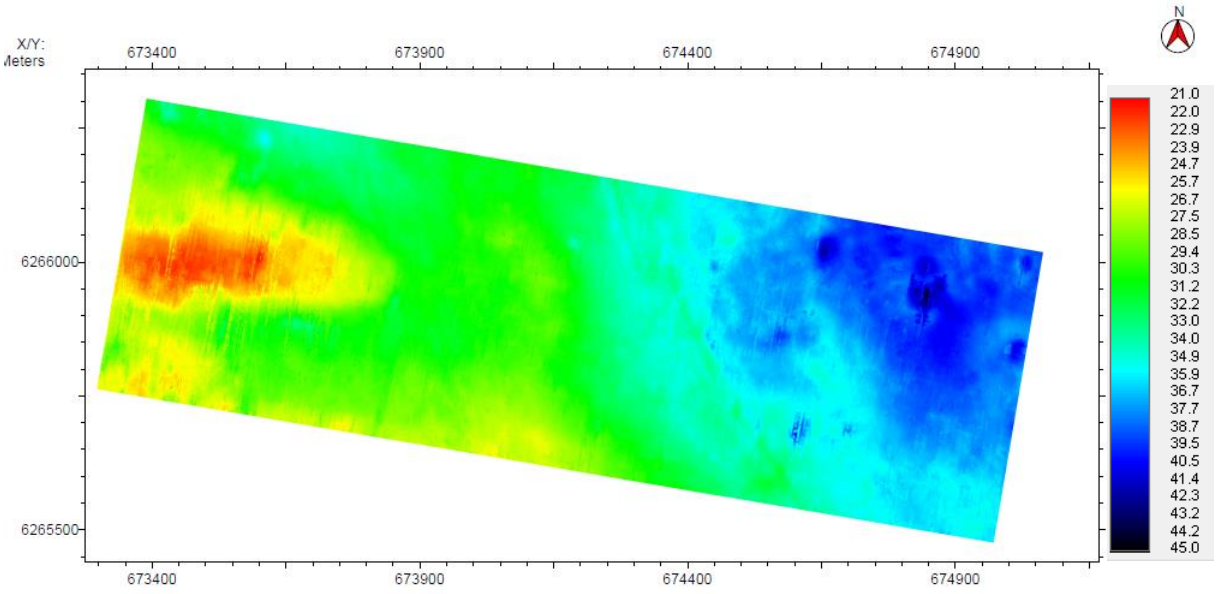

Figure 4.10: Thickness map of Unit D in metres at OSS1 site.

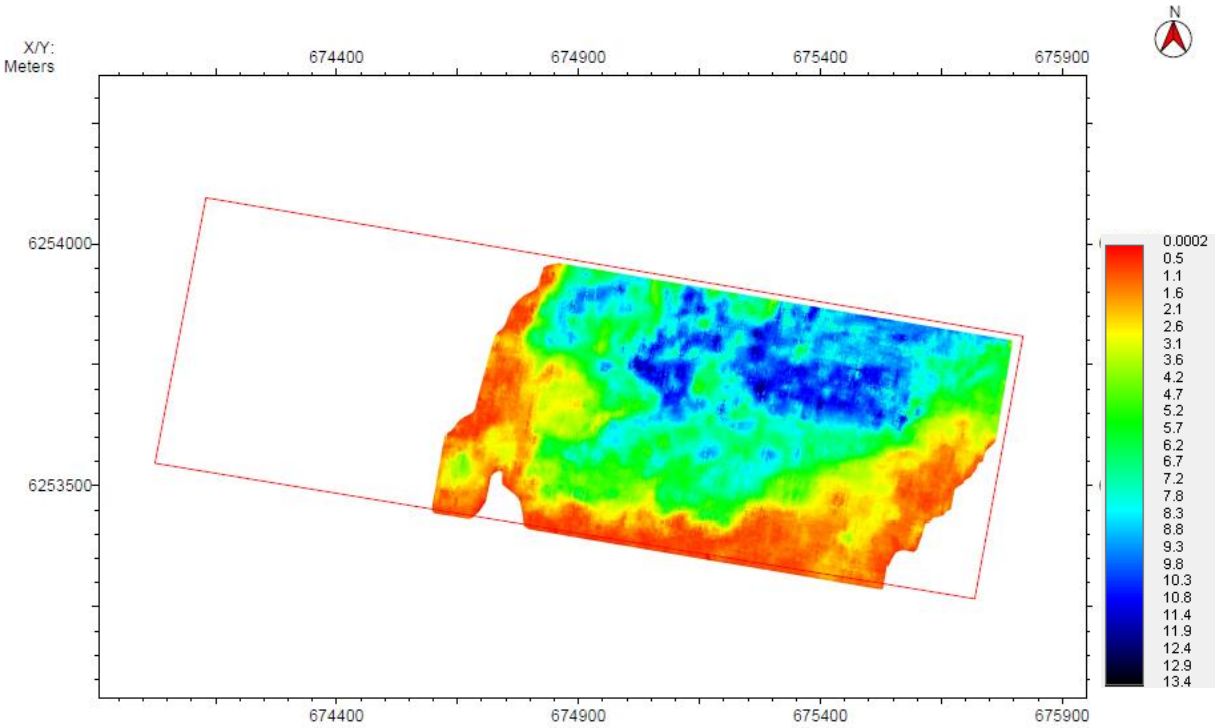

Figure 4.11: Thickness map of Unit D in metres at the OSS2 site.

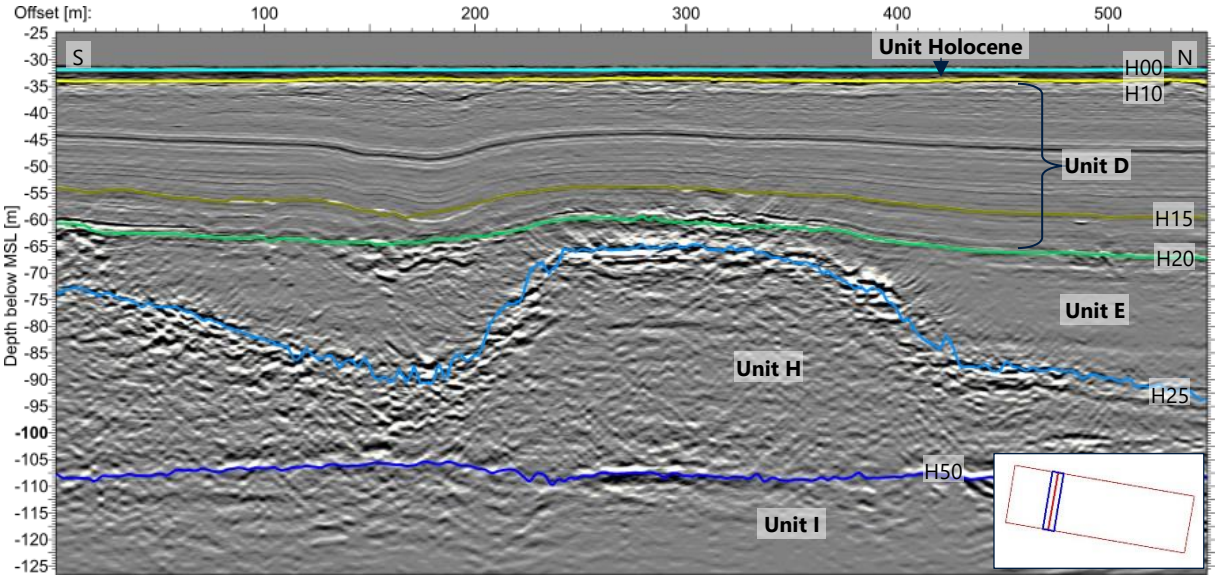

Figure 4.12: Crossline 2005 in OSS1. Data example of Unit D, Unit E and Unit H.

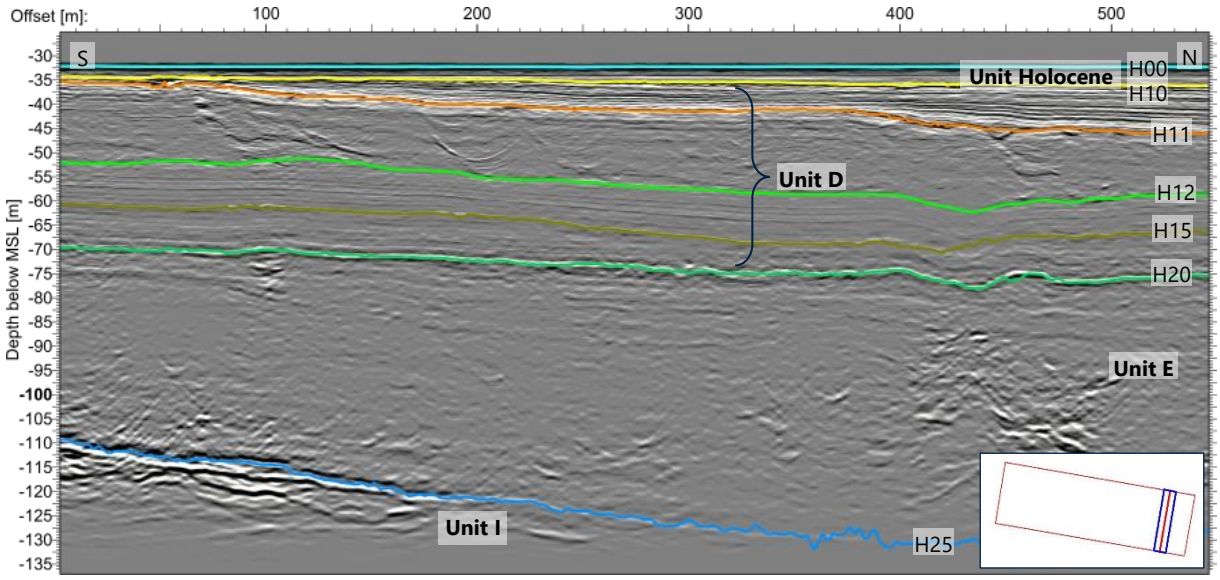

Figure 4.13: Crossline 4151 in OSS1. Data example of Unit D and Unit E.

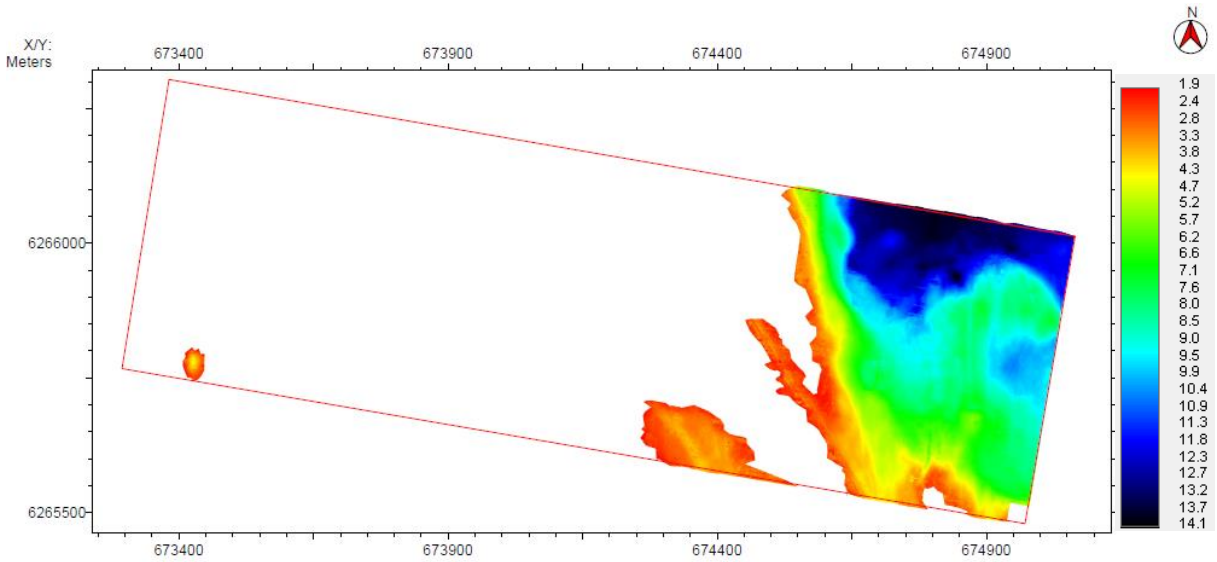

Figure 4.14: Depth to internal Horizon H11 (metres MSL) in Unit D at the OSS1 site.

4.3.3 Unit E

Unit E is present across both OSS1 and OSS2 sites. The unit varies substantially in thickness at the OSS1 site (Figure 4.15) between 0.6 m in the west and 59 m in the east. At the OSS2 site the unit varies in thickness between 15 m in the central part and 36 m in the west and south-east (Figure 4.16).

Unit E is topped by Horizon H20 and its base is represented by Horizon H25. The internal seismic character of Unit E is semi-transparent to chaotic (Figure 4.5,Figure 4.12, Figure 4.13, Figure 4.17). Locally, laterally limited steep internal reflectors are present (Figure 4.6), what suggests that Unit E is locally glacially deformed (see Section 4.4.5).

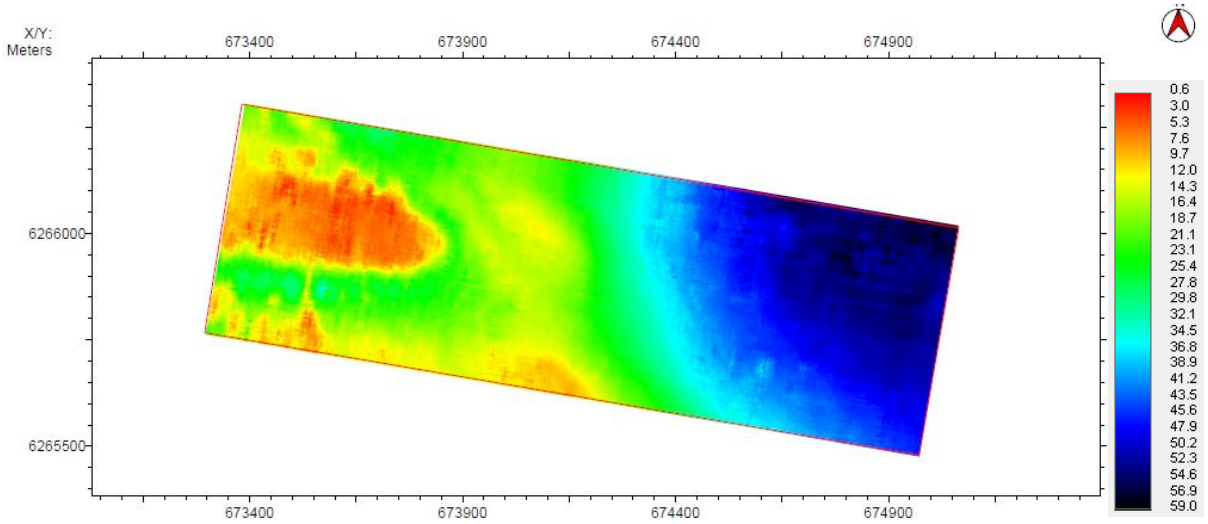

Figure 4.15: Thickness map of Unit E in metres at the OSS1 site.

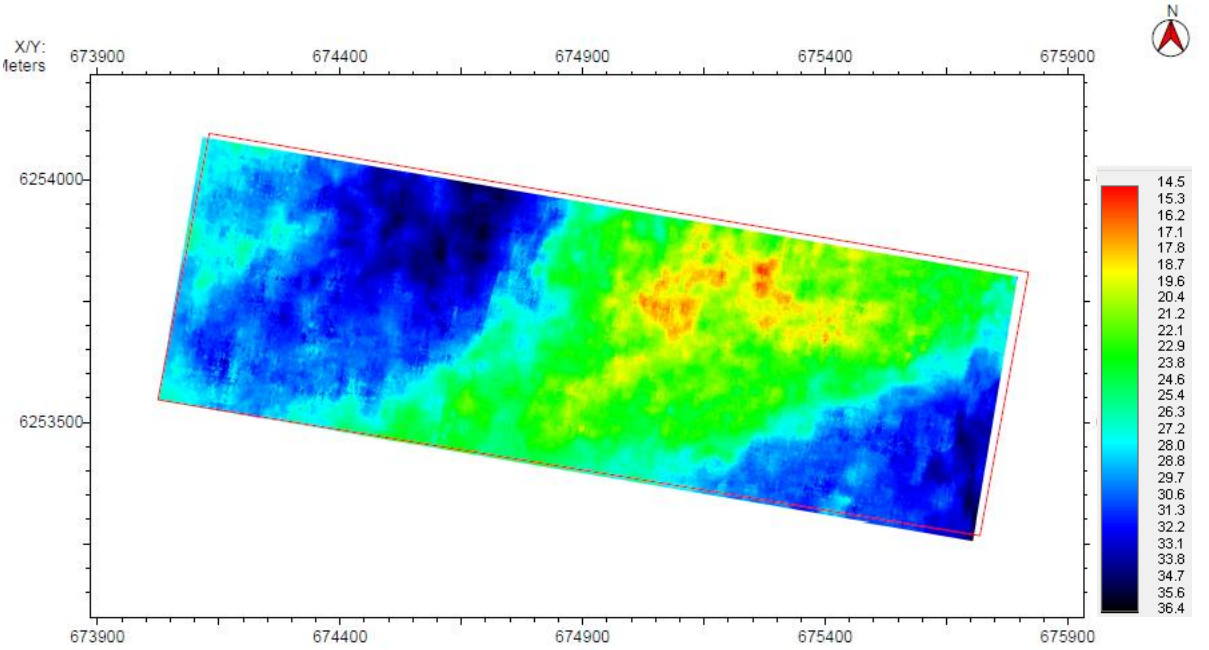

Figure 4.16: Thickness map of Unit E in metres at the OSS2 site.

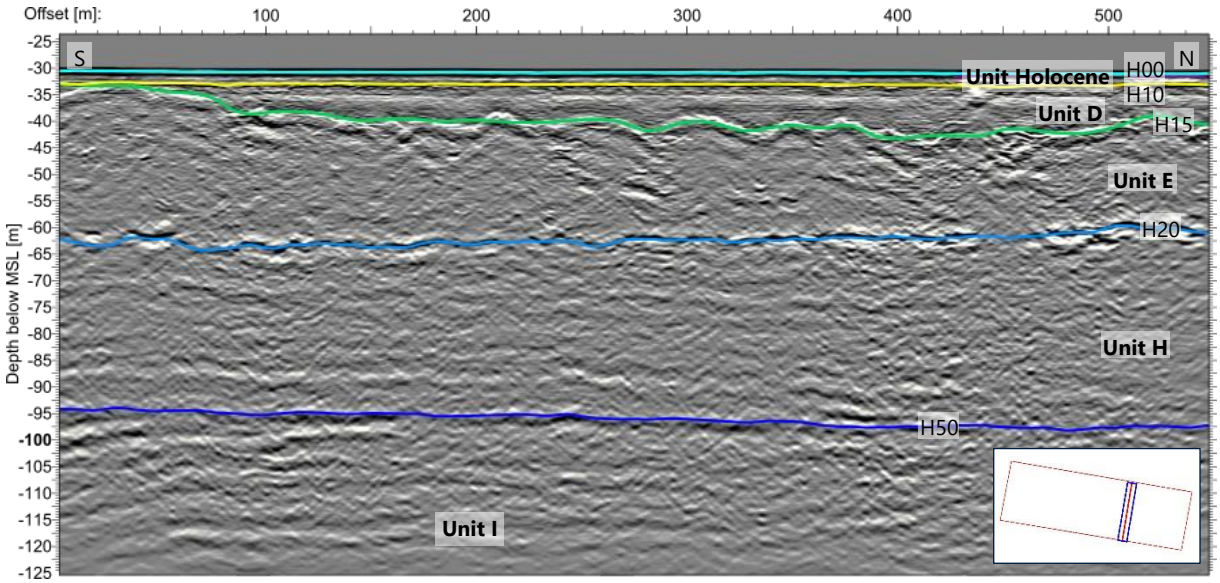

Figure 4.17: Crossline 9066 in OSS2. Data example of Unit E, Unit H and Unit I.

4.3.4 Unit H

Unit H is present in the western part of the OSS1 site and in the entire OSS2 site. In the OSS1 site, it varies in thickness between a couple of metres in the east, where it has been cut by the overlying Unit E (Figure 4.18), to more than 49 m in the west, where it forms an east to west oriented ridge.

In the OSS2 site, it varies from typical thicknesses of 25 m to 30 m in the east and west of the site to approximately 39 m in the central part, forming a south-west to north-east oriented ridge (Figure 4.19).

The internal seismic character of Unit H is very variable. At the OSS1 site it is acoustically transparent to chaotic (Figure 4.5, Figure 4.12), while at the OSS2 site it is semi-transparent with some medium amplitude parallel reflectors (Figure 4.6, Figure 4.17).

Unit H is interpreted as early Pleistocene sediments, deposited in glacial, periglacial and/or glaciomarine conditions. The observed ridges could represent remnants of moraine ridges of pre-Weichselian glaciations.

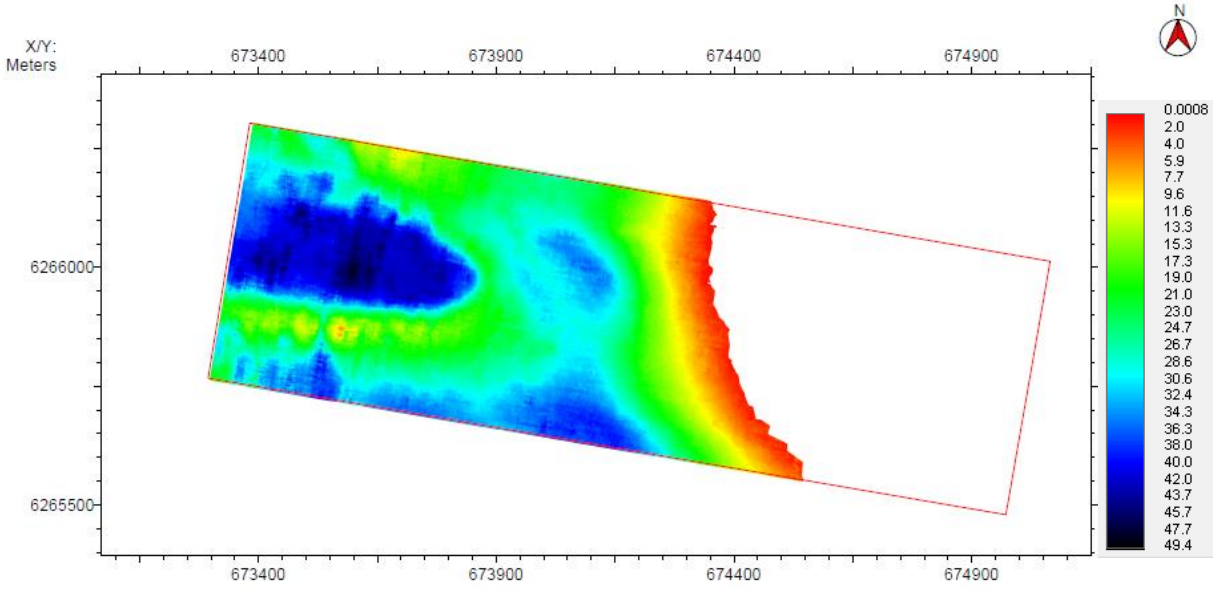

Figure 4.18: Thickness map of Unit H in metres at the OSS1 site.

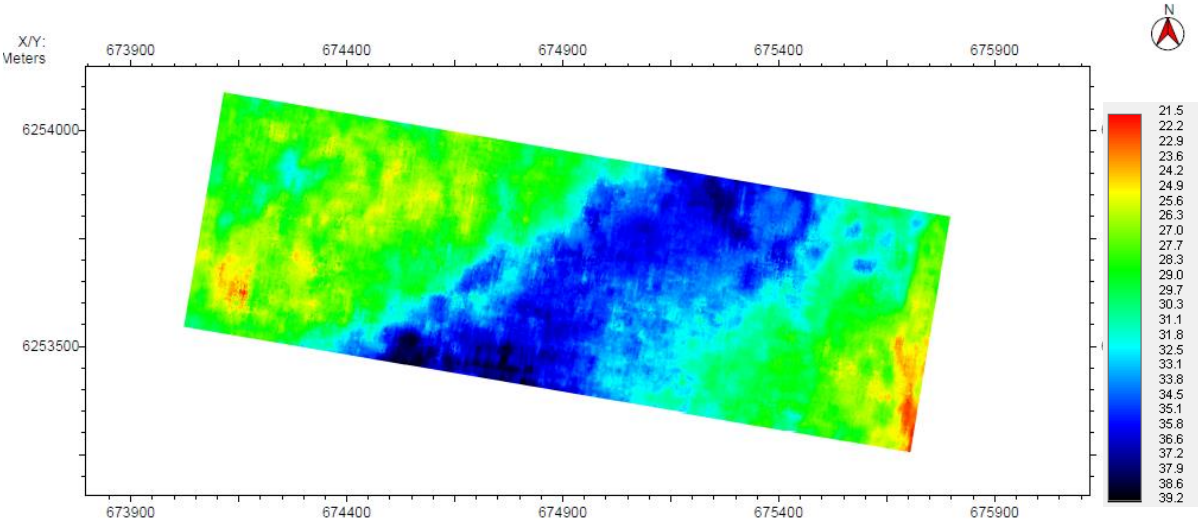

Figure 4.19: Thickness map of Unit H in metres at the OSS2 site.

4.3.5 Unit I

Unit I is interpreted as pre-Quaternary bedrock and expected to be present over the entire OSS1 and OSS2 sites. The top is represented by Horizon H50 or Horizon H25 and forms an angular unconformity (Figure 4.5, Figure 4.6, Figure 4.17).

In the western part of the OSS1 site, the top of Unit I is located between 68 m and 81 m BSF (Figure 4.20). In the eastern part of the OSS1, at the margin of the large pre-Quaternary depression, the top of Unit I is below the penetration depth of the 3D-UHR data. In this part of the OSS1 site, the base of Unit E (Horizon H25) incises deeply into Unit I.

At the OSS2 site the top of Unit I is situated between 86 m and 98 m BSF, increasing slightly in depth in the central and north-eastern part of the site (Figure 4.21).

The internal seismic character shows predominantly low to medium amplitude, low frequency parallel reflectors (Figure 4.6; Figure 4.17). Locally at both sites it can be acoustically semi-transparent.

Where Unit I shows parallel reflectors, the top (Horizon H50) represents an angular unconformity with the overlying units.

Based on GEUS (2020) the bedrock at the OSS1 site represents Jurassic sandy mudstone and the bedrock at the OSS2 site Upper Cretaceous limestone and glauconitic sandstone.

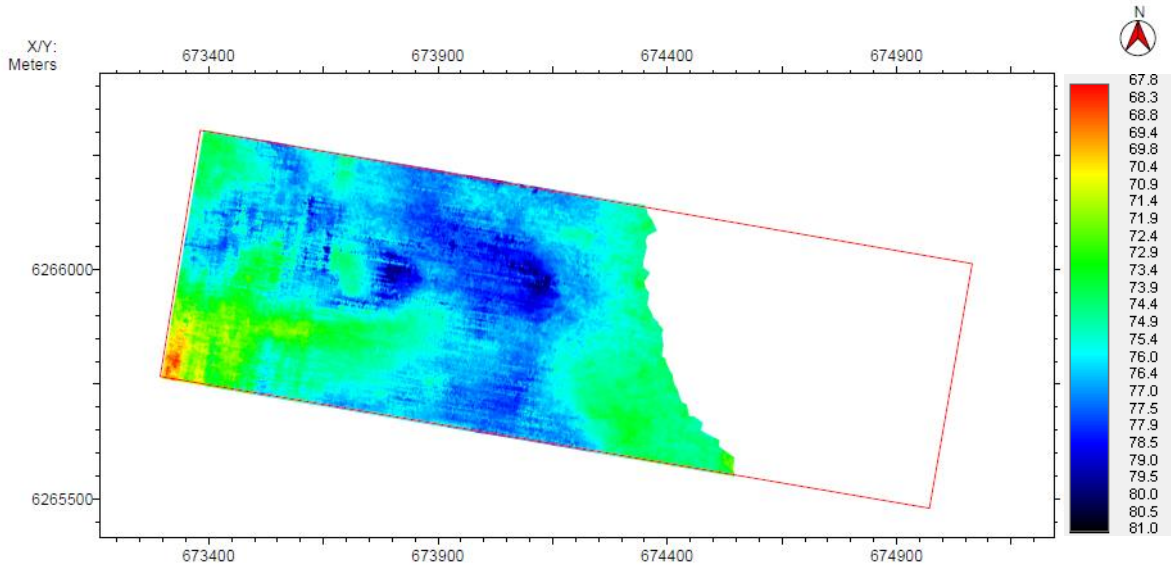

Figure 4.20: Depth to Horizon H50 (top bedrock) in metres BSF at the OSS1 site.

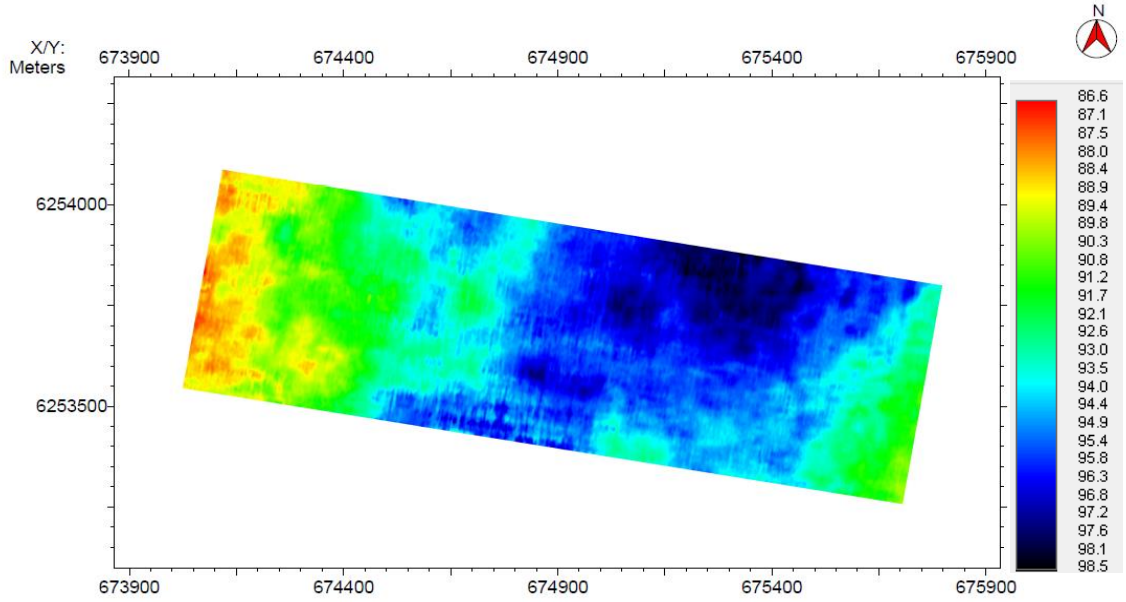

Figure 4.21: Depth to Horizon H50 (top bedrock) in metres BSF at the OSS2 site.

4.4 Geological Features

4.4.1 Local Enhanced Amplitude Anomalies - Postglacial Anomalies

Locally, enhanced amplitude parallel reflectors, with a varying spatial extent were observed in Unit Holocene, Unit D and Unit E in both OSS sites (Figure 4.22; Figure 4.23). They are particularly abundant in the OSS2 site. Occasionally acoustic blanking and/or signal distortion is observed below these anomalies. They are typically topped by a high-amplitude negative reflector. The width of these features varies from approximately 10 m up to 100 m and they vary from circular to more cloud shaped in plan view (Figure 4.23).

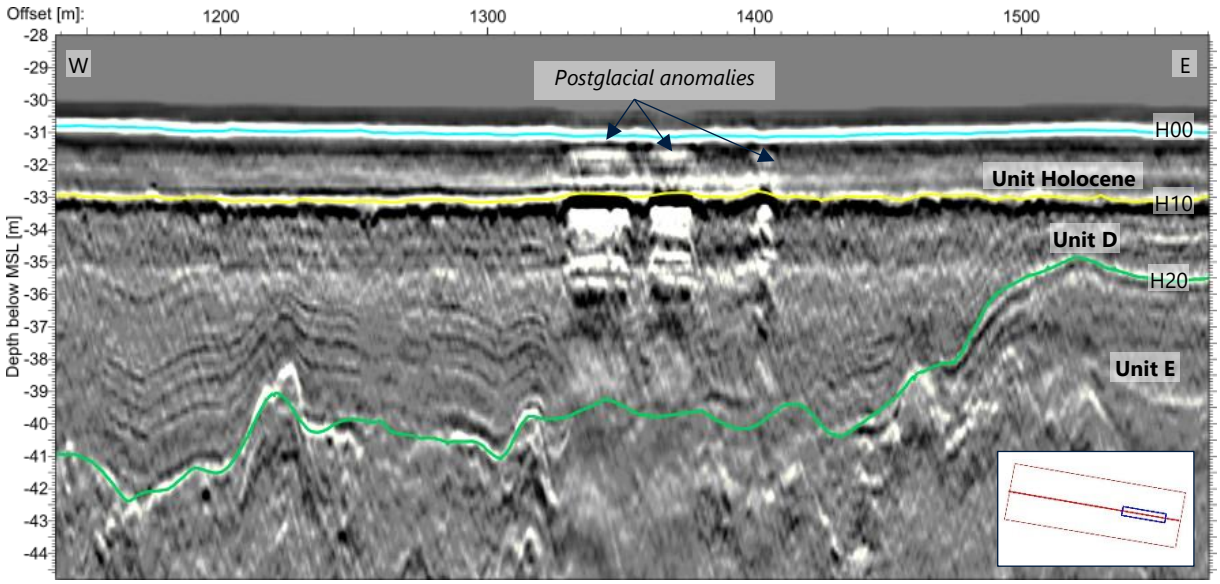

Figure 4.22: Inline 12400 in OSS2. Data example of Postglacial anomalies.

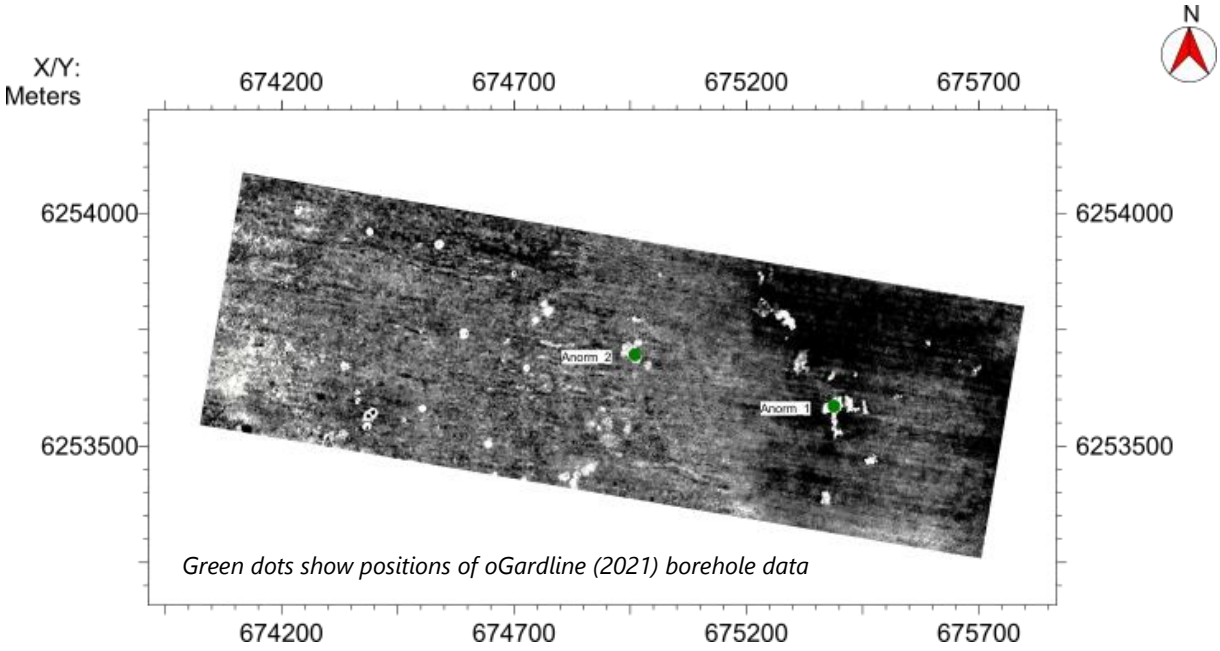

Figure 4.23: Depth slice example of the OSS2 site (31.75 m MSL) in Unit Holocene with Postglacial anomalies (white dots).

Correlation with Geotechnical Data and Interpretation

The local enhanced amplitude anomalies were also observed in the SBP and 2D-UUHR data from WPA (report F172145-REP-GEOP-001). It is not likely that these features represent acquisition artefacts. These features are considered to have a geological origin. The exact origin cannot be determined with confidence. Several explanations for these features are described below.

Four (4) Postglacial anomalies were sampled for ground truthing (Gardline, 2021). Two (2) geotechnical borehole locations are in the OSS2 site (Figure 4.23). Representative data examples showing the geotechnical borehole locations projected on 3D-UHR seismic sections are presented in Figure 4.24 and Figure 4.25.

The top of the anomalies, as observed in the seismic data, occurs in Unit A. Geotechnical boreholes penetrating these anomalies indicate that their tops occur within very low strength CLAY (Unit Holocene), which is underlain by a bed of SAND varying in thickness between 0.1 m and 1.2 m. This sand bed is associated with Unit B or Unit C and its base is associated with Horizon H10.

This SAND bed is slightly to highly calcareous and includes (frequent) shell fragments. It is locally silty, gravelly and may contain cobbles (described as 'cobbly' (Gardline (2021)). At the Anorm_2 geotechnical borehole location, the top of the SAND bed corresponds to a local high amplitude positive reflector (Figure 4.25).

Below the SAND bed, slightly to highly calcareous, low to medium strength CLAY with black organic staining or slight organic odour is present.

The geotechnical borehole data show that the soil conditions and properties vary over the vertical interval covered by the anomaly: i.e. the top of the anomaly may coincide with CLAY, whilst lower parts of the anomaly are associated with slightly to highly calcareous SAND. Cemented sand was not observed at the sampled locations.

Possible origins for these local enhanced amplitude anomalies are listed below:

- The Postglacial anomalies appear to be related to the SAND beds observed in Unit B and Unit C, and associated with Horizon H10. Bendixen et al. (2015) and Jensen et al. (2002) reported that PG II (corresponding to Unit B in this report) comprises laminated SILT and CLAY. This deviates from the geotechnical properties of Unit B as observed at the Anorm_2 borehole location and the base of Unit B at Anorm_1: i.e. SAND. This may suggest that Unit B and Unit C are generally associated with SILT and CLAY and that local occurrences of SAND (e.g. very local sand bars) are present. This lateral change in soil conditions (and possible accumulation of gravel and cobbles within the sand bed) may be the cause for a relatively large acoustic contrast and hence a local enhanced amplitude anomaly.

- Acoustic blanking and signal distortion were observed below some of these anomalies. This suggests that (small amounts of) free gas may present in sediment below the anomalies and that the anomalies themselves may reflect the approximate position of where the gas is trapped below or within the clayey sediments of Unit A. At these shallow depths, sealing capacity of normally consolidated soils is expected to be low and possibly insufficient to contain gas accumulations. The natural buoyancy of the free gas bubbles may be in equilibrium with capillary forces in pores within the fine-grained sediments of Unit A.
- The northern Kattegat is known for methane-derived authigenic carbonates (MDAC) or 'bubble reefs' (Jensen et al., 1992). These features are associated with gas seeps and/or expulsion and are evidenced by the presence carbonate-cemented sandstone structures (e.g. mounds). Where they are associated with active gas seepage, they are often accompanied by a diverse marine ecosystem (Judd and Hovland, 2007). The geotechnical borehole data at the investigated anomalies do not indicate the presence of a carbonate-cemented sandstone. Within the sampled sands (Unit B, Unit C and Horizon H10), only (small) shell fragments were described (i.e. not a diverse marine ecosystem). From this it may be concluded that the targeted anomalies do not resemble fully developed MDAC features. In addition, these features are covered by recent sediment that may suggest that gas seepage activity has ceased in past, effectively stopping authigenic carbonate formation. As such, these features may resemble an early stage form of an MDAC at the onset of carbonate cementation (as evidence by varying carbonate contents with the sampled sands).

Only a limited number of local enhanced amplitude anomalies were sampled. The results of the acquired geotechnical data and integration with the seismic data result in various potential origins of these features. A definite, single origin for the sampled features could however not be deduced. These features could result from various processes. Therefore, the origins of the sampled features and the non-sampled features remain speculative without further ground truth information (e.g. soil sampling and CPT testing, geochemical analysis, high resolution geological logging).

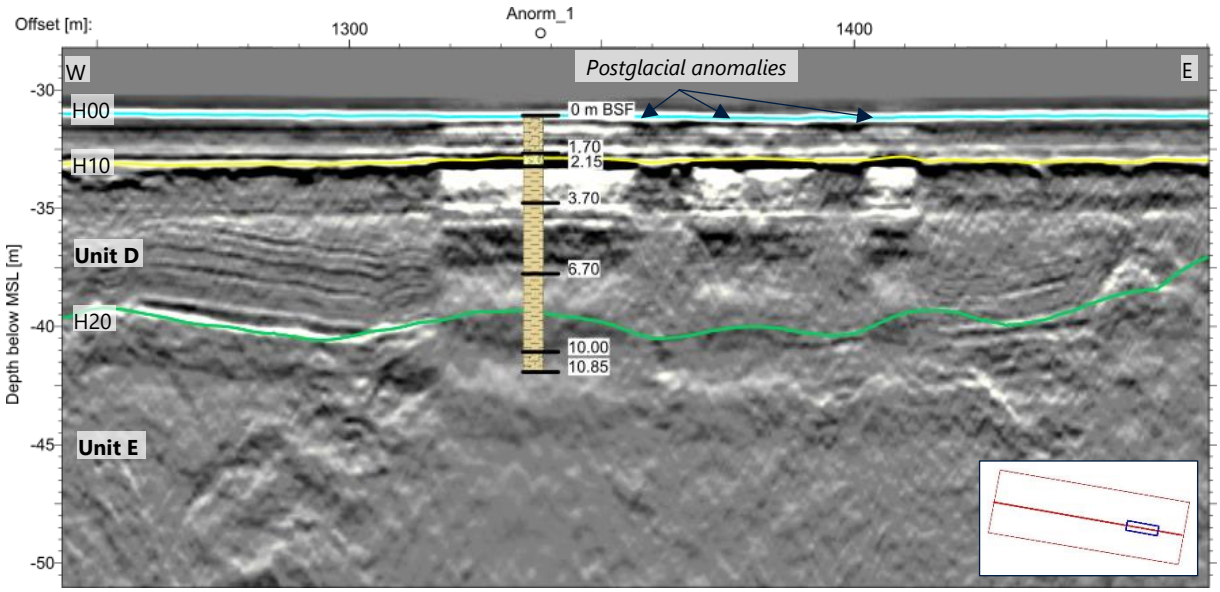

Figure 4.24: Inline 12410 in OSS2. Borehole log of Anorm_1 projected on a 3D-UHR seismic line.

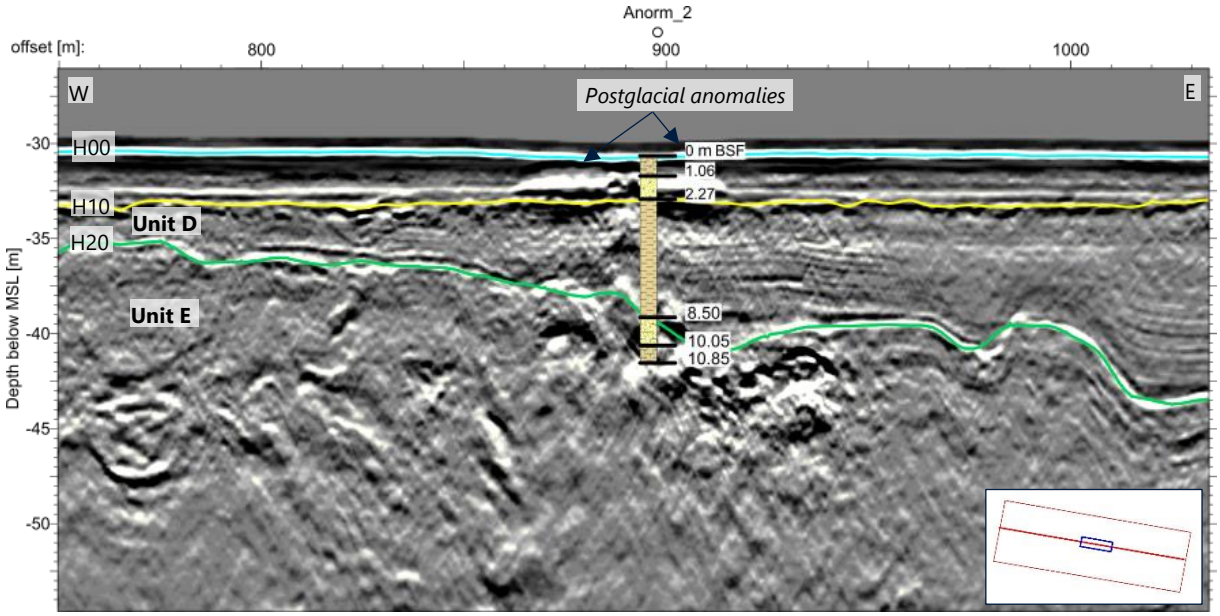

Figure 4.25: Inline 12370 in OSS2. Borehole log of Anorm_2 projected on a 3D-UHR seismic line.

4.4.2 Boulders, Cobbles and Gravel

In the OSS1 site, point anomalies were observed in Unit D, Unit E and Unit H. A total of 576 positive point anomalies were interpreted in the OSS1 site, where they are particularly abundant in Unit D. No point anomalies were observed in the OSS2 site. In the unmigrated 3D-UHR data, they correspond with diffraction hyperbolas (Figure 4.26;Figure 4.27).

The point anomalies or hyperbolic diffractions are interpreted as predominantly gravel, cobbles and/or boulders. As Unit D is interpreted as glaciomarine and glaciolacustrine deposits, these point anomalies may possibly represent ice-rafted debris.

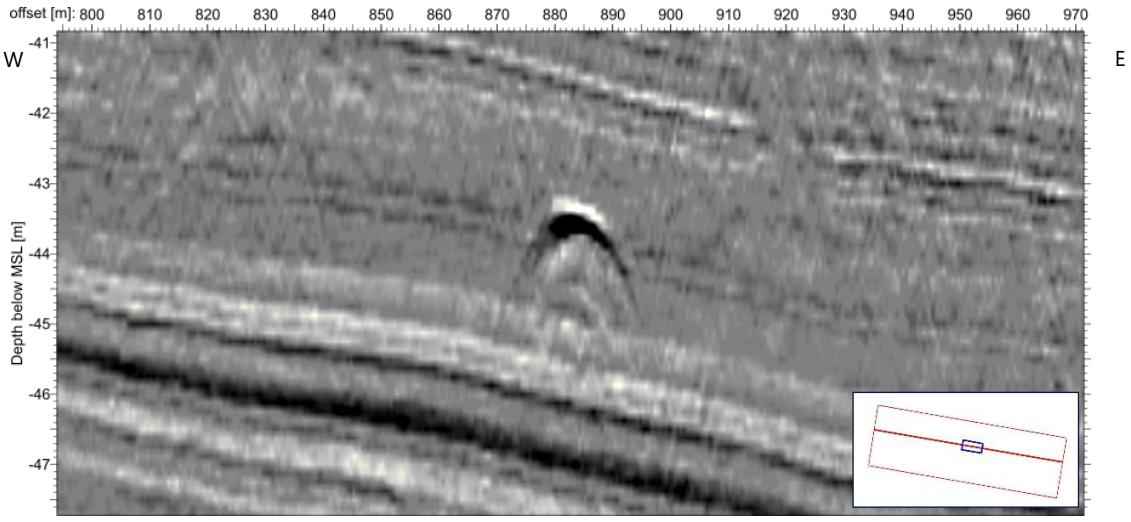

Figure 4.26: Inline 434 in OSS1. Data example of a diffraction hyperbola in Unit D in unmigrated 3D-UHR data.

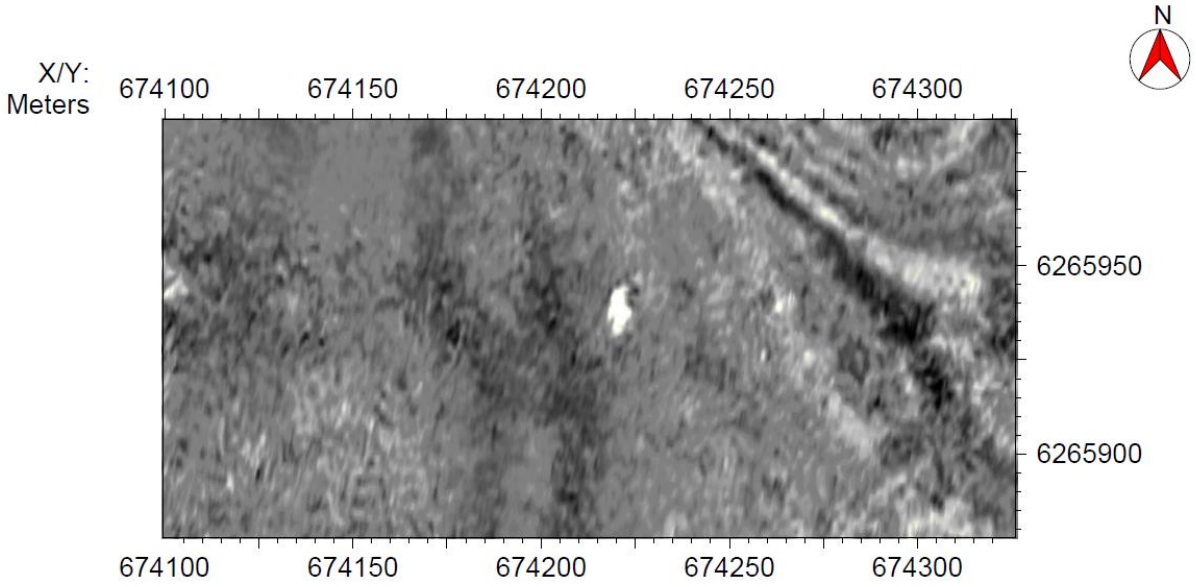

Figure 4.27: Depth slice example (41.5 m MSL) of a point anomaly (the same as in figure above) in migrated 3D-UHR data.

4.4.3 Buried Channels

Horizon H11 is a negative reflector that forms the base of channels in the upper part of Unit D. The H11 channels are predominantly present in the eastern part of the OSS1 site, but one small channel feature is also observed in the western part of this site (Figure 4.9). The thicknesses of channel-fills vary and can be up to 11 m. The seismic character of the channel infill is defined by high amplitude parallel stratified reflectors. This is in contrast with the stratified seismic character from the rest of Unit D, which is generally characterised by low to medium amplitude reflectors.

The channels related to Horizon H11 are interpreted to be of a fluvial or tidal origin.

4.4.4 Faults

Faults are expected to occur in the sites associated with the Sorgenfrei–Tornquist (fault) Zone. The sub-surface architecture, changes in unit thickness and erosive contact between units within the pre-Quaternary depression may imply tectonic activity during Quaternary.

Large faults were not identified in the seismic data. They may occur at deeper levels, beyond the penetration depth of the seismic data. Faults are likely to be present in the bedrock (Unit I).

Small-scale faulting was observed in Unit D, which is possibly related to mass transport processes (see Section 4.4.6).

4.4.5 Glacial Deformation

The HOWF site have been affected by glacial processes during the Quaternary. In particular, evidence of the Weichselian ice movement can be expected (GEUS, 2020). Ice sheet advance and retreat cycles may have deformed the Weichselian and older deposit resulting in folding or thrusting. They are present in the seismic data as undulating and steeply inclined, discontinuous reflectors, respectively

In both OSS sites, locally, Unit D is slightly folded and Unit E shows wavy and steeply inclined, discontinuous reflectors (Figure 4.6), which may imply glacial deformation.

In the HOWF site, Unit E increases in thickness and the seismic character becomes more chaotic towards the south. This may be attributed to increased glacial deformation due to ice sheet advance south of the HOWF site (GEUS, 2020).

4.4.6 Mass Transport Deposits

Evidence for mass transport deposits (MTDs) was observed at multiple stratigraphic levels in Unit D in the HOWF site. These MTDs are associated with different seismic characters, which may be a result of different types of past sediment failure. One stratigraphic level of MTDs was observed in the OSS1 site, which is described below. No MTDs were observed in the OSS2 site.

Channel-like features demarcated at the base by Horizon H12 occur towards the top of Unit D. These channel-like features are present in the eastern part of the OSS1 site and reach thickness up to approximately 31 m (Figure 4.28). The seismic character of the channel infills varies from transparent to chaotic with the presence of irregular, wavy reflectors (Figure 4.13; Figure 4.29:).

To the west of Horizon H12, Unit D comprises intervals which display small faults separating (rotated) blocks of sediments with intact stratification (Figure 4.29; Figure 4.30).

Horizon H12 appears to be on the same stratigraphic level on which these small faults terminate (i.e. decollement or glide plane). These faulted areas generally display normal fault

movements, creating either horst and graben-like structures or rotated sediment blocks and transition laterally into undisturbed Unit D (i.e. parallel reflectors).

The MTDs levels in Unit D show deviating seismic characters from the dominant character (i.e. parallel layered reflectors). They are likely the result of multiple large-scale sediment failures, triggered by fault movement along the Sorgenfrei–Tornquist Zone. Temporal variation in tectonic activity during the deposition of Unit D may have influenced the stratigraphic position of MTD occurrences in the unit.

Where faulted, Unit D may have been subject to (translational) failure, resulting in blocks of undeformed Unit D bounded by faults. In case the seismic character is chaotic or transparent, sediment deformation was likely higher and past sediment failure likely represented slumps. The geotechnical behaviour of these remobilised deposits may differ from the surrounding non-mobilised Unit D.

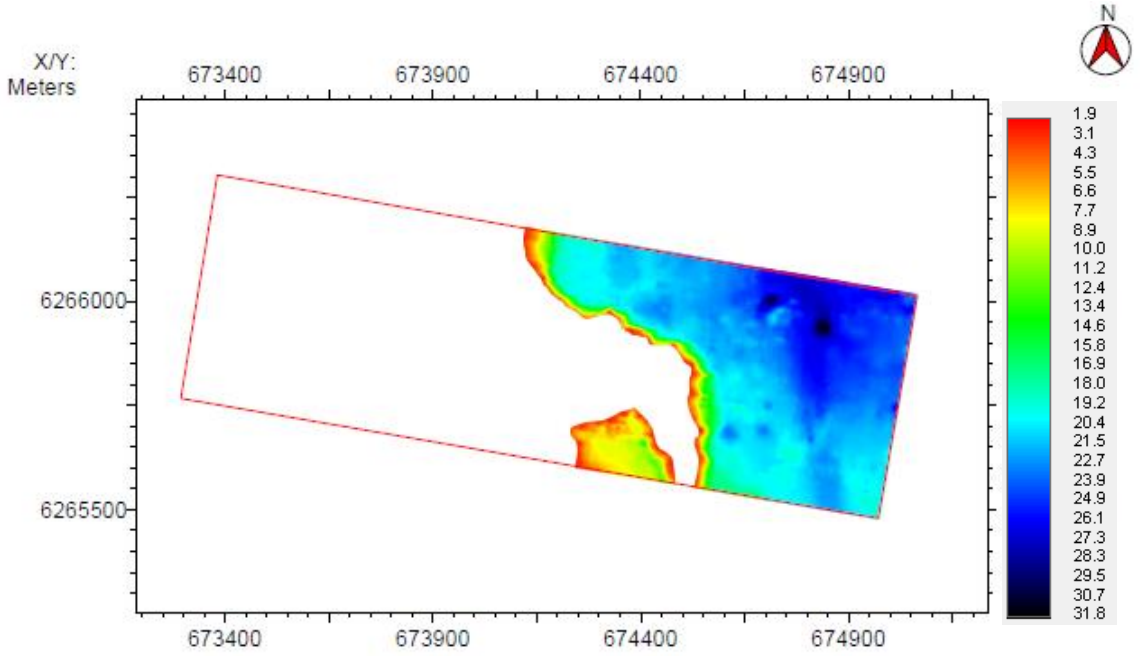

Figure 4.28: Thickness of channel-like features at H12 in metres BSF at the OSS1 site.

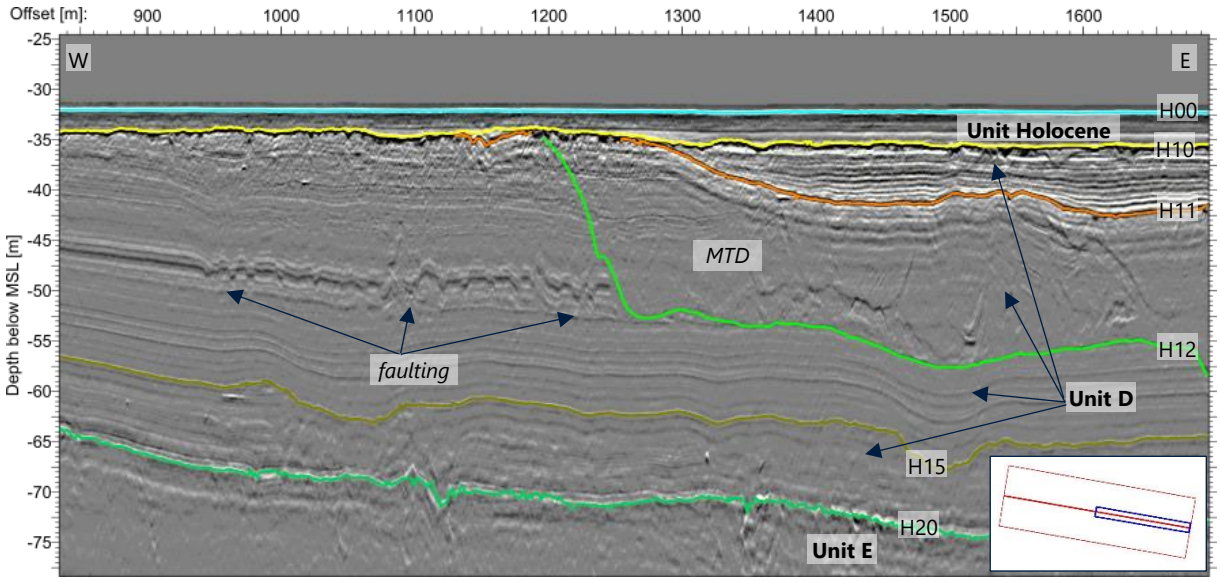

Figure 4.29: Inline 485 in OSS1. Data example of MTD and faulting in Unit D.

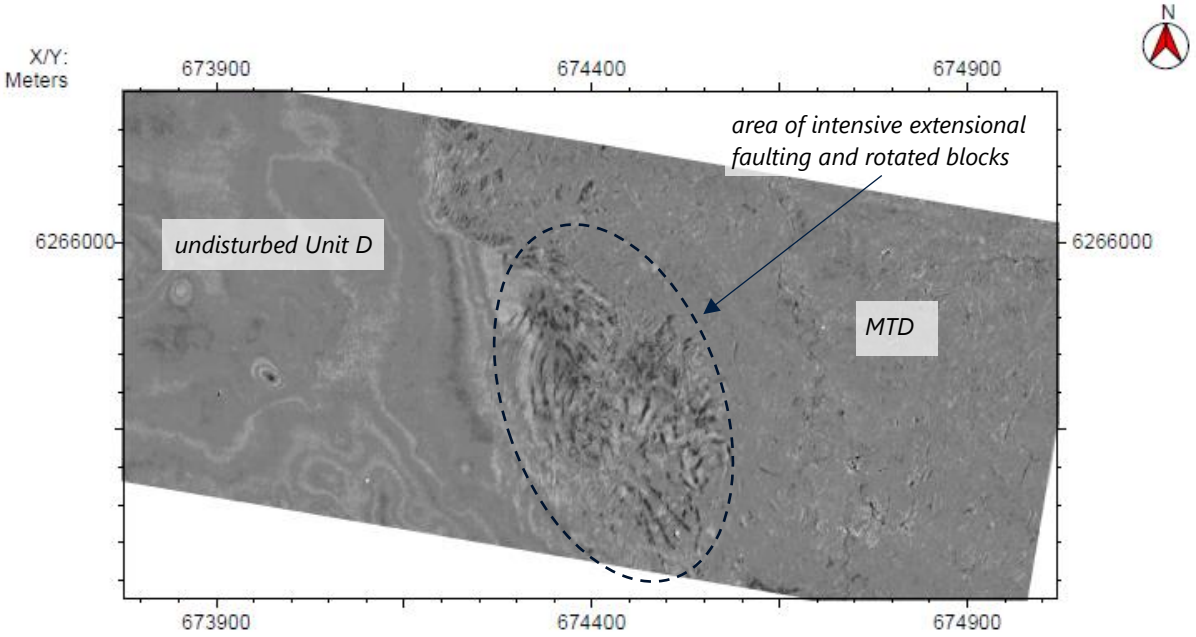

Figure 4.30: Depth slice example (49 m MSL) in the OSS1 site showing faulting and MTD in Unit D.

5. Processing and Interpretation Methodology

5.1 Data Processing

Detailed description of the processing flow applied to the 3D-UHR seismic data acquired during the survey is presented in the seismic processing report in Appendix C.

5.2 Data Interpretation

The following strategy was applied for 3D-UHR data interpretation:

- Compilation of historical geotechnical, geophysical and geological data from client-provided sources, literature and Fugro database;
- Interpretation of seismically distinct units and horizons in the time-domain applying the interpretation framework used for the 2D-UUHR data (refer to 'Geophysical Survey Report (WPA scope)' F172145-REP-GEOP-001);
- Identification and interpretation of key geological features, which can be potential hazards (geohazards) for offshore infrastructures;
- Time–depth conversion of horizons and features using a RMS velocity model based on velocity picking;
- Creation of polygons encompassing the horizon interpretation to define areas where soil units and horizons were not observed and areas where soil units and horizons were not present.
- Gridding (and contouring) of unit boundaries/horizons in metres BSF and in metres below MSL and isochore unit thicknesses in metres.

The following needs to be considered for the 3D-UHR data:

- The quality of the 3D-UHR data is good with a typical penetration depth of over 100 m BSF;
- Interpretation was initiated by manually interpreting a framework of mainlines and crosslines with approximately 10 m to 50 m distance. This was followed by applying a 3D interpolation algorithm to create a 3D horizon interpretation surface.
- Gridding of horizons was performed within IHS Kingdom Suite 2018. All gridding was done with the 'flex gridding' algorithm and parameters were kept the same among all 3D-UHR horizons. The cell size was 0.5 m by 0.5 m. The search distance was set at 0.5 m, to make sure there were no gaps in the grids. Minimum curvature was applied, and smoothness was set to halfway (6).

5.3 3D-UHR Seismic Data Quality

The acquired 3D-UHR Seismic data was QC'd onboard on a line by line basis. Observer and Navigation logs were checked after acquisition and any problems noted and/or rectified.

A vertical resolution of at least 0.3 m was achieved and a typical penetration of more than 100 m BSF, which is better than the technical requirements of 60 m BSF (Energinet, 2020). The vertical resolution and penetration is generally better in the OSS1 site compared to the OSS2 site. This is due to the presence of significantly more Late Glacial clays (Unit D) at the OSS1 site and more glacially deformed deposits at the OSS2 site (Unit E).

The on-board quality control consisted of the following processes:

5.3.1 Shot gathers display

Shot gathers were checked during acquisition to identify problems in the data such as bad/dead channels, faulty streamers, to analyse noise levels, identify potential noise sources and check offsets (Figure 5.1).

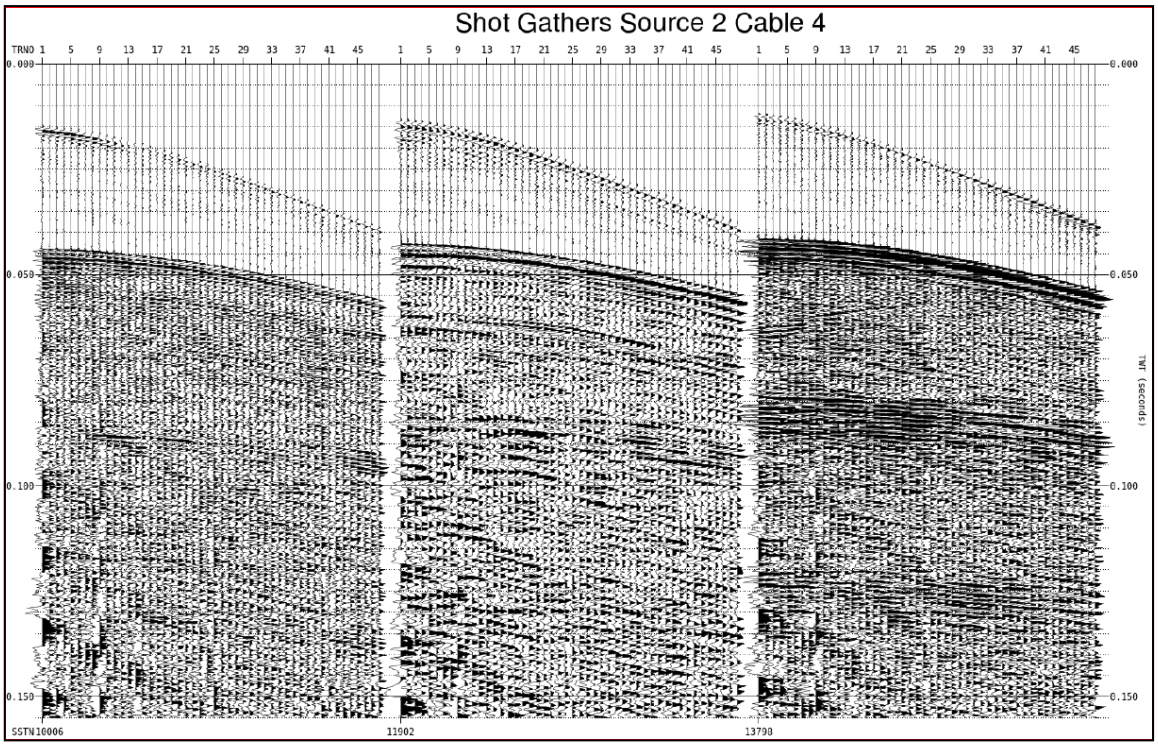

Figure 5.1: Shot gather display from EOL QC .pdf

5.3.2 Near Trace Gathers

Near trace gathers were generated to control the source-receiver offset along the line and to assess the presence of bad shots and recording system problems Figure 5.2.

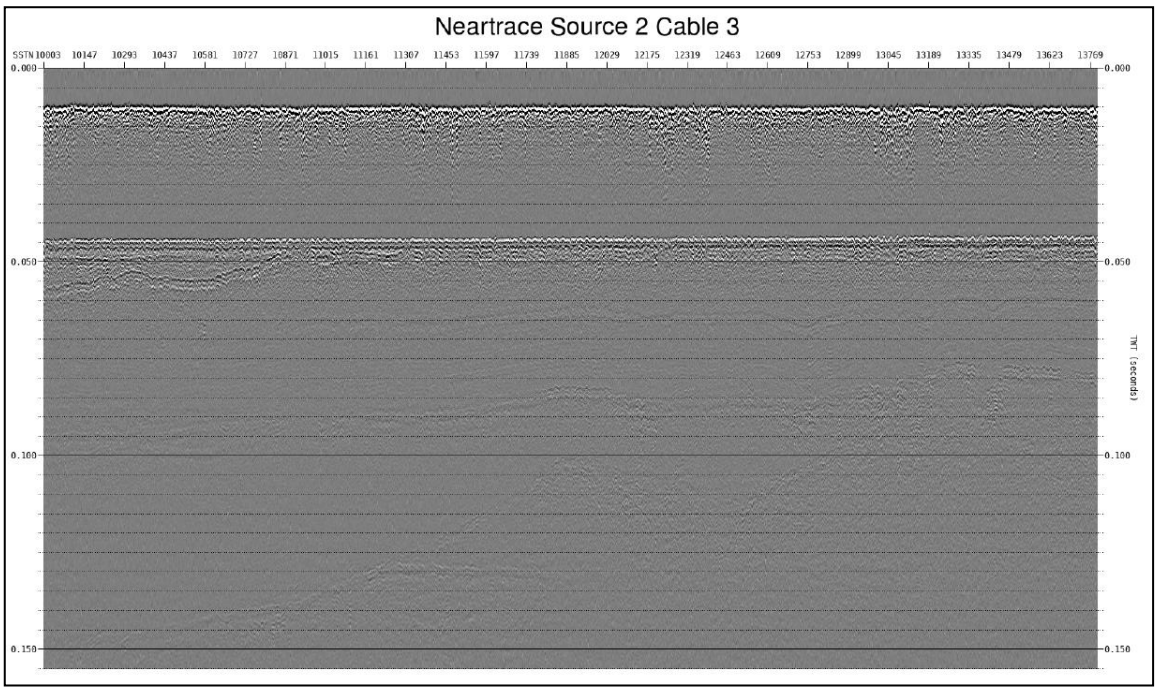

Figure 5.2: Near Trace Gather used for data QC.

5.3.3 Brute Stacks

Brute stacks were generated for assessing the data a quality and noise levels.

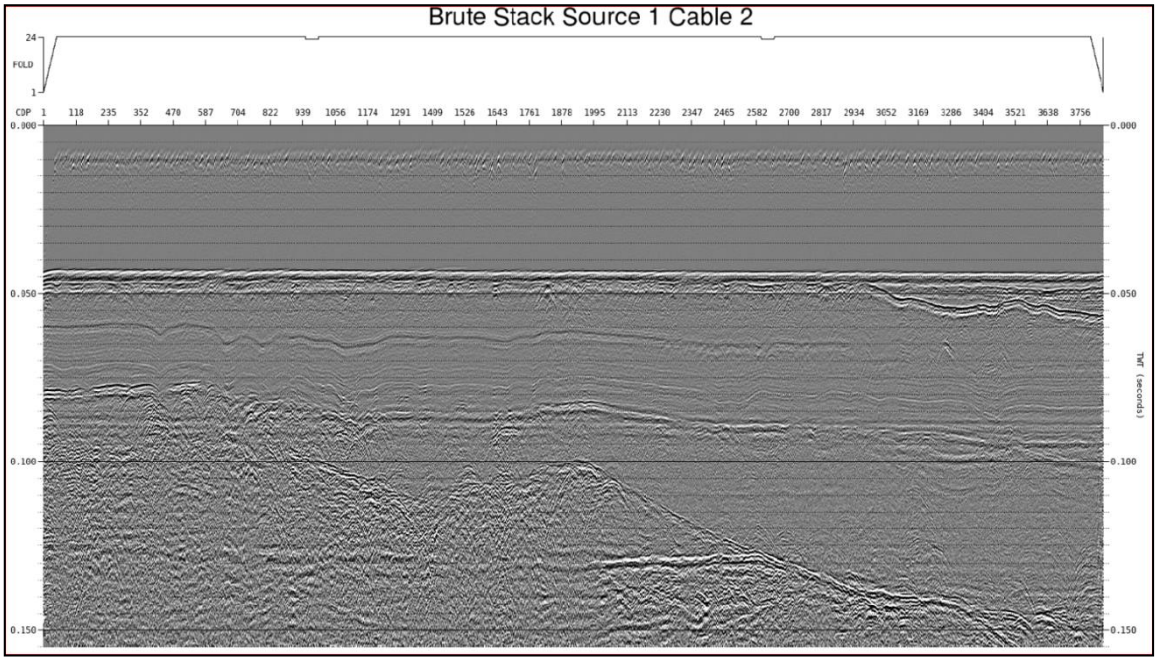

Figure 5.3: Brute Stack.

5.3.4 Noise Plots

The noise plots are based on RMS amplitude analysis within two time windows on recorded shots. Each shot is stacked to produce one trace per shot display of the RMS amplitude along

the entire line. The signal RMS amplitude plots are calculated using a parabolic time window starting at the sea bed to include the primary signal down to include the first water bottom multiple (Figure 5.4). For this survey this time window was set at 30ms in length. The noise RMS amplitude plots are based on a time window at the bottom of the shot record. For this survey the top of the analysis window was set at 110ms across the shot record, and the bottom of the analysis window was set at 150ms across the shot record (Figure 5.5).

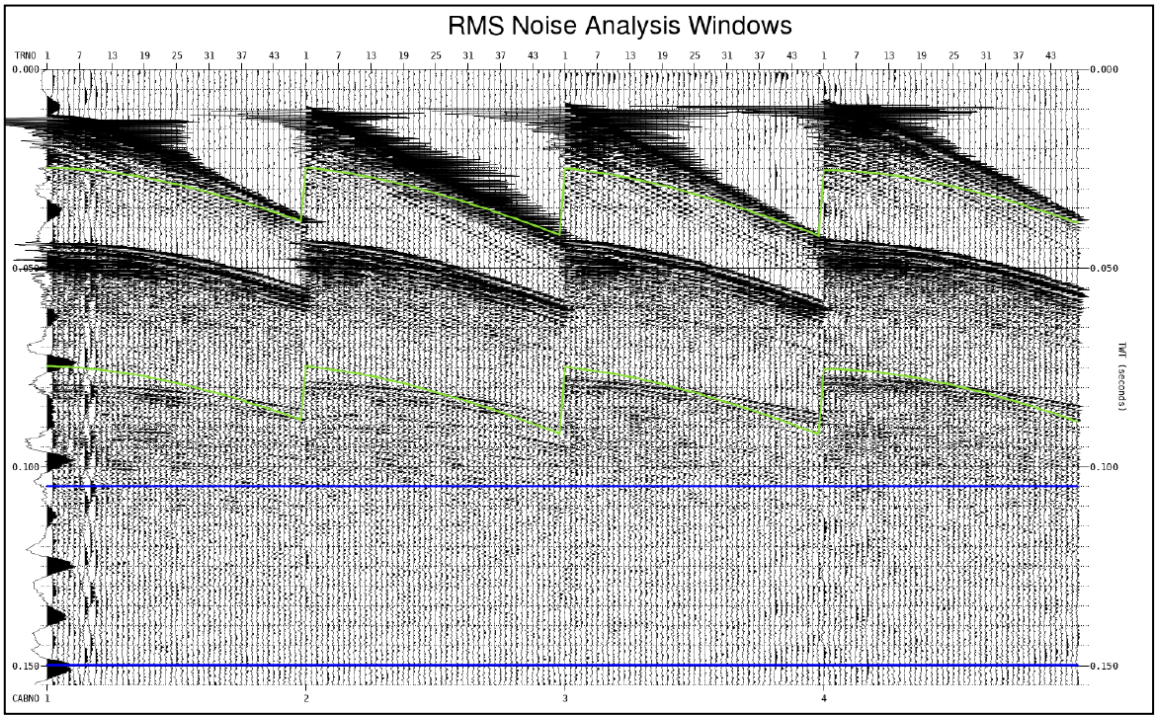

Figure 5.4: RMS Noise Analysis Windows for signal and noise analysis. Signal analysis window is green and the Noise analysis window.

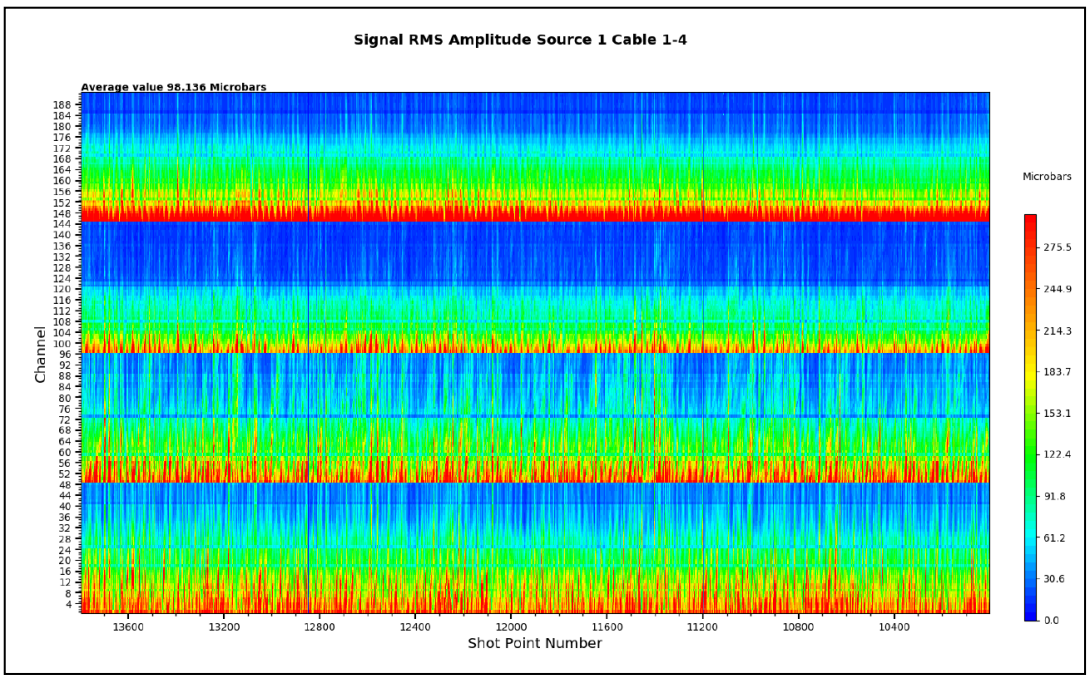

Figure 5.5: RMS Amplitude Signal Plots for the different source cable combinations (microbars). X-axis indicates shot point number, Y-axis indicates channel number. Source 1 Cable 1 to 4 is shown here.

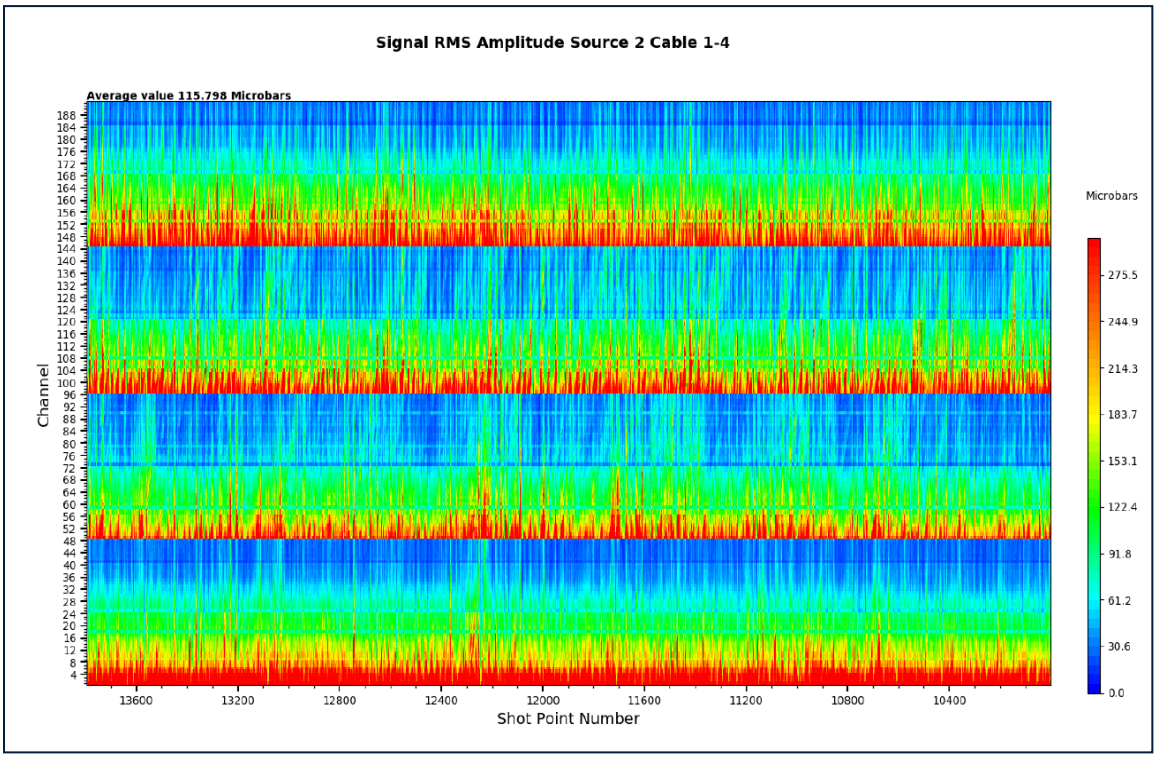

Figure 5.6: RMS Amplitude Signal Plots for the different source cable combinations (microbars). X-axis indicates shot point number, Y-axis indicates channel number. Source 2 Cable 1 to 4 is shown here.

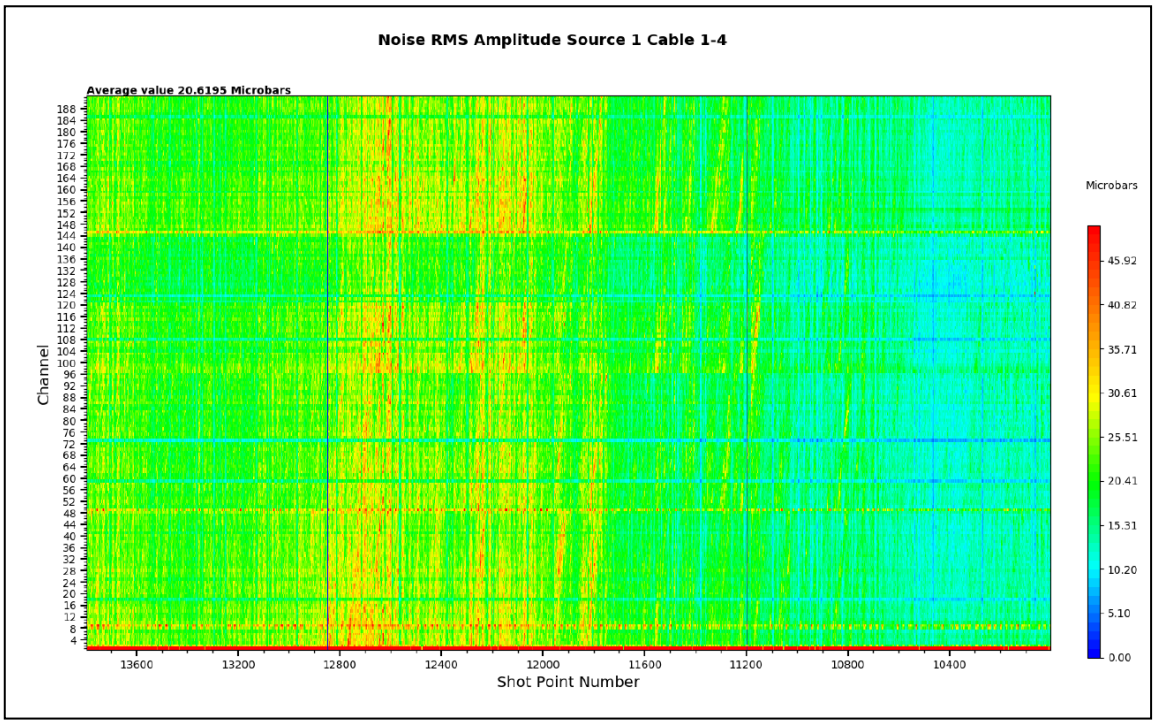

Figure 5.7: RMS Amplitude Signal Plots for the different source cable combinations (microbars). X-axis indicates shot point number, Y-axis indicates channel number. Source 1 Cable 1 to 4 is shown here.

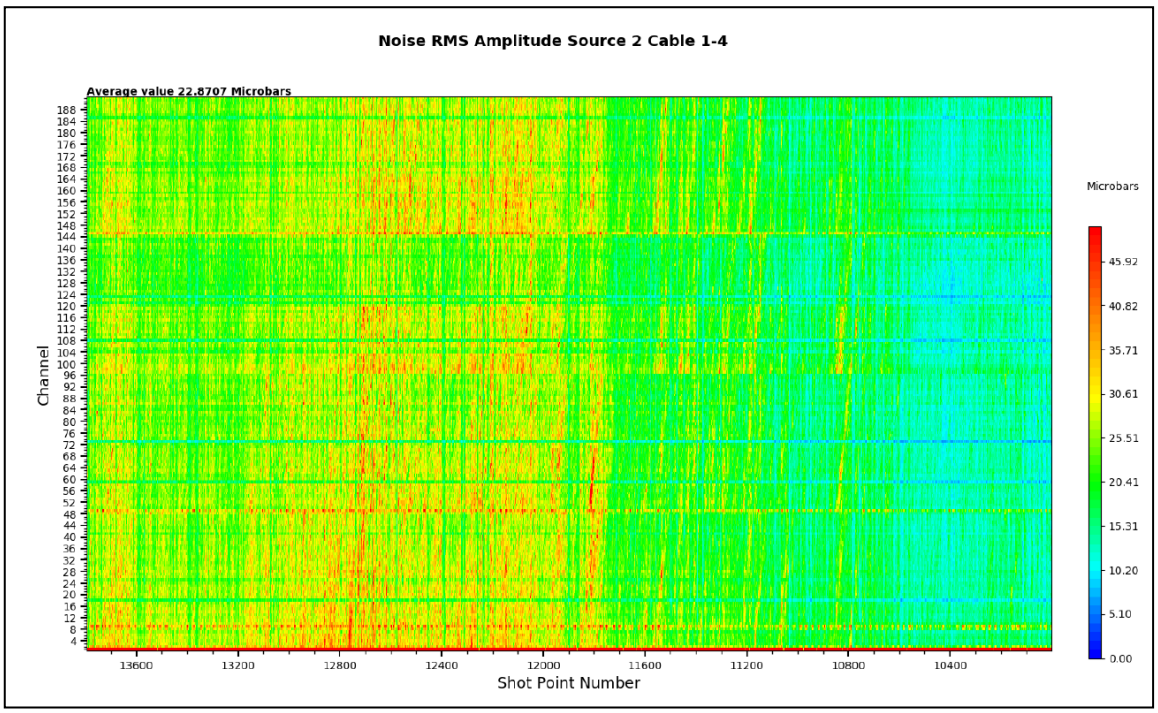

Figure 5.8: RMS Amplitude Signal Plots for the different source cable combinations (microbars). X-axis indicates shot point number, Y-axis indicates channel number. Source 2 Cable 1 to 4 is shown here.

5.3.5 Start-End of line Noise Plots

The Start-End of line (SOL) noise plots are generated using ten consecutive noise records at the start and end of each line. The RMS amplitude analysis is done for each of the ten noise files, each noise file being stacked to give one trace per file. See Figure 5.9 for an example of a Start of Line Noise file. The noise plots generated from the noise files collected at SOL and End of Line (EOL) were used to assess the noise levels in acquisition due to the effects weather conditions (sea state) and are used in conjunction with the seismic data to assess the threshold at which acquisition should stop.

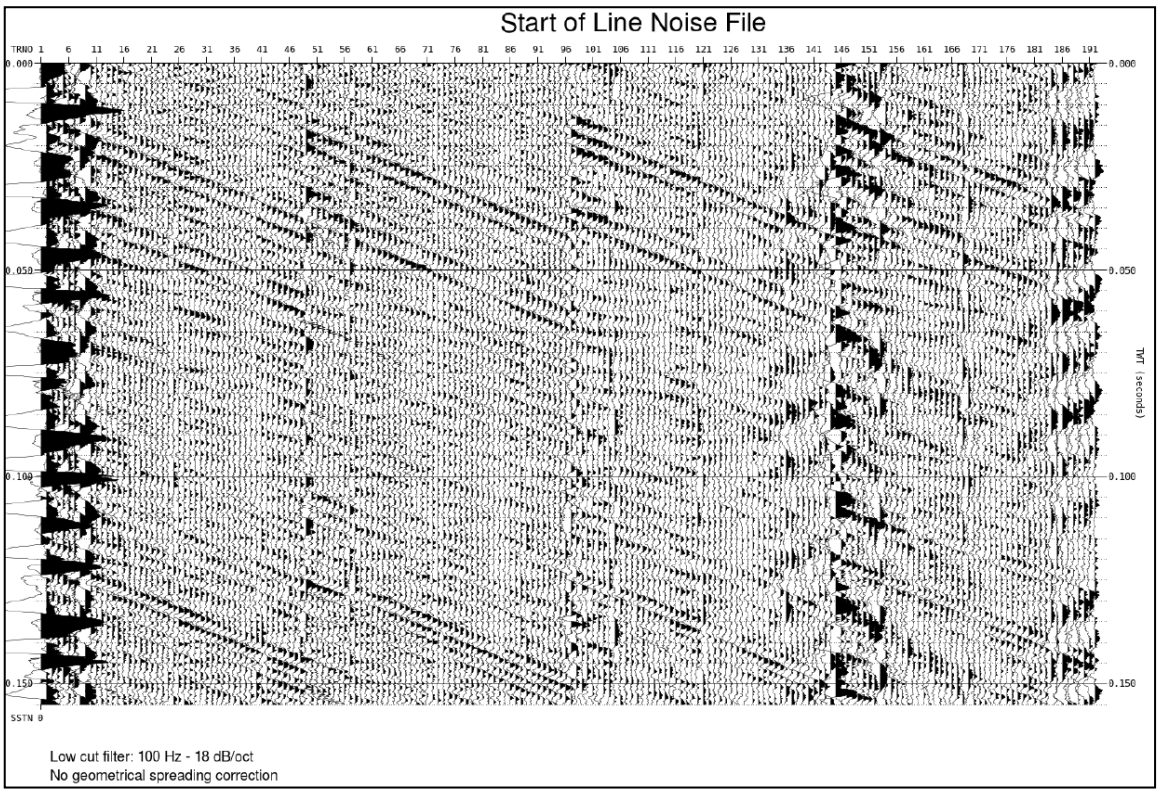

Figure 5.9: Start-End of line Noise File.

5.3.6 Navigation comparison

After navigation merge, the near (channel 1), mid (channels 12 and 24) and far (channel 48) offsets direct arrival times were calculated from the navigation P190 files and compared with the direct arrival picked offsets on the data to check consistency and ensure offset stability (Figure 5.10).

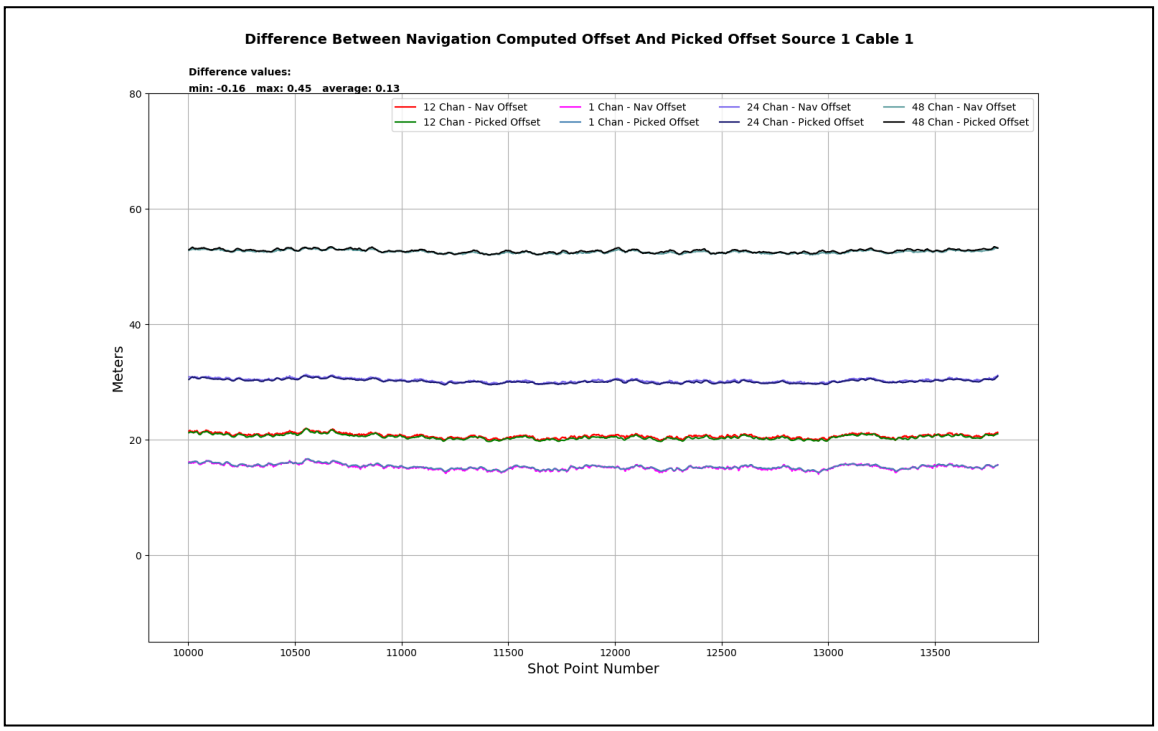

Figure 5.10: Comparison between navigation calculated and direct arrival picked offset.

5.3.7 Navigation, Coverage and Feather Angle Quality Control

Navigation quality control was made using VBA Proc and the feather angle quality control was made using the end of line plots generated by Starfix NG, see Figure 5.12. Coverage was monitored using CoverPoint with Surveyors steering to the un-flexed bin grid to ensure the best coverage and infill designed based on the flexed bin grid coverage (Figure 5.11).

Rerun or infill was decided when the acquired lines were out of specification, the coverage did not meet requirements or data quality was sub-standard.

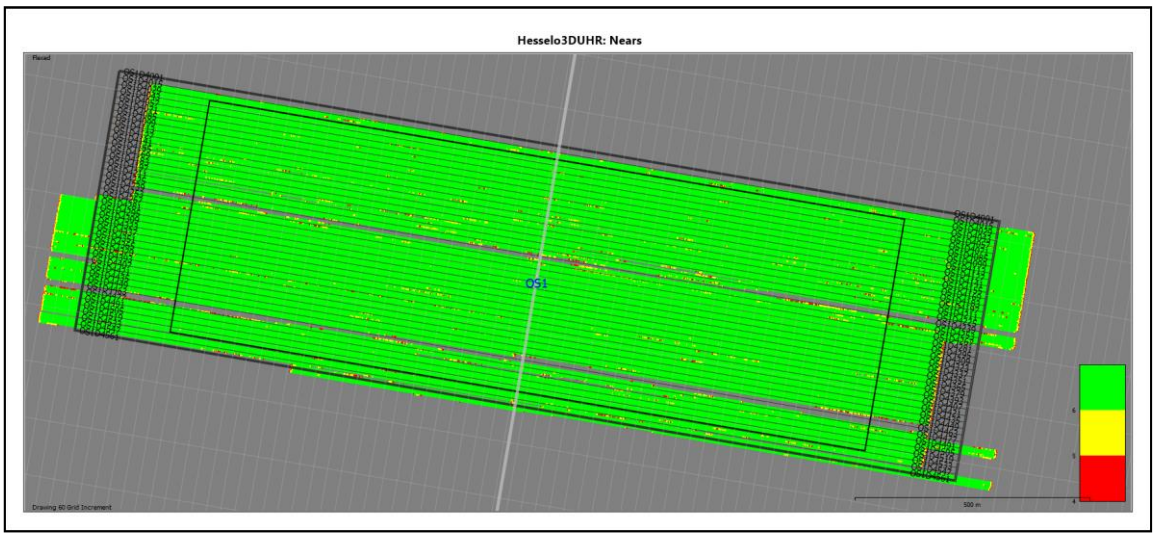

Figure 5.11: Coverage as seen on CoverPoint.

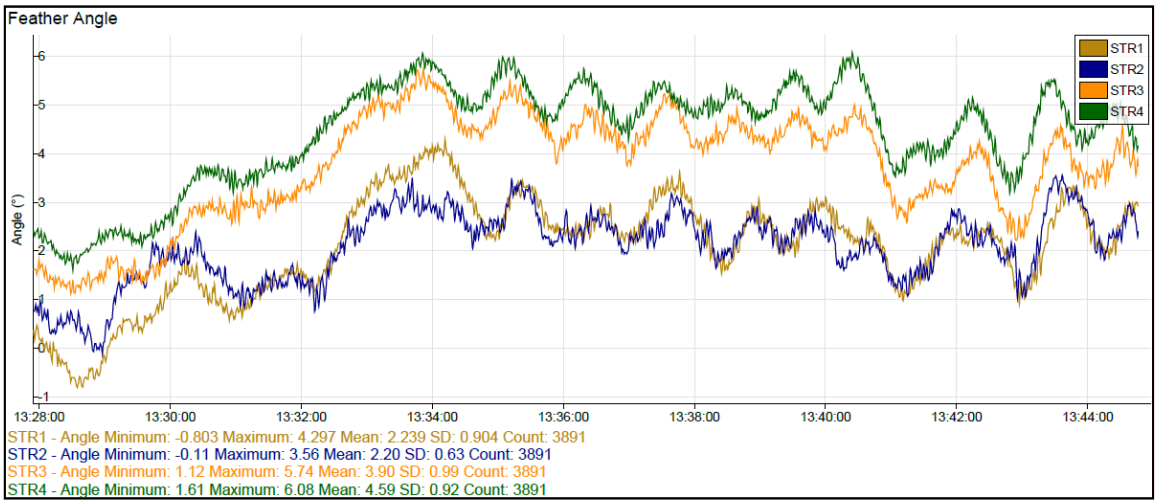

Figure 5.12: Feather Angle plot for quality control.

6. References

Andersen, S. (1998). Israndslinier i Norden. Nordic Council of Ministers.

Andrén, T., Jorgensen, B.B., Cotterill, C. and Green, S. (2015a). IODP expedition 347: Baltic Sea basin paleoenvironment and biosphere. Scientific Drilling, 20, 1-12.

Andrén, T., Jorgensen, B.B., Cotterill, C., Green, S. and the Expedition 347 Scientists (2015b). Expedition 347 summary, Proceedings of the Integrated Ocean Drilling Program, Volume 347.

Bendixen, C., Jensen, J.B., Boldreel, L.O., Clausen, O.R., Bennike, O., Seidenkrantz, M.-S., Nyberg, J., and Hübscher, C. (2015). *The Holocene Great Belt connection to the southern Kattegat, Scandinavia: Ancylus Lake drainage and Early Littorina Sea transgression*. Boreas 46(1), 53-68. https://doi.org/10.1111/bor.12154

Bendixen, C., Boldreel, L.O., Jensen, J.B., Bennike, O., Hübscher, C., and Clausen, O.R. (2017). *Early Holocene estuary development of the Hesselø Bay area, southern Kattegat, Denmark and its implication for Ancylus Lake drainage*. Geo-Marine Letters 37, 579-591. https://doi.org/10.1007/s00367-017-0513-7

Erlström, M., and Sivhed, U. (2001). *Intra-cratonic dextral transtension and inversion of the southern Kattegat on the southwest margin of Baltica – Seismostratigraphy and structural development*. Sverige Geologiska Undersökning. Research Paper C 832.

Energinet. (2020). Geophysical survey, Hesselø offshore wind farm – Scope of Services – Enclosure 1 - Technical requirements, Document No. 20/03856-4, dated 01 July 2020.

Gardline, (2021). Preliminary borehole logs (PDF format) of four (4) locations within the HOWF site. Provided by Energinet to Fugro on 10 June 2021.

GEUS. (2020). *General geology of southern Kattegat; the Hesselø wind farm area; Desk Study*. GEUS Rapport 2020/53.

Houmark-Nielsen, M., and Kjær, K.H. (2003). *Southwest Scandinavia, 40–15 kyr BP: palaeogeography and environmental change*. Journal of Quaternary Science 18(8), 169-186. https://doi.org/10.1002/jqs.802

Jensen, P., Aagaard, I., Burke Jr., R.A., Dando, P.R., Jorgensen, N.O., Kuijpers, A., Laier, T., O'Hara, S.C.M. and Schmaljohann, R. (1992). 'Bubbling reefs' in the Kattegat: Submarine landscapes of carbonate-cemented rocks support a diverse ecosystem at methane seeps. Marine Ecology Progress Series, V. 83, P. 103-112.

Jensen, J.B., Petersen, K.S., Konradi, P., Kuijpers, A., Bennike, O., Lemke, W., and Endler, R. (2002). *Neotectonics, sea level changes and biological evolution in the Fennoscandian Border Zone of the southern Kattegat Sea*. Boreas 31(2), 133-150. https://doi.org/10.1111/j.1502-3885.2002.tb01062.x

Larsen, N.K., Knudsen, K.L., Krohn, C.F., Kronborg, C., Murray, A.S., and Nielsen, O.B. (2009). Late Quaternary ice sheet, lake and sea history of southwest Scandinavia – a synthesis. Boreas 38(4), 732-761. https://doi.org/10.1111/j.1502-3885.2009.00101.x

Appendices

Appendix A

Guidelines on Use of Report

This report (the "Report") was prepared as part of the services (the "Services") provided by Fugro for its client (the "Client") and in accordance with the terms of the relevant contract between the two parties (the Contract"). The Services were performed by Fugro in accordance with the obligations in the Contract and based on requirements of the Client set out in the Contract or otherwise made known by the Client to Fugro and any other information affecting the Services at the time; save that the extent to which Fugro relied on Client or third party information in carrying out the Services was set out in the Contract.

Fugro's obligations and liabilities to the Client or any other party in respect of the Services and this Report are limited to the extent and for the time period set out in the Contract (or in the absence of any express provision in the Contract as implied by the law of the Contract) and Fugro provides no other representation or warranty whether express or implied, in relation to the Services, or for the use of this Report, for any other purpose. Furthermore, Fugro has no obligation to update or revise this Report based on any future changes in conditions or information which emerge following issue of this Report unless expressly required by the provisions of the Contract.

The Services were performed by Fugro exclusively for the Client and any other party expressly identified in the Contract, and any use and/or reliance on the Report or the Services for purposes not expressly stated in the Contract, will be at the Client's sole risk. Any other party seeking to rely on this Report does so wholly at its own and sole risk and Fugro accepts no liability whatsoever for any such use and/or reliance.

Appendix B

Charts

Charts (detailed below) have been presented as a separate PDF file.

Chart Type	Chart Name
3D-UHR TRACK POSITION (COMMON DEPTH POINT)	SN2020_031_Hesselo_OWF_01_NU_50k_OVERVIEW
3D-UHR TRACK POSITION (COMMON DEPTH POINT) AT OSS1 LOCATION	SN2020_031_Hesselo_OWF_02_NU_2'5k_TRK_3DUHR_OSS1
3D-UHR TRACK POSITION (COMMON DEPTH POINT) AT OSS2 LOCATION	SN2020_031_Hesselo_OWF_03_NU_2'5k_TRK_3DUHR_OSS2
DEPTH TO HORIZON H10 (METRES BSF & MSL) - BASE OF UNIT HOLOCENE - OSS1	SN2020_031_Hesselo_OWF_04_NU_2'5k_SBG_DEPTH_BSF_MSL_H10_OSS1
DEPTH TO HORIZON H15 (METRES BSF & MSL) - INTERNAL HORIZON IN UNIT D - OSS1	SN2020_031_Hesselo_OWF_05_NU_2'5k_SBG_DEPTH_BSF_MSL_H15_OSS1
DEPTH TO HORIZON H20 (METRES BSF & MSL) - BASE OF UNIT D (OSS1)	SN2020_031_Hesselo_OWF_06_NU_2'5k_SBG_DEPTH_BSF_MSL_H20_OSS1
DEPTH TO HORIZON H25 (METRES BSF & MSL) - BASE OF UNIT E (OSS1)	SN2020_031_Hesselo_OWF_07_NU_2'5k_SBG_DEPTH_BSF_MSL_H25_OSS1
DEPTH TO HORIZON H50 (METRES BSF & MSL) - BASE OF UNIT H (OSS1)	SN2020_031_Hesselo_OWF_08_NU_2'5k_SBG_DEPTH_BSF_MSL_H50_OSS1
THICKNESS UNIT HOLOCENE & UNIT D (METRES)	SN2020_031_Hesselo_OWF_09_NU_2'5k_SBG_THICKNESS_UNIT_HOLOCENE_UNIT_D_OSS1
THICKNESS UNIT E & UNIT H (METRES)	SN2020_031_Hesselo_OWF_10_NU_2'5k_SBG_THICKNESS_UNIT_E_UNIT_H_OSS2
GEOLOGICAL FEATURES CHART	SN2020_031_Hesselo_OWF_11_NU_2'5k_GEOF_OSS1
DEPTH TO HORIZON H10 (METRES BSF & MSL) - BASE OF UNIT HOLOCENE - OSS2	SN2020_031_Hesselo_OWF_12_NU_2'5k_SBG_DEPTH_BSF_MSL_H10_OSS2
DEPTH TO HORIZON H20 (METRES BSF & MSL) - BASE OF UNIT D - OSS2	SN2020_031_Hesselo_OWF_13_NU_2'5k_SBG_DEPTH_BSF_MSL_H20_OSS2
DEPTH TO HORIZON H25 (METRES BSF & MSL) - BASE OF UNIT E - OSS2	SN2020_031_Hesselo_OWF_14_NU_2'5k_SBG_DEPTH_BSF_MSL_H25_OSS2
DEPTH TO HORIZON H50 (METRES BSF & MSL) - BASE OF UNIT H - OSS2	SN2020_031_Hesselo_OWF_15_NU_2'5k_SBG_DEPTH_BSF_MSL_H50_OSS2
THICKNESS UNIT HOLOCENE & UNIT D (METRES)	SN2020_031_Hesselo_OWF_16_NU_2'5k_SBG_THICKNESS_UNIT_HOLOCENE_UNIT_D_OSS2
THICKNESS UNIT E & UNIT H (METRES)	SN2020_031_Hesselo_OWF_17_NU_2'5k_SBG_THICKNESS_UNIT_E_UNIT_H_OSS2
GEOLOGICAL FEATURES CHART	SN2020_031_Hesselo_OWF_18_NU_2'5k_GEOF_OSS2

Appendix C

3D-UHR Processing Report

3D-UUHR Processing Report

Energinet Denmark Hesselø Geophysical Survey | *Denmark, Inner Danish Sea, Kattegat*

F172145-REP-PROC-002 01 | 19 April 2021
Complete

Energinet Eltransmission A/S

Document Control

Document Information

Project Title	Hesselø Offshore Wind Farm, 3D Seismic Survey
Document Title	3D-UUHR Processing Report
Fugro Project No.	F172145
Fugro Document No.	F172145-REP-PROC-002
Issue Number	01
Issue Status	Complete

Client Information

Client	Energinet Eltransmission A/S
Client Address	Tonne Kjærsvej 65, DK-7000 Fredericia, Denmark
Client Contact	Nicky Hein Witt
Client Document No.	N/A

Revision History

Issue	Date	Status	Comments on Content	Prepared By	Checked By	Approved By
01	19 Apr 2021	Complete		GS	RC	CIW

Project Team

Initials	Name	Role
MT	Maria Theander	Global Product Owner – Seismic Processing Marine Site Characterisation
PB	Patrick Burn	Operations Supervisor - Seismic Processing Marine Site Characterisation
GS	Graeme Scott	Inhouse Seismic Processing Geophysicist
IW	Iain Walby	Onboard Seismic Processing Geophysicist – Pioneer
SB	Sanket Bhattacharya	Onboard Seismic Processing Geophysicist – Pioneer
CIW	Chris Wright	Geophysical Deliverables Coordinator

Contents

Appendices

Figures

Tables

Abbreviations

3D-UUHR	Three-Dimensional Ultra Ultra High Resolution
CDP	Common Depth-point
CMP	Common Mid-Point
DGPS	Differential Global Positioning System
FTP	File Transfer Protocol
F-K	Frequency - wave number
F-X	Frequency - space domain
GPS	Global Positioning System
LNA	Linear Noise Attenuation
MLSS	Multi-Level Stacked Sparker
MSL	Mean Sea Level
NMO	Normal Move Out
PoSTM	Post-Stack Time Migration
QC	Quality Control
SFT	Secure File Transfer
SRME	Surface Related Multiple Elimination
TWTT	Two-Way Travel Time
UTM	Universal Transverse Mercator
WB_ZO	Water Bottom Zero Offset Time
X-T	Space – Time Domain
.csv	Comma Separated Values

1. Introduction

Energinet Eltransmission A/S (Energinet) is developing a new offshore wind farm in the inner Danish Sea, Kattegat, the Hesselø Offshore Windfarm (HOWF). The project area is located between Denmark and Sweden approximately 30 km North of Sjælland.

The seismic processing report aims to detail the step by step processes used to get the best imaging of the seismic data. The techniques involved aim to reduce the noise in the datasets, improve signal to noise ratios, and improve upon the acquisition brute bandwidth of the data.

1.1 Scope of Work

Fugro acquired 3D Ultra Ultra High Resolution (3D-UUHR) seismic data at the Hesselø offshore wind farm, utilising the Fugro Pioneer. The data were QC'd offshore and processed onshore, using Fugro *Uniseis* software.

The aim of this survey was to acquire and provide high quality and high resolution data of the two 3D work locations. These were both 0.5 km x 1.5 km in size. The data from the survey will assist the client to determine the water depth, seabed sediment types, seabed features, and obstructions identifying any hazards larger than 1 m in the shallow section (seabed risk assessment). A minimum target depth of 60 m penetration below the seabed was a requirement.

In general data was of high quality. Lines were assessed onboard between the QC and client to determine if a client concession could be issued for lines that were technically out of spec.

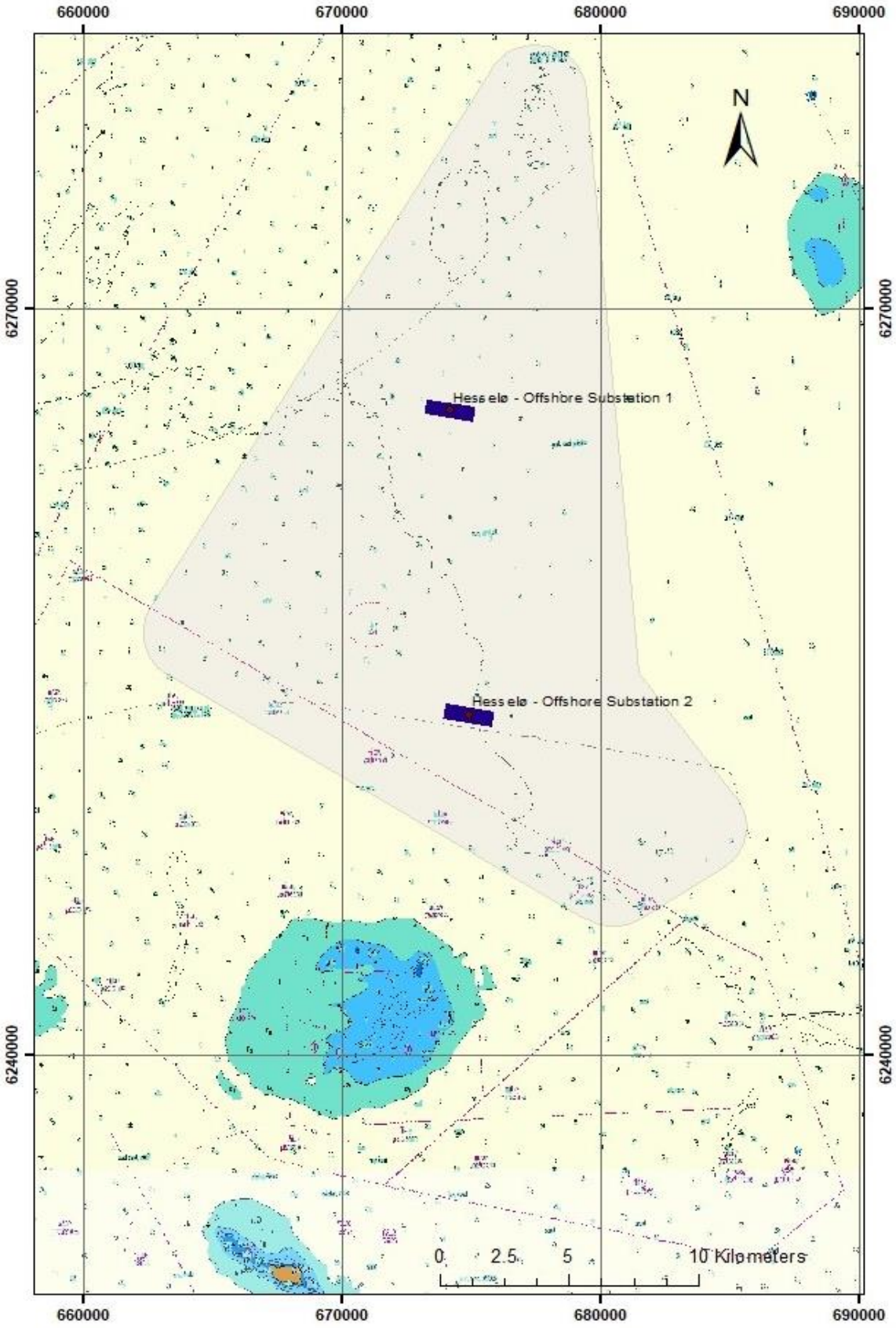

Figure 1.1: Hesselø 3D-UUHR location overview

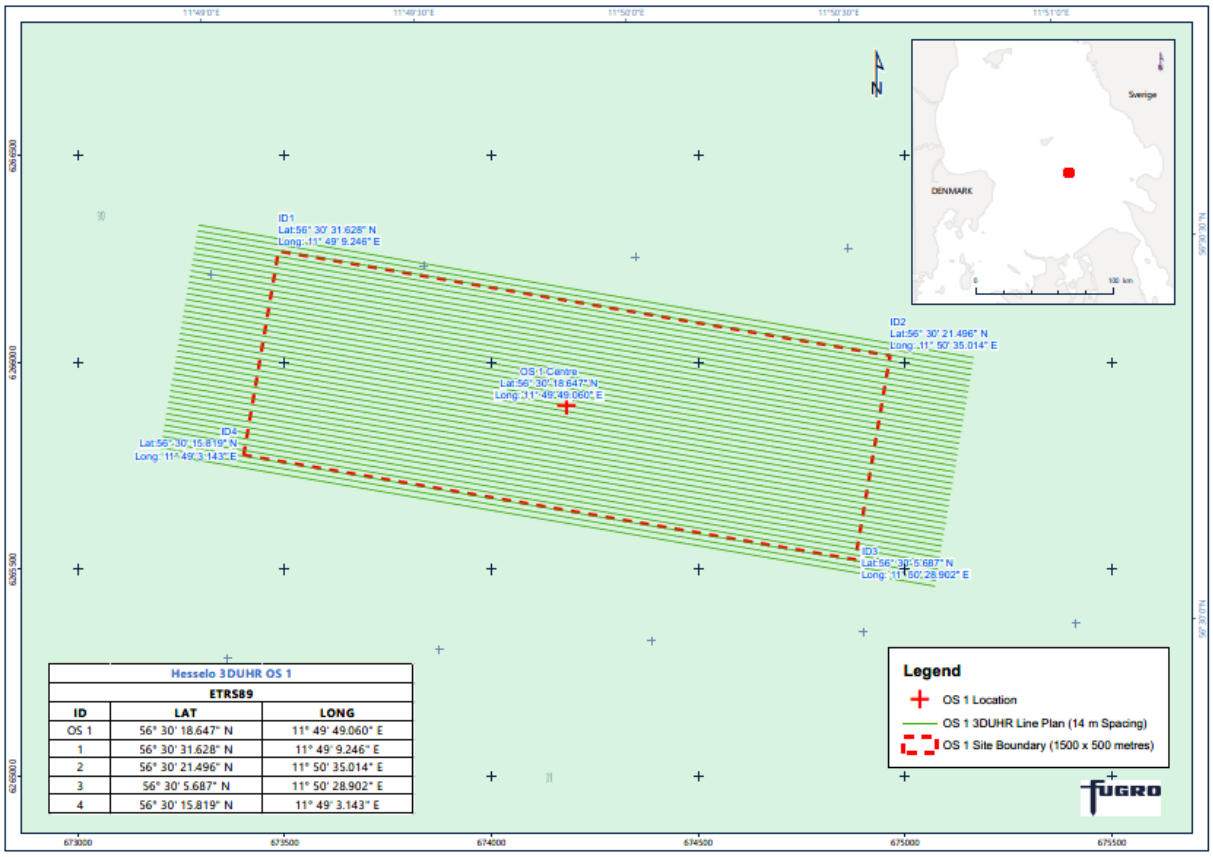

Hesselo 3DUHR OS 1		
ETRS89		
ID	LAT	LONG
OS 1	56° 30' 18.647" N	11° 49' 49.060" E
1	56° 30' 31.628" N	11° 49' 9.246" E
2	56° 30' 21.496" N	11° 50' 35.014" E
3	56° 30' 5.687" N	11° 50' 28.902" E
4	56° 30' 15.819" N	11° 49' 3.143" E

Figure 1.2: Hesselø 3D-UUHR line plan for offshore substation 1

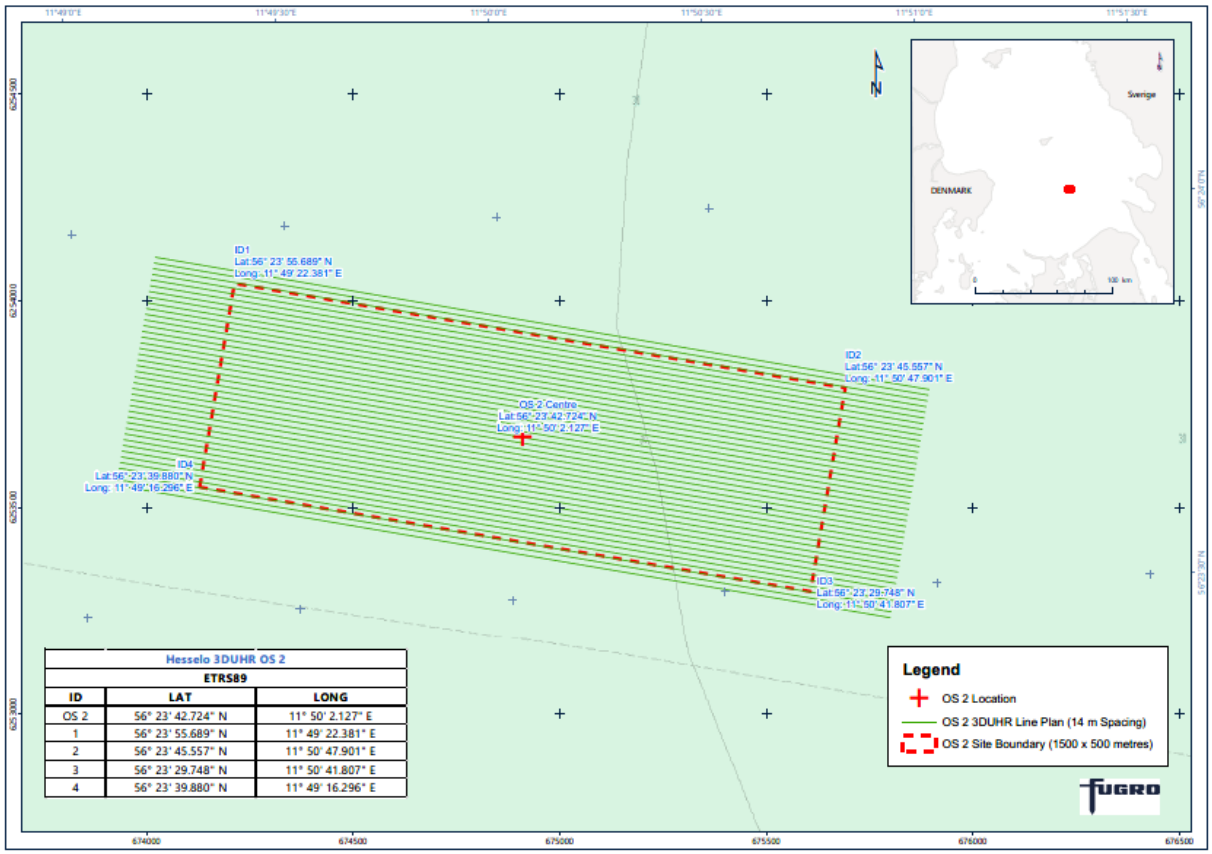

Hesselo 3DUHR OS 2		
ETRS89		
ID	LAT	LONG
OS 2	56° 23' 42.724" N	11° 50' 2.127" E
1	56° 23' 55.689" N	11° 49' 22.381" E
2	56° 23' 45.557" N	11° 50' 47.901" E
3	56° 23' 29.748" N	11° 50' 41.807" E
4	56° 23' 39.880" N	11° 49' 16.296" E

Figure 1.3: Hesselø 3D-UUHR line plan for offshore substation 2

1.2 Acquisition Configuration

Table 1.1: 3D-UUHR Acquisition parameters

Acquisition	
Source	
Type	2 x Multi Level Stacked Sparker
Power	700 Joules / 360 Tips
Shot Interval	0.5 m (1 m same sparker)
Depth	0.52, 0.67, 1.12 m
Streamer	
Model	GeoEel gel filled
Groups per cable	48 @ 1 m
Cables / Separation	4 / 8 m
Depth	1.4 m
Near Offset	~10 m
Recording System	
Model	Geode
Sample interval / Length	0.125 ms / 155.875 ms
Format	SEG-D

Table 1.2: 3D-UUHR Processing Grid Parameters Offshore Substation 1

Grid				
Corner Point 1	IL 210	XL 1200	X 673389.26	Y 6266305.31
Corner Point 2	IL 210	XL 4600	X 675064.96	Y 6266018.93
Corner Point 3	IL 760	XL 1200	X 673296.60	Y 6265763.17
Corner Point 4	IL 760	XL 4600	X 674972.31	Y 6265476.79
Datum / CM / Projection	ETRS89 / 9° E / UTM Northern Hemisphere 32 N			
Processing Bin Size Inline / Xline	1 m / 0.5 m (Acquisition at 2 m / 0.5 m)			

Table 1.3: 3D-UUHR Processing Grid Parameters Offshore Substation 2

Grid				
Corner Point 1	IL 12130	XL 6750	X 674116.61	Y 6254088.19
Corner Point 2	IL 12130	XL 10160	X 675797.24	Y 6253800.97
Corner Point 3	IL 12680	XL 6750	X 674023.96	Y 6253546.05
Corner Point 4	IL 12680	XL 10160	X 675704.59	Y 6253258.83
Datum / CM / Projection	ETRS89 / 9° E / UTM Northern Hemisphere 32 N			
Processing Bin Size Inline / Xline	1 m / 0.5 m (Acquisition at 2 m / 0.5 m)			

2. Processing 3D-UUHR

2.1 3D-UUHR Processing Summary

The agreed processing flow was applied to all the lines as follows:

- Reformat from SEG-D
- Apply recording delay correction static: 0 ms
- Apply low-cut filter: 20Hz / 18 dB/Oct
- Apply T^2 spherical divergence
- Merge seismic with source & receiver navigation, update offsets, assign 2D & 3D geometry
- Pick zero offset seabed – assign hyperbolic seabed time per channel
- Edit out bad shots / channels identified from offshore QC
- Shot domain swell noise attenuation
- Channel domain swell noise attenuation
- Receiver domain swell noise attenuation
- Temporary statics application (to aid QC – statics reassessed after final velocities)
- Linear noise attenuation
- 2D SRME
- Deghosting
- Apply tidal static correction
- Preliminary 3D statics
- 3D Velocity analysis in Pegasus: 160 m picking grid
- Final 3D statics
- Regrid to processing grid
- 3D Fourier interpolation and regularisation
- Sort to 3D CMP domain
- NMO using picked velocity
- PASTA statics application
- Outer trace final mute
- Stack using 1/N trace normalisation – 24 fold max
- Post stack Kirchhoff time migration
- Footprint removal
- Deconvolution shaping and denoise
- Zero phase filter application using data derived wavelet (positive seabed)
- Deconvolution remnant demultiple
- Surface wave noise attenuation
- Time variant bandpass filter
- FK filter, dBgain and denoise up to 100 Hz
- Apply source and receiver datum correction
- Cosmetic seabed mute
- NLMEAN timeslice image denoise
- Output to SEG-Y (trimmed to exclude low fold edges)

2.2 Reformatting and Navigation Merge

For each sequence, raw field data in SEG-D format was reformatted into *Uniseis* internal processing format. As part of the reformatting process a bulk shift is applied to the data to compensate for any delay in the recording system. The Geode recoding system has zero start of data delay, so the trace data kept the original acquired 155.875 ms record length at a sample rate of 0.125 ms. A de-bias low-cut filter of 20 Hz / 18 dB/Octave was applied to the data in order to remove low frequency noise and instrument DC bias prior to processing. A spherical divergence correction (time squared) was applied to the data to aid in QC and further processing.

A QC of the data was conducted on the vessel so that any missing shots, bad channels and noisy records that may have an adverse effect on data quality could be identified.

Geometry was assigned in order to give each trace a CMP number and source / receiver positions were merged into the seismic dataset in order to get accurate offsets and 3D locations for the data prior to velocity picking. Correct CMP locations enabled trends from nearby lines to be used in order to help with consistency and accuracy of velocity picks.

Finally, at this stage, near trace gathers were used to interactively pick a zero offset water bottom time (near trace seabed time with normal moveout applied) for use in later processing.

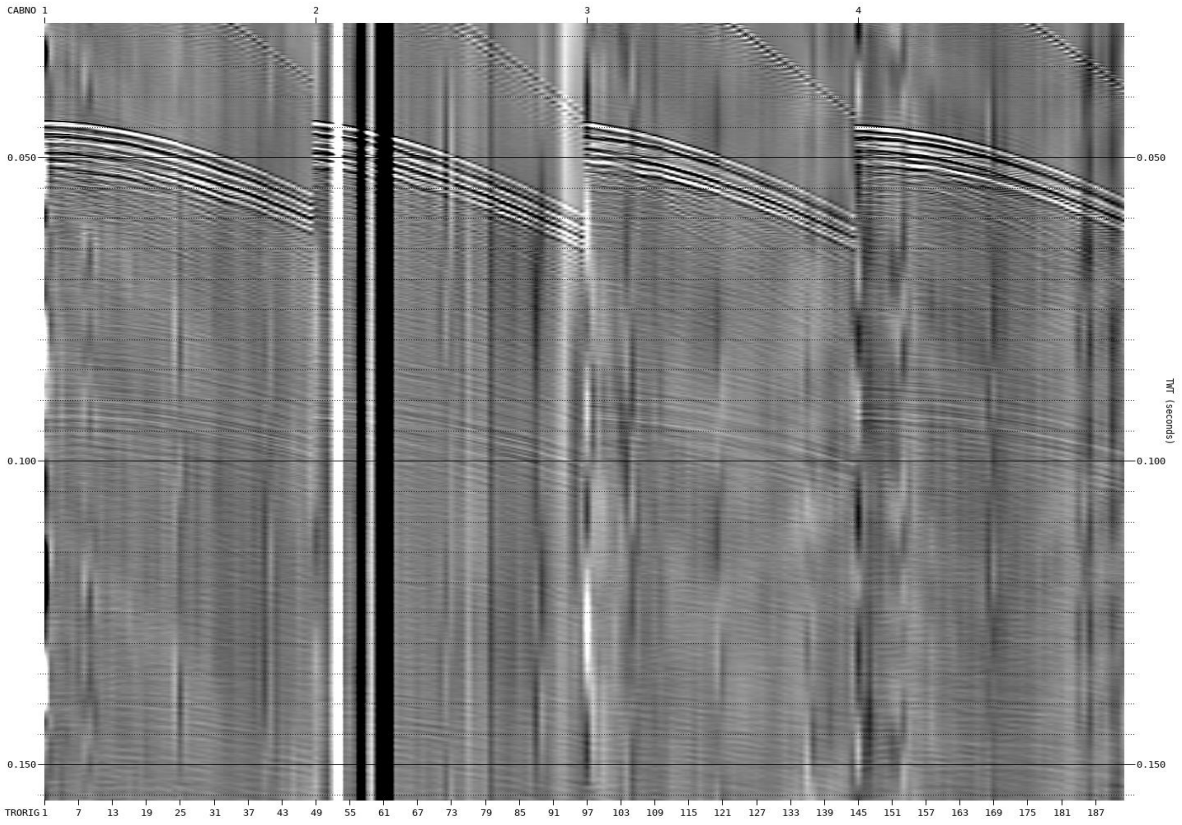

Figure 2.1: Reformat: raw shots

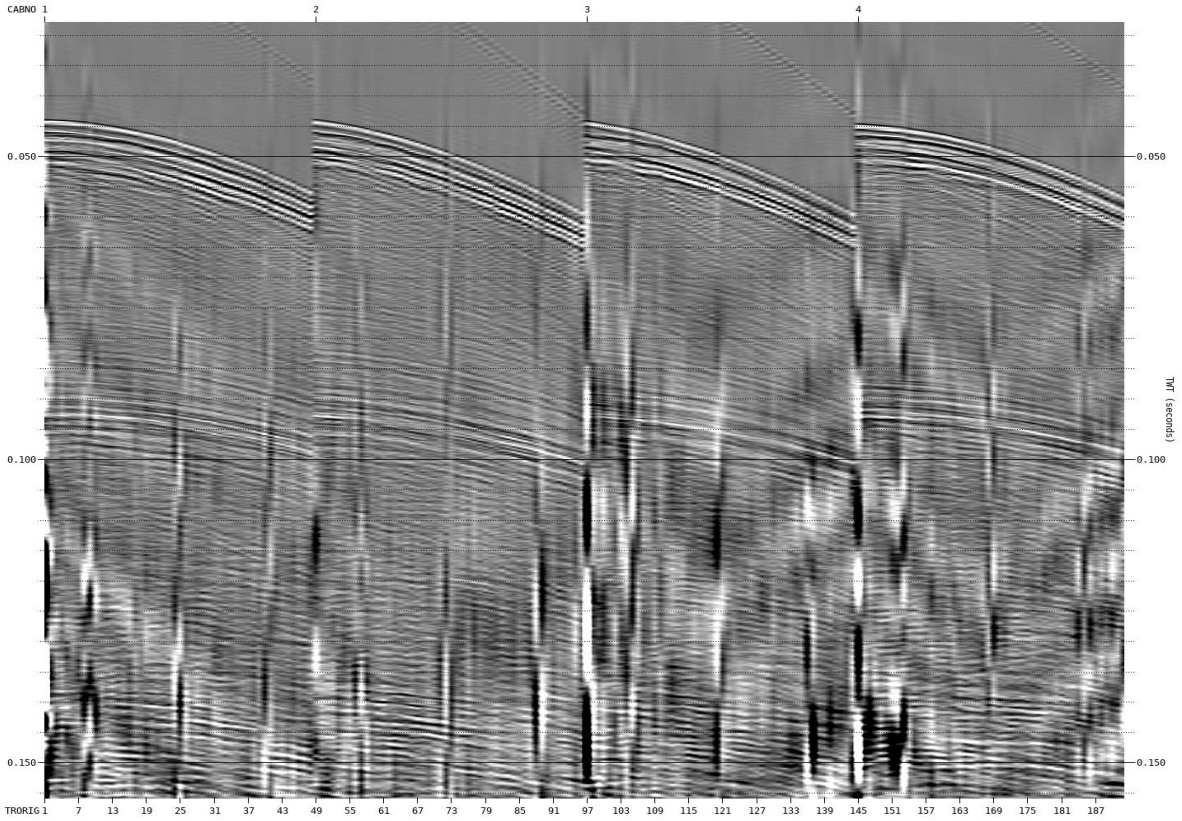

Figure 2.2: Reformat: low cut and geometrical spreading

2.3 Swell Noise Attenuation

Swell noise was effectively attenuated using the *Uniseis 'SWNA'* and *'TFDN'* tools. The *'TFDN'* algorithm makes use of the fact that, unlike an impulsive source such as a shot, the amplitude of the swell noise will not decay with time since it is being continuously generated during recording. The process decomposes the trace data into signal and noise components, down-weighting or removing the noise to leave a clean trace.

An initial pass of de-swell (*TFDN*) was applied to frequencies up to 100 Hz in the shot domain. Dip attenuation (*SWNA*) was then applied to attenuate any non-physical dips up to 100Hz below 1000 m/s apparent velocity. This was followed by a second pass of *TFDN* / *SWNA* performed in the channel domain up to 100 Hz, and a third pass of *TFDN* / *SWNA* in the receiver domain up to 150 Hz.

Higher values than 150 Hz were tested, but these did not show any improvement in swell noise attenuation, as it is predominantly a lot lower frequency than this. The maximum value of 150 Hz was based on no improvement to the denoise routine, only an increase in CPU runtime if we went any larger.

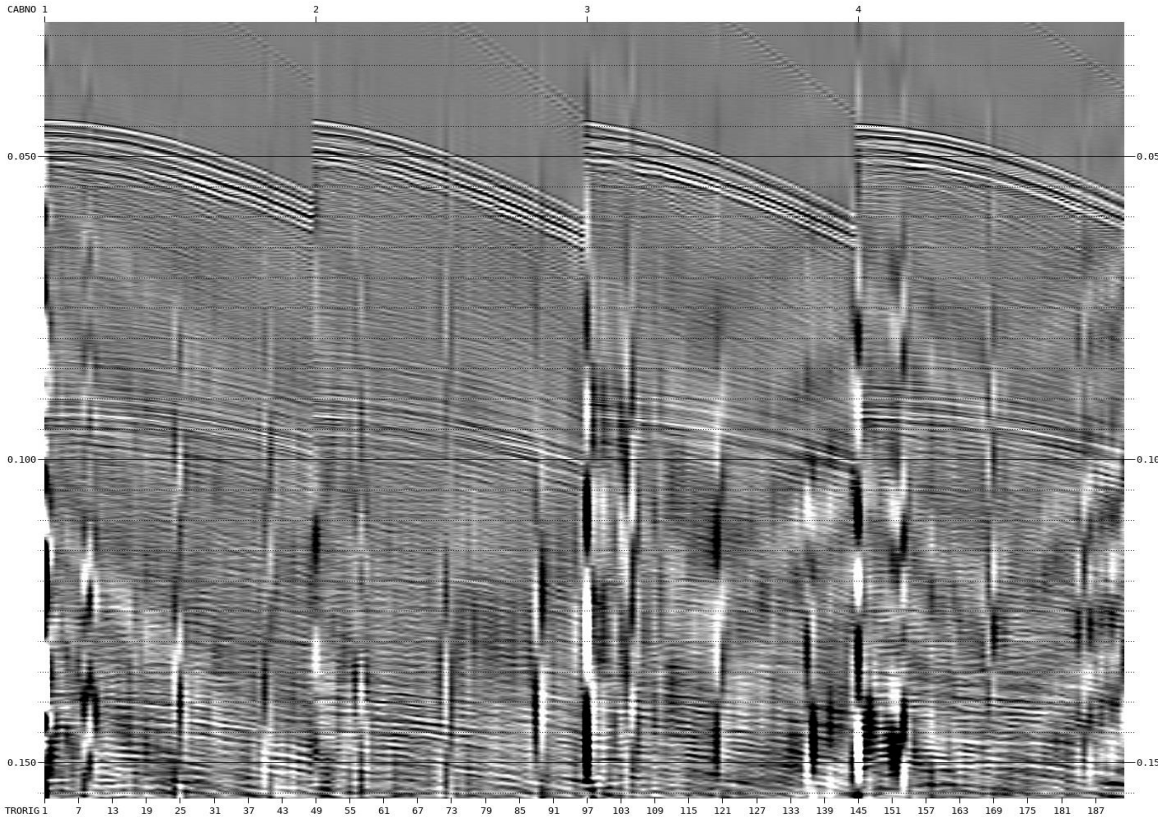

Figure 2.3: Denoise: input shots

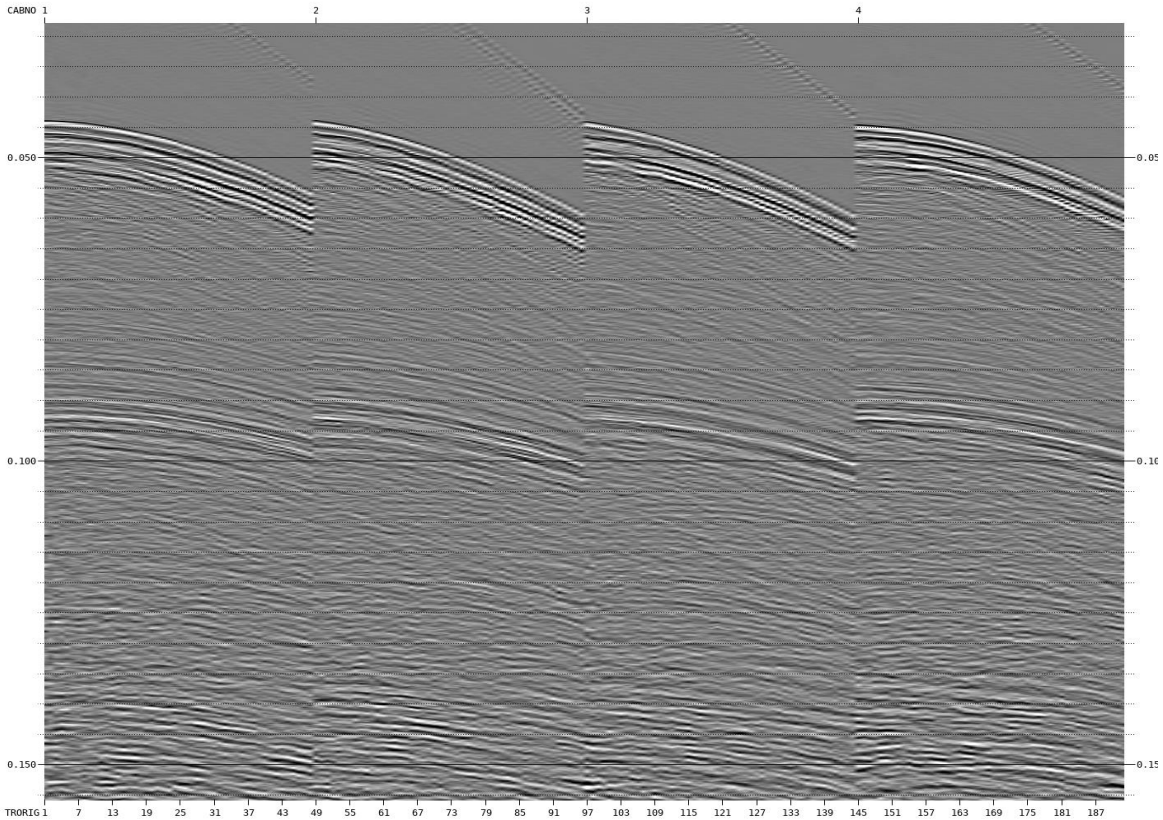

Figure 2.4: Denoise: output shots

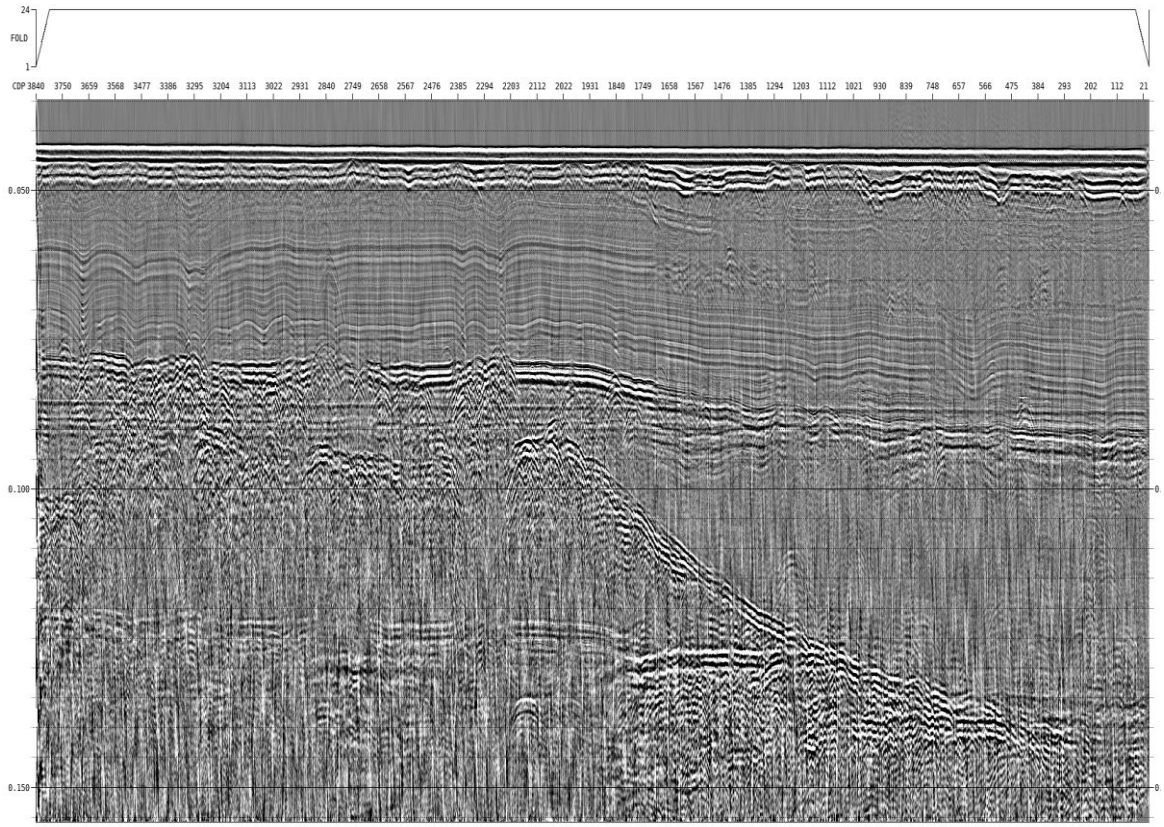

Figure 2.5: Denoise: input stack

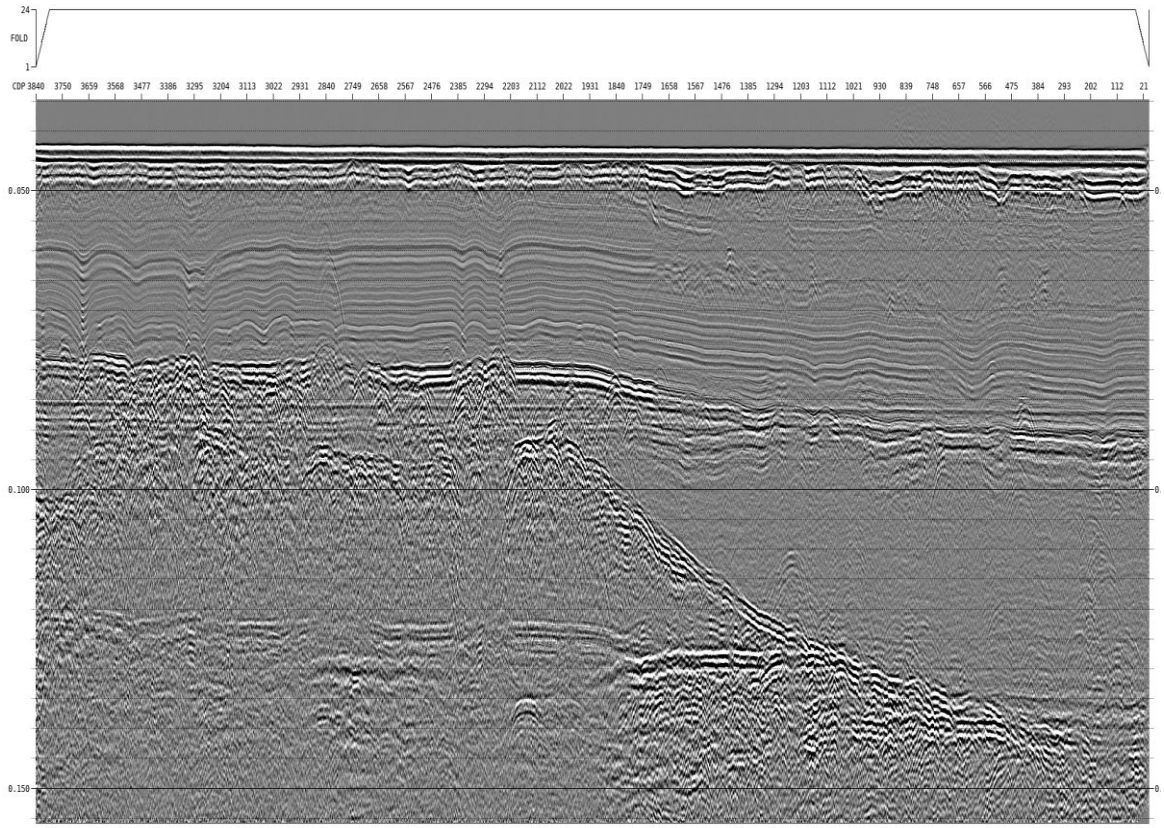

Figure 2.6: Denoise: output stack

2.4 Preliminary Shot Statics

Due to the fine sampling rate, shot statics were a large factor in the resolution of the shallow section of the data. It was important at this stage, once data was relatively free of low frequency swell noise, to apply some preliminary shot statics to aid the QC of some of these further processes. It is particularly useful to have shot statics applied prior to deghosting as it is difficult with this resolution of data to identify what the process is doing if shot statics are still predominant.

To achieve this, a provisional shot statics computation was ran using the *Uniseis* module *'NEPTUNE'*. This is ran on NMO corrected CMPs, creating a pilot trace for each CMP using a weighted mix of local stacked traces. Cross-correlations of the pilot trace with the traces in its respective CMP gather are used to assess the static, and this is ran in multiple iterations. With each iteration, the static computed is applied and the pilot trace is correspondingly updated. This run focused solely on the shot static which is a short period effect that locally damages the stack. 5 iterations were chosen, as there was a slight uplift from 3 iterations. Any more than 5 iterations were where the static had already converged to the accepted value and would only unnecessarily increase the runtime.

Later in the processing, once the data is deghosted and velocities are picked, we rerun this computation in 3D (essential before interpolation) and add in a final component to correct for the streamer depth static using the module *'PASTA'*.

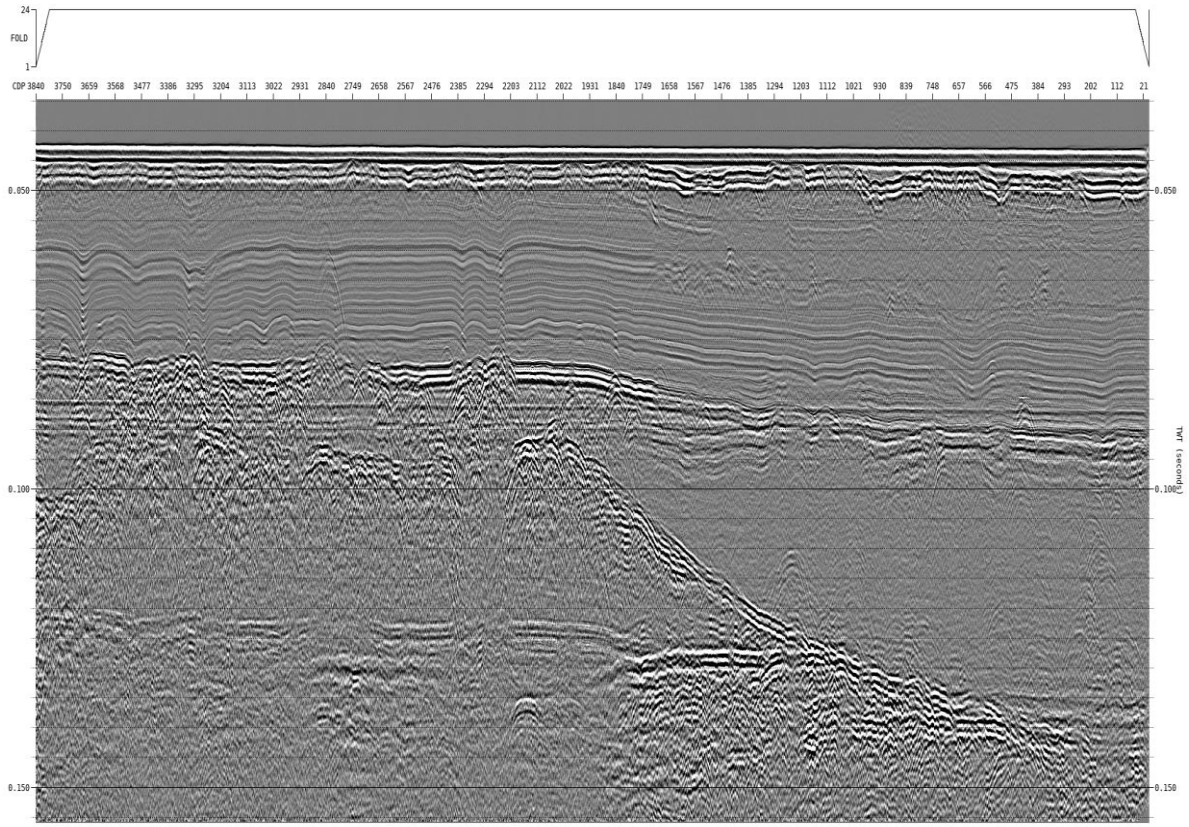

Figure 2.7: Preliminary shot statics: input stack

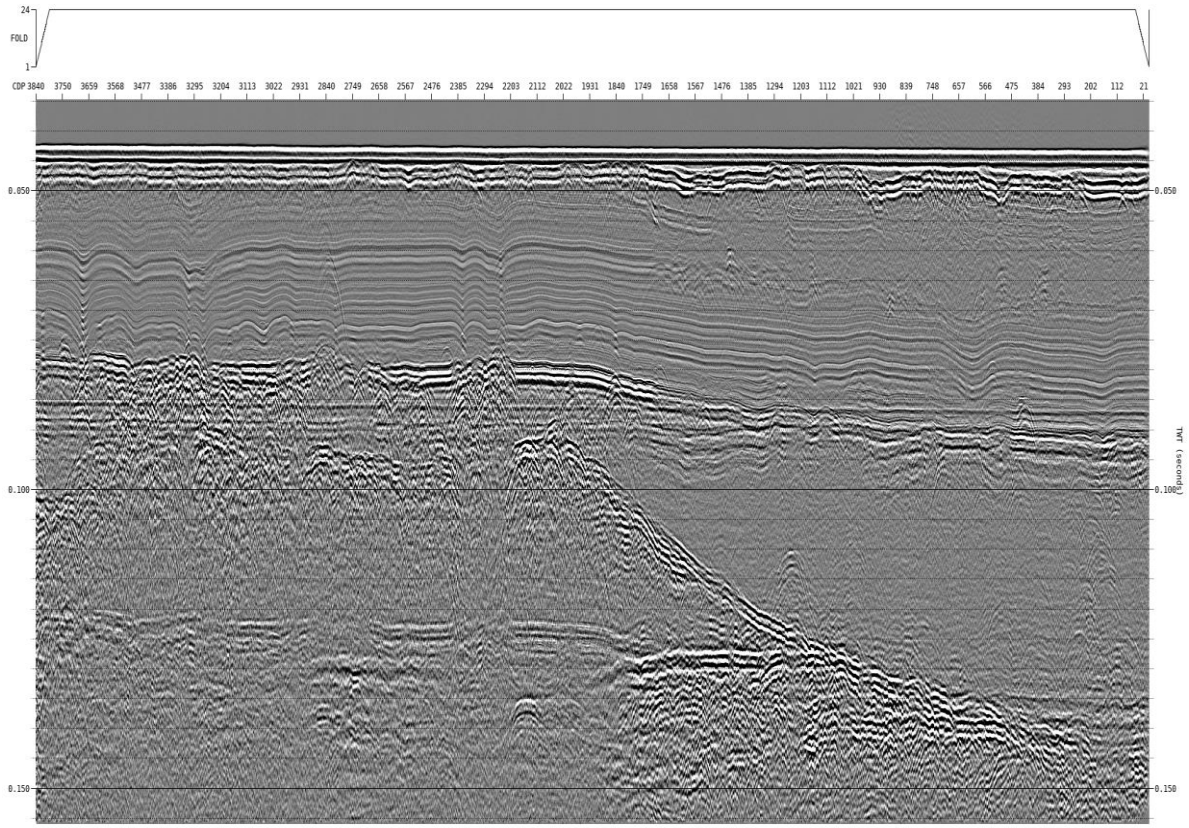

Figure 2.8: Preliminary shot statics: output stack

2.5 Linear Noise Attenuation

Linear noise was observed on most lines in this survey. A Tau-P linear transform was applied to the data to effectively attenuate this noise. Data in the Tau-P domain with dip greater than 20 ms at maximum offset was muted from the full Tau-P transform. Values of ±15 ms transform range began to show hints of primary removal, and ±25 ms was less effective at linear noise attenuation.

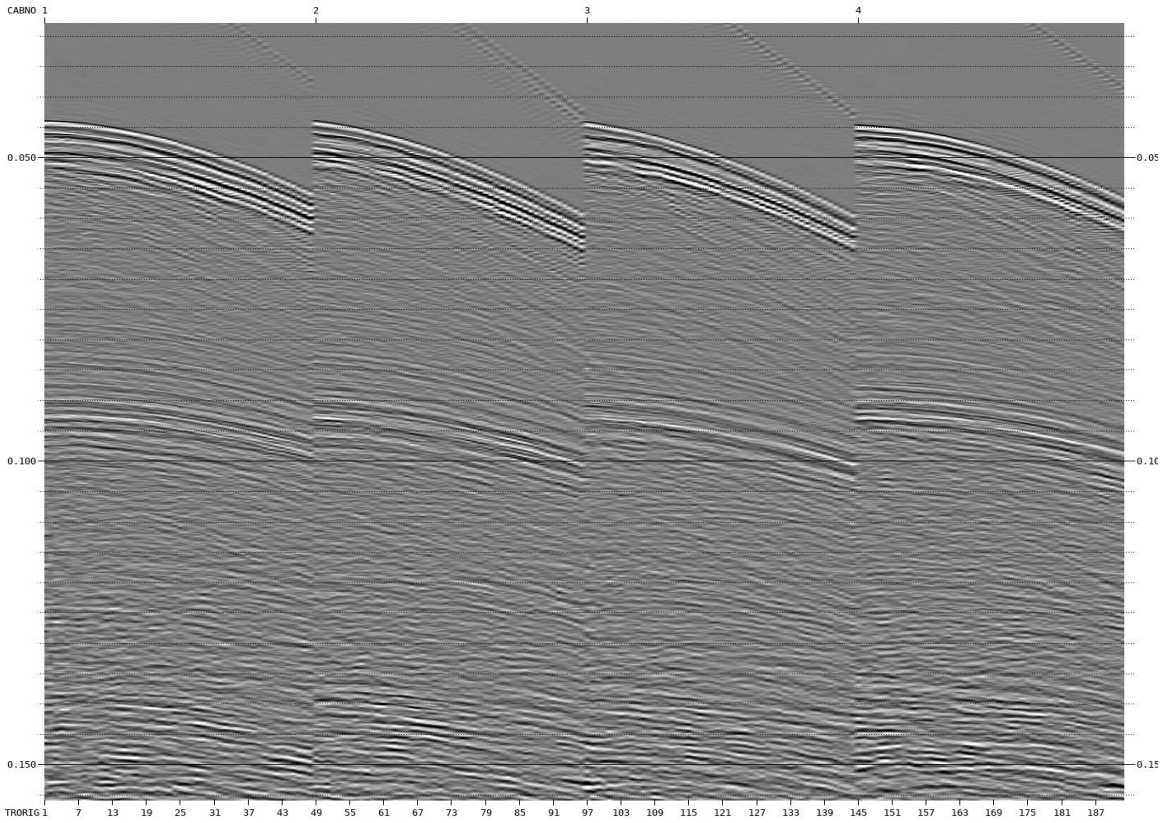

Figure 2.9: LNA: input shots

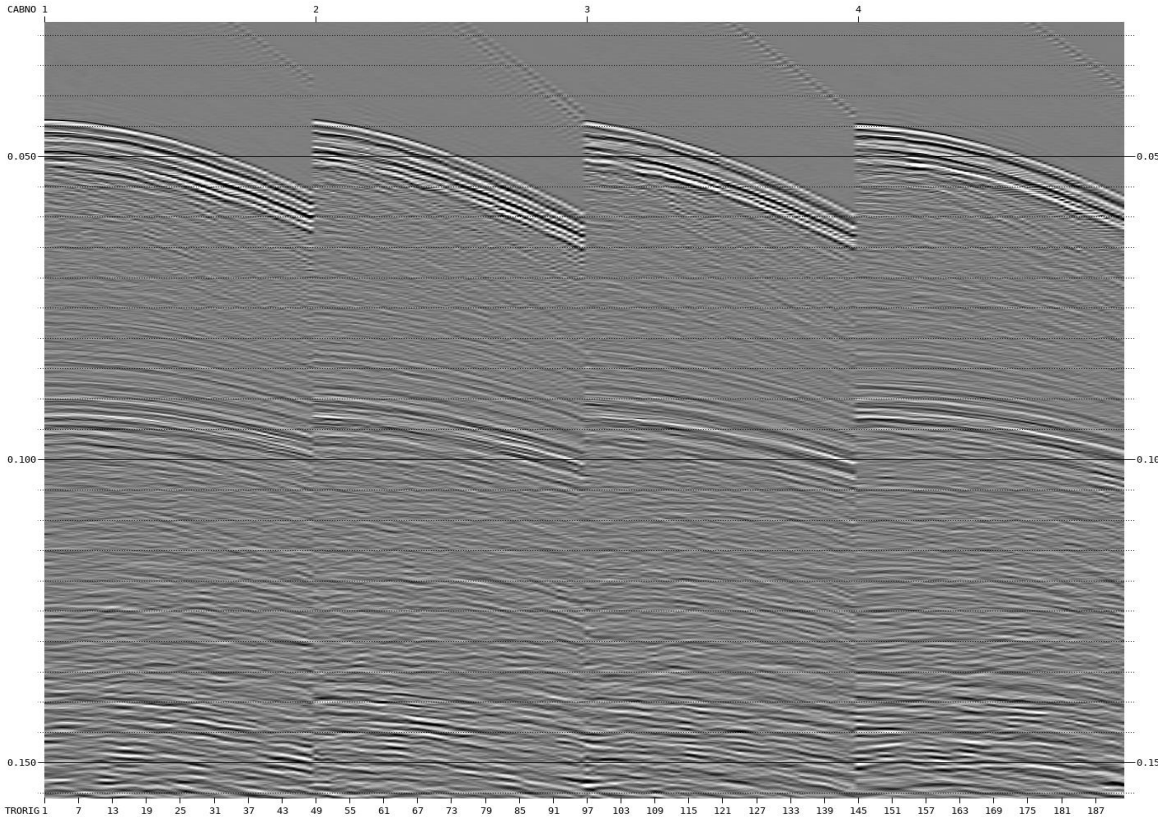

Figure 2.10: LNA: output shots

2.6 Surface Related Multiple Elimination (SRME)

There was significant multiple energy within the data, mainly associated with the water bottom. To attenuate multiple energy, SRME (Surface Related Multiple Elimination) was carried out. SRME uses the geometry of shot recording to estimate all possible multiples that can be generated by the surface. Before evaluating the multiple model, the recorded data was extrapolated to zero offset and a mute was applied to the input shot records to remove direct arrival and guided wave energy. The predicted multiple energy was removed from the input gathers with a double adaptive matching algorithm, the first done in the common channel domain and the second in the shot domain. The adaption in the common offset domain was computed over 211 neighbouring shots, with a filter length of 15 ms and an operator of 50 ms which was longer than the seabed reflection time. Less traces than 211 can cause the SRME to be too harsh (with a small SP interval of 0.5 m this is just over 100 m), and conversely a higher number of traces can often lead to a degraded model where there is steeply dipping and variable multiple. Before adaptive subtraction, the modelled multiples were muted above the first seafloor multiple. SRME was found to be effective in attenuating multiple energy whilst preserving primary events.

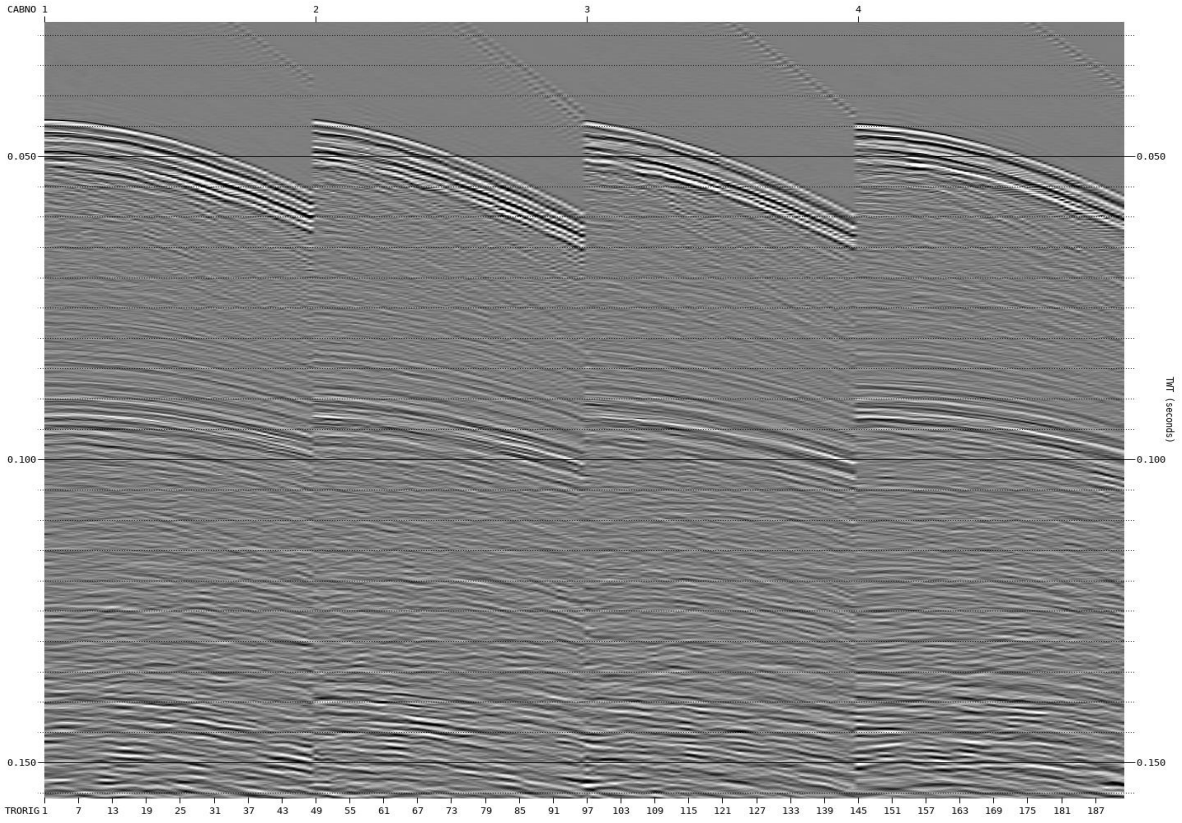

Figure 2.11: SRME: input shots

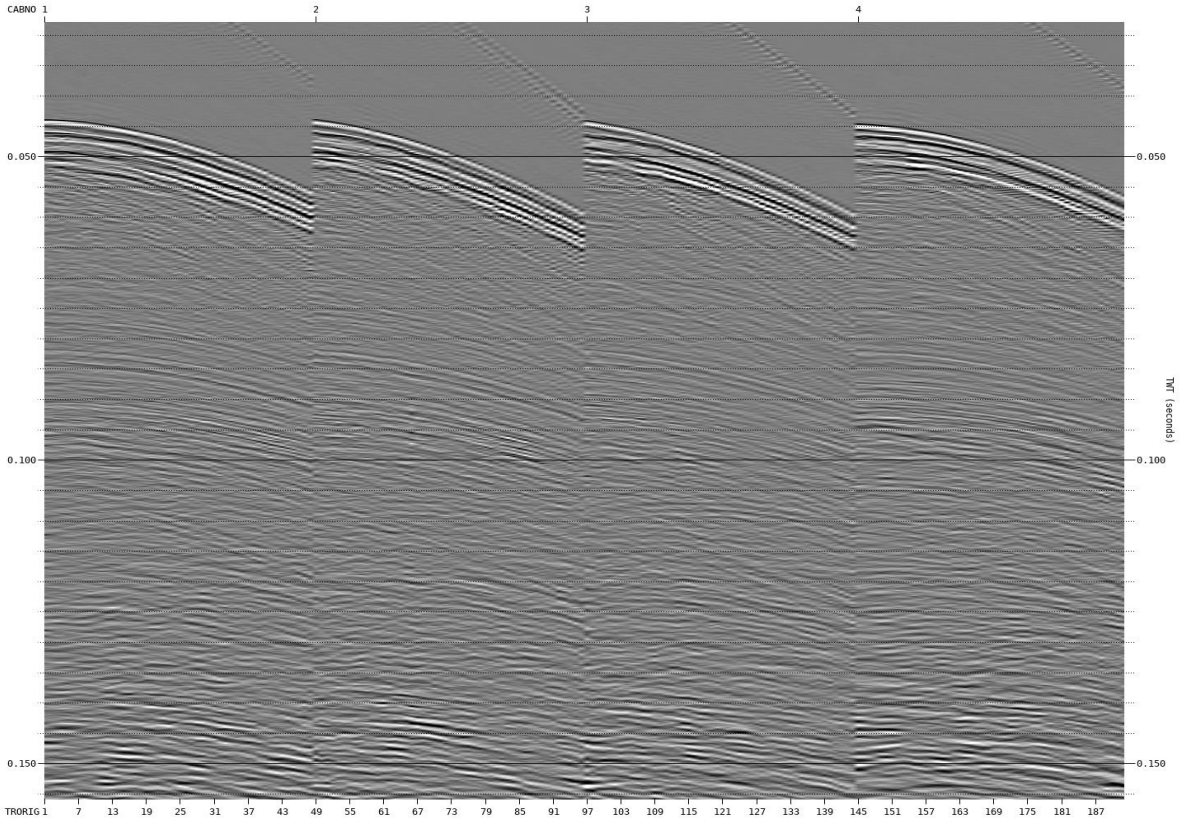

Figure 2.12: SRME: output shots

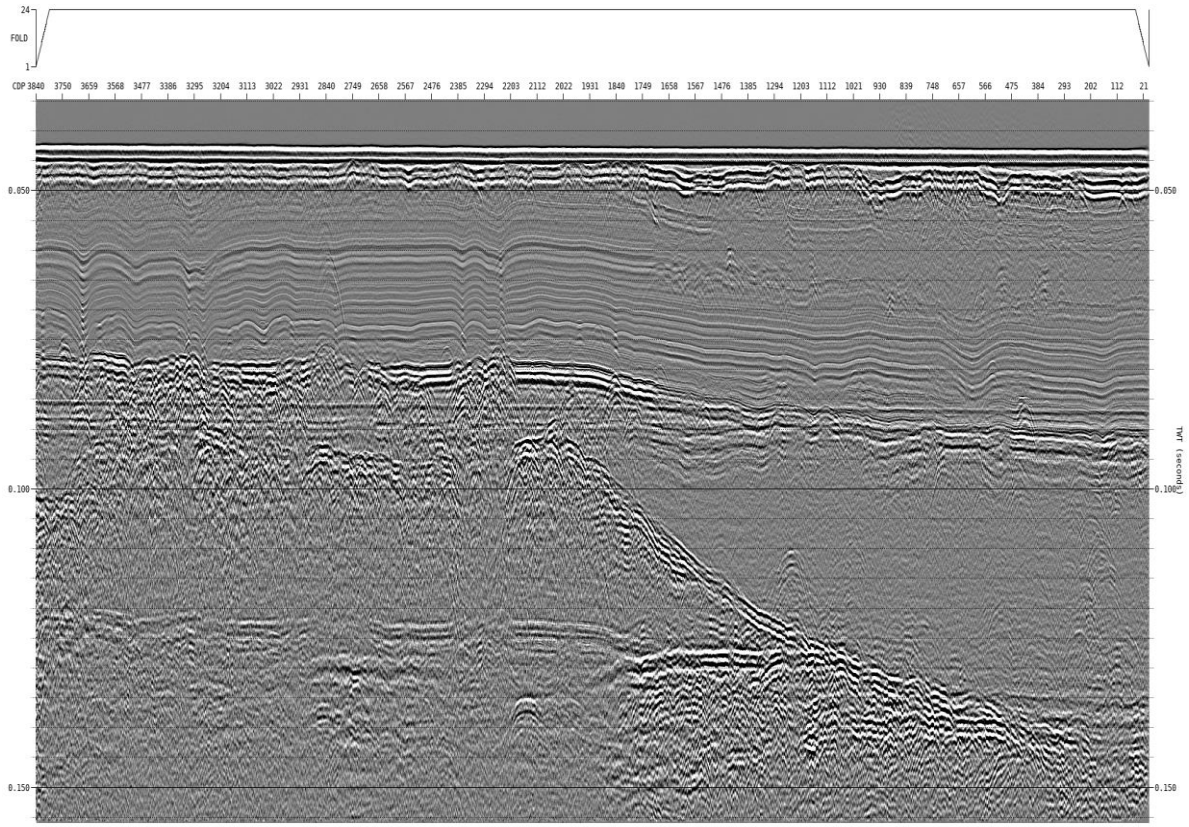

Figure 2.13: SRME: input stack

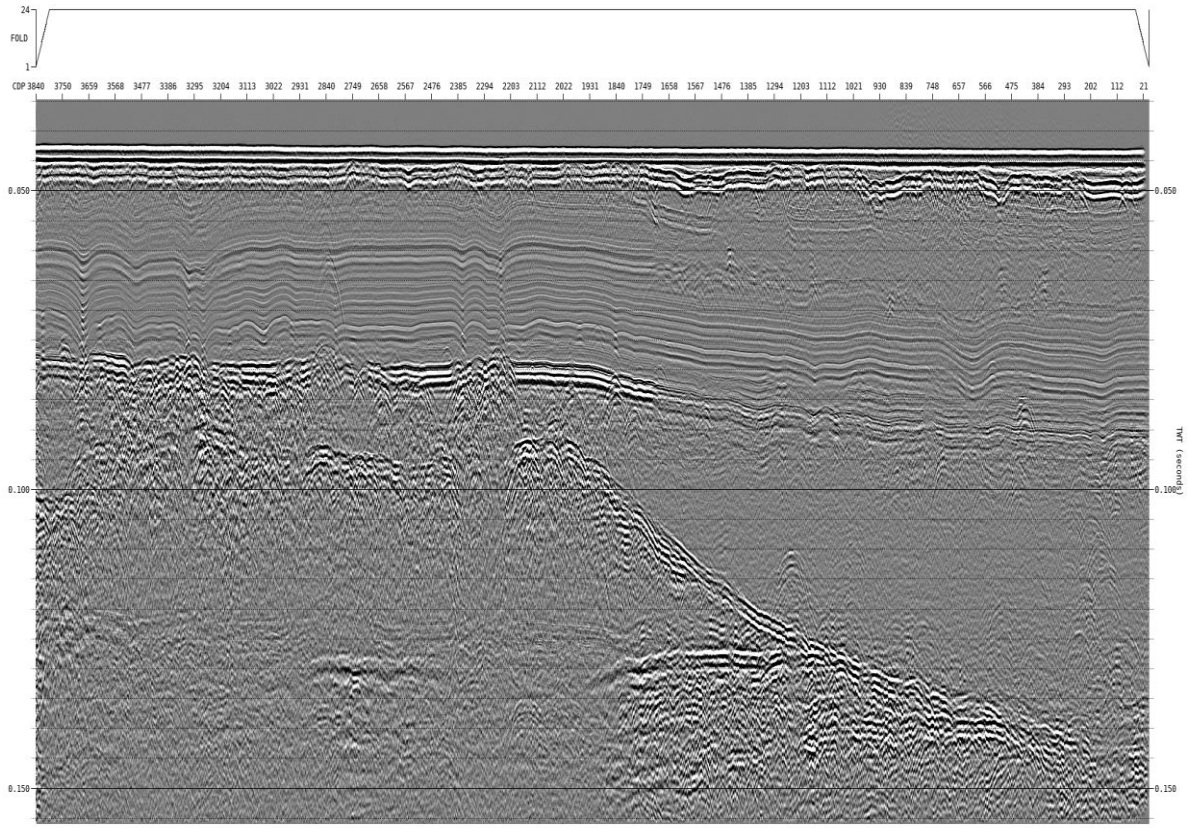

Figure 2.14: SRME: output stack

2.7 Source and Receiver Deghosting

The high acoustic impedance contrast between the water column and the sea surface causes the latter to act as a near perfect reflector of acoustic energy. Consequently, some of the acoustic energy from a seismic source reflects at this interface before being recorded at the receivers and this is referred to as (source/receiver) ghost, thereby limiting the wavefield spectral band.

To attenuate source, receiver and combined source / receiver ghosts, the *Uniseis 'DEGHOST'* module was applied. *'DEGHOST'* attempts to separate the primary energy from the secondary ghosted wavefield. The primary upcoming wavefield should be more representative of the subsurface reflectivity required for interpretation & well-log matching. Reflections should become shorter, less complex wavelets and be more representative of their characteristic reflectivity in magnitude and polarity. The consequence of this is that we improve the resolution and achieve a broader spectrum. Various tests showed the standard reflection coefficient of -1 for the source and receiver deghosting worked well to attenuate the ghost. A 0.5 m wave height allowance for the frequency dependent scattering model was applied to the source deghosting and 0.2 m for receiver side. This helped to reduce ringing from the deghosting process.

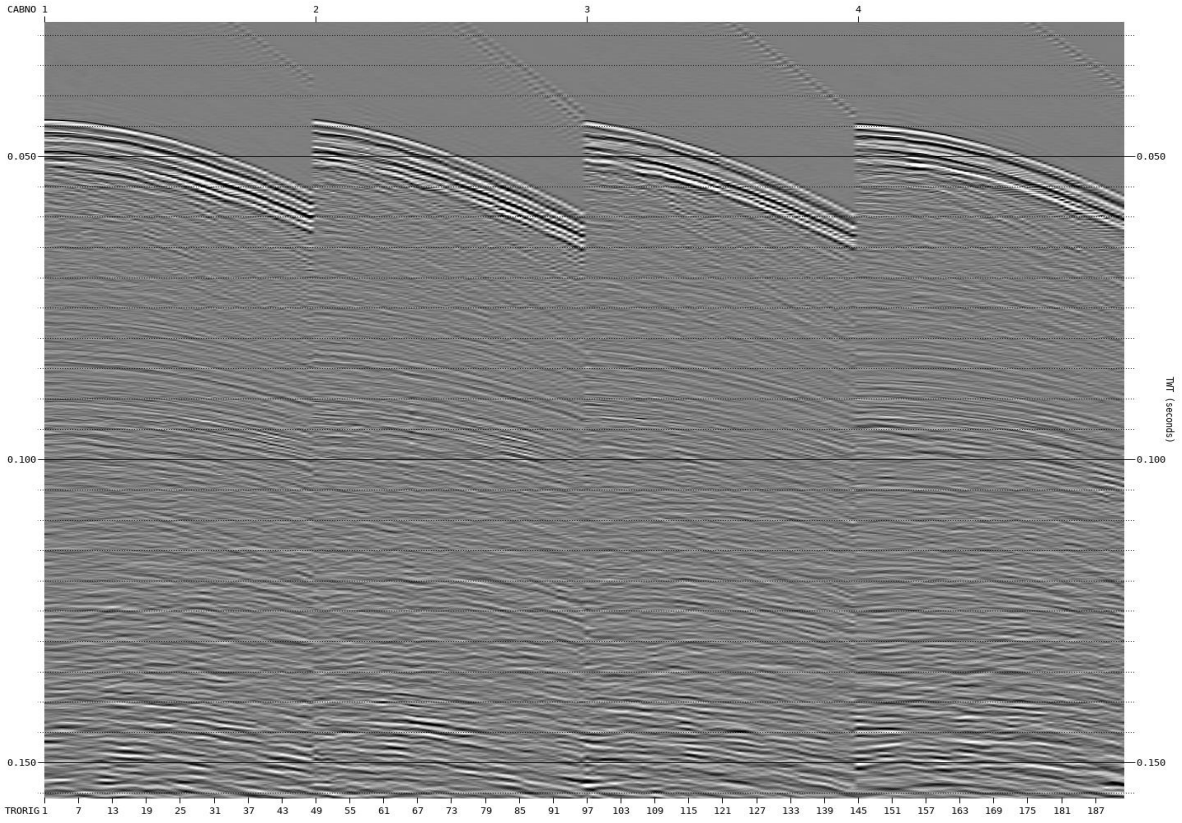

Figure 2.15: Deghost: input shots

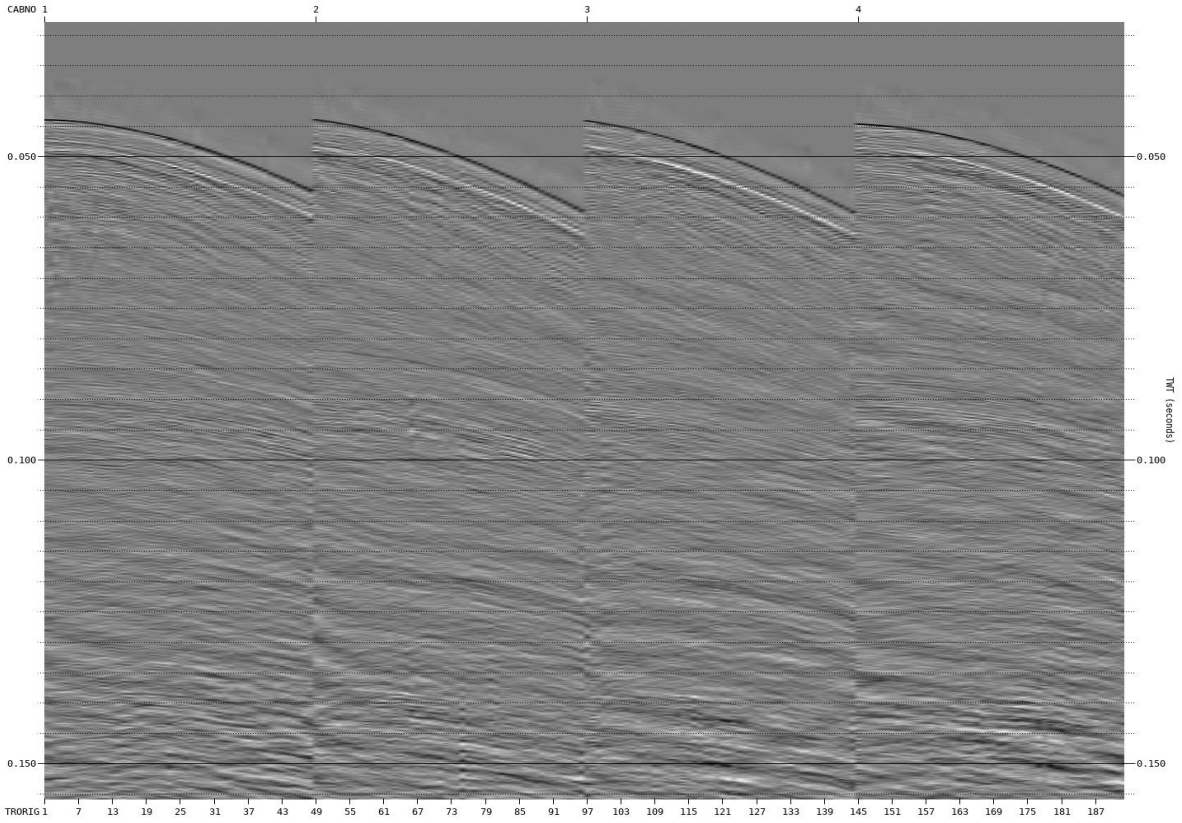

Figure 2.16: Deghost: source & receiver deghost shots

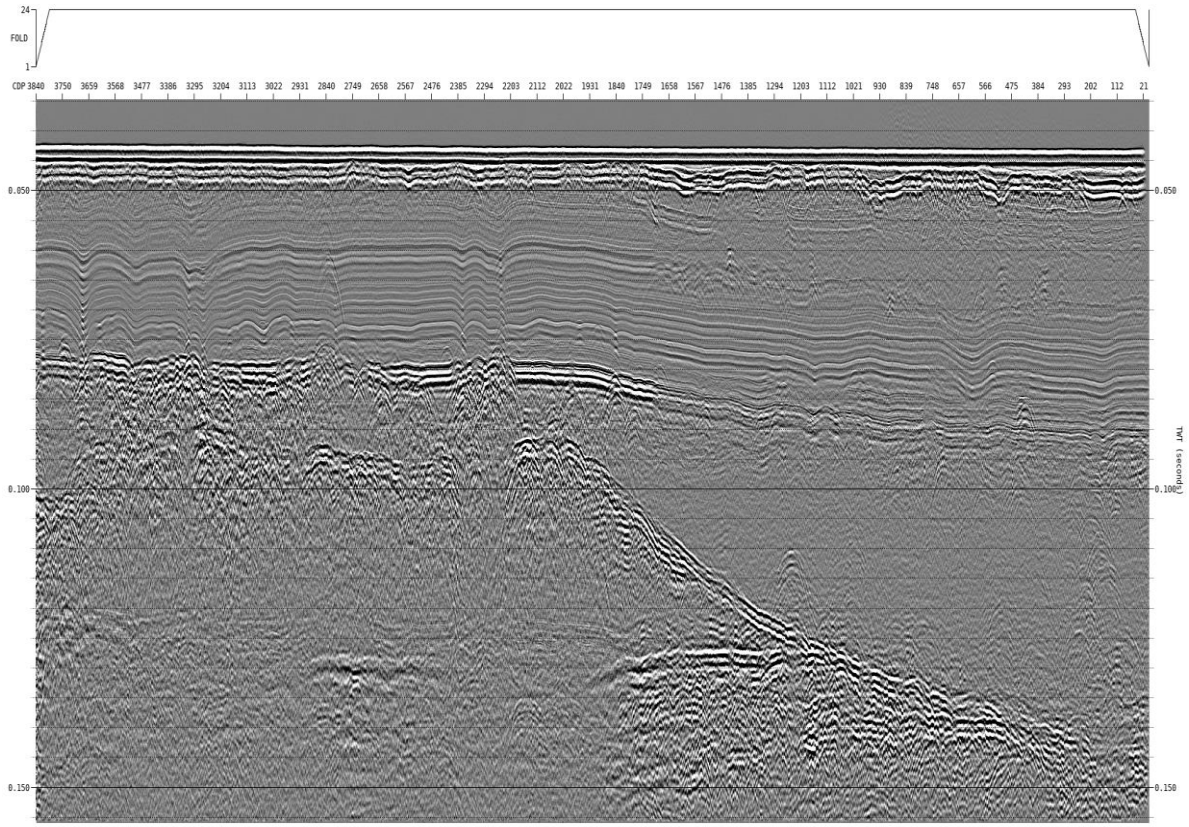

Figure 2.17: Deghost: input stack

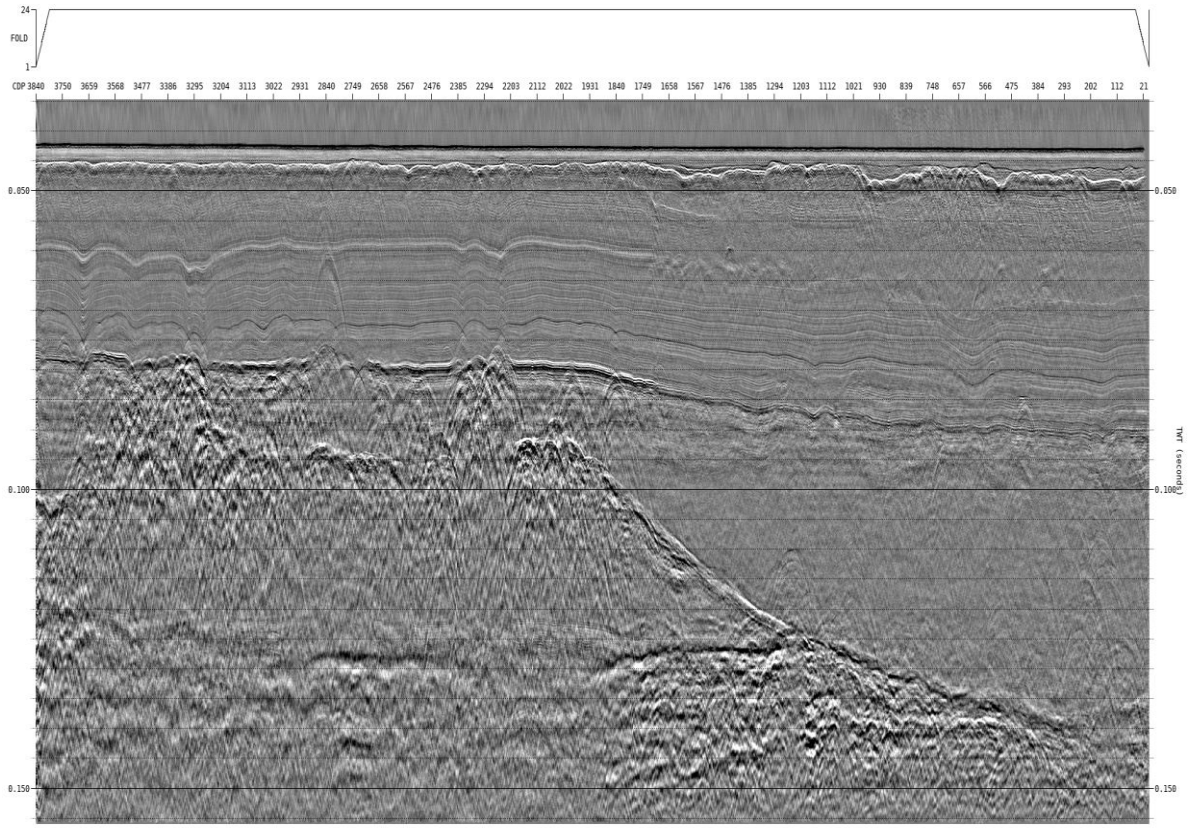

Figure 2.18: Deghost: source & receiver deghost stack

2.8 Velocity Analysis

A high-resolution velocity analysis using 2nd order NMO correction was conducted using the interactive velocity analysis software *Pegasus*. The analysis was performed at 160 m intervals in both inline and crossline directions with each location being compared to and constrained by neighbouring locations. This ensured that consistency was maintained between adjacent lines and velocity locations. Preliminary 3D shot statics were applied at this stage to improve the semblance and stacking. More detail on the 3D statics is available in "Tides and Final 3D Shot Statics". The example below shows the displays generated by *Pegasus* for the purposes of velocity analysis. This image shows the semblance, NMO corrected gather, multi velocity stacks, real time stack and the picking map.

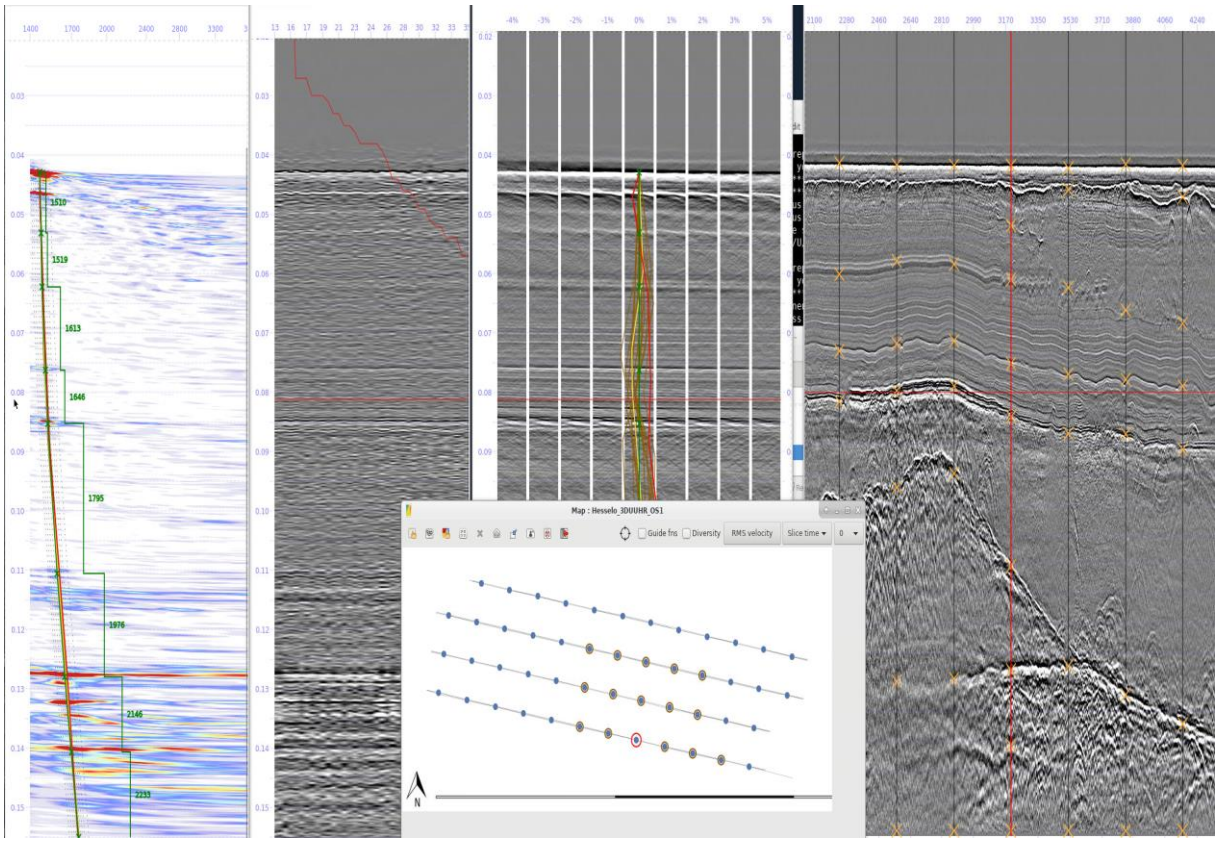

Figure 2.19: Pegasus 3D velocity picking example on OS1

2.9 Tides and Final 3D Shot Statics

Similar to Section 2.4 on preliminary shot statics, and to compensate for any remaining timing variations, residual shot statics are recomputed in a 3D domain. Observed tides were applied up front, followed by the computation and application of the residual shot static.

The process is very similar to the 2D application, but this time the cdps are 3D cdps of common inline and crossline, with varying offset. The only big difference is that a supergather is created for each 3D cdp that includes the traces from 5 inlines either side and 5 crosslines either side. This supergather then becomes the pilot trace and the same iterative cross correlative approach is then ran through 5 iterations.

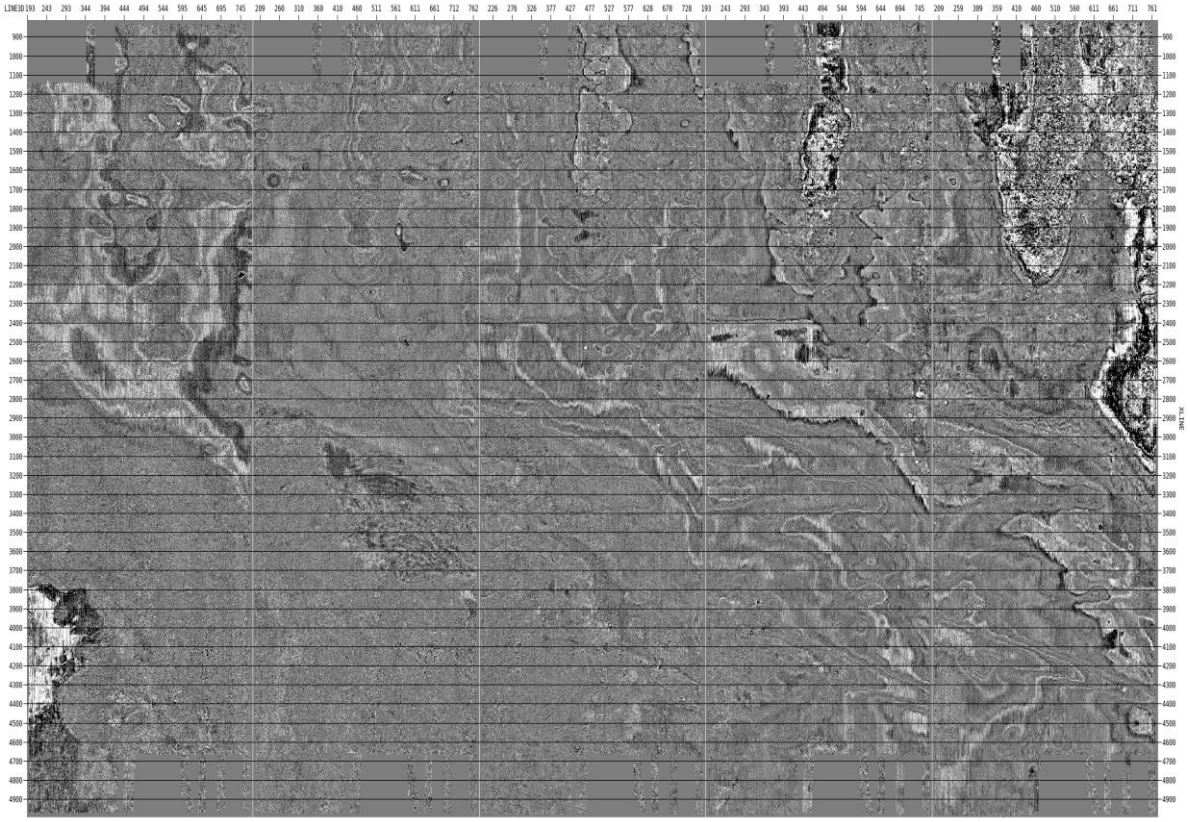

Figure 2.20: 3D OS1 timeslice 60-85 ms: without final statics

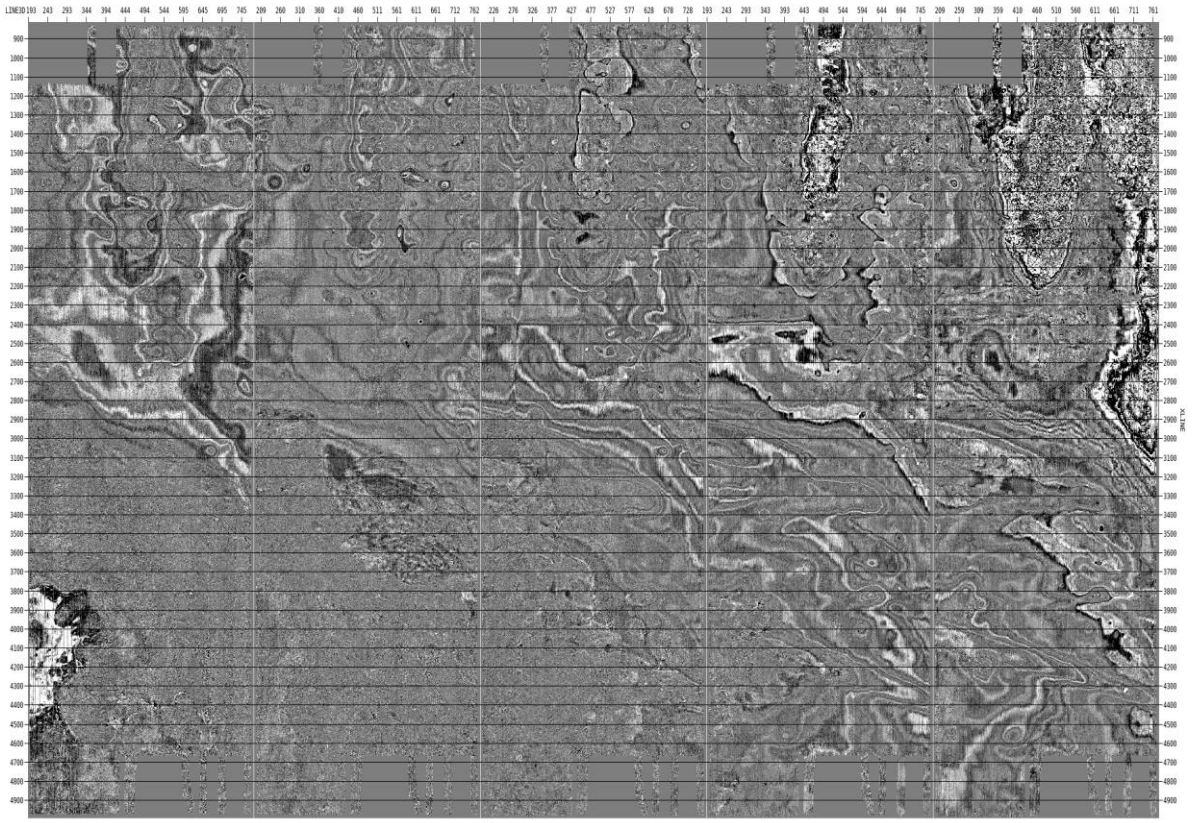

Figure 2.21: 3D OS1 timeslice 60-85 ms: with final statics

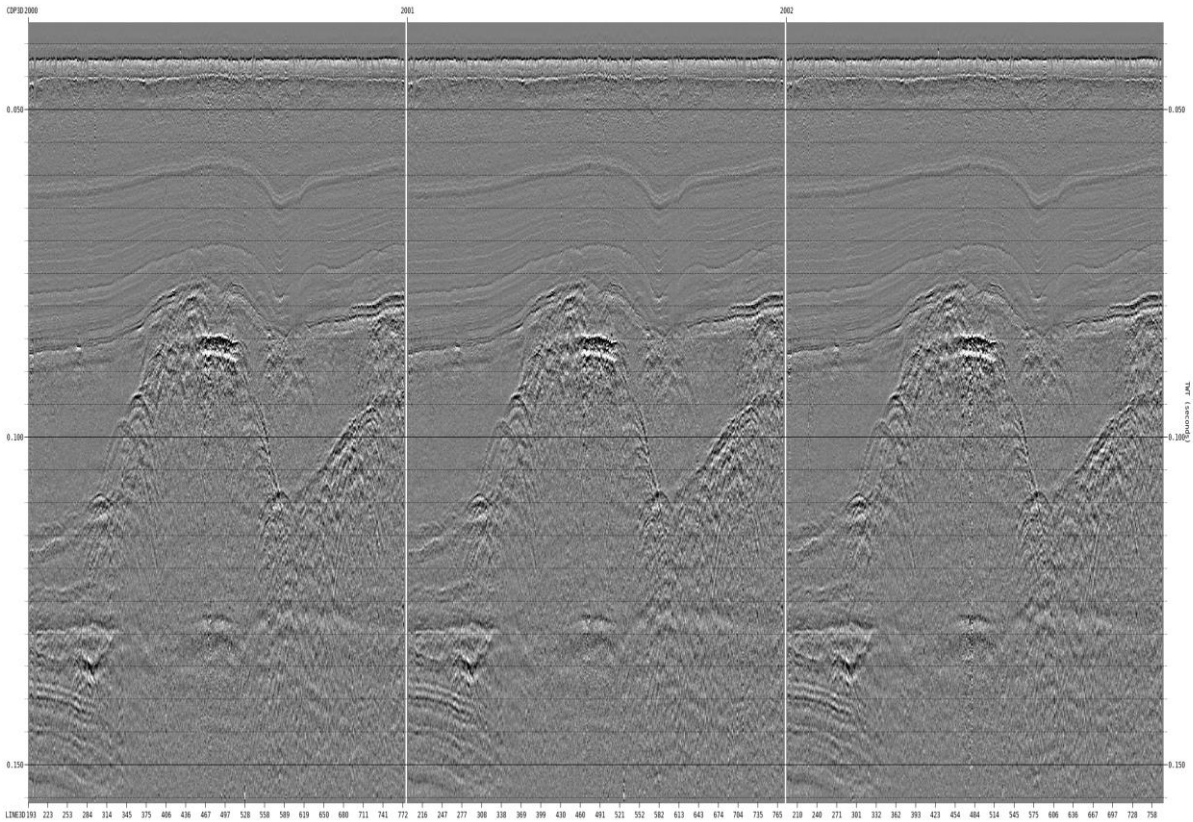

Figure 2.22: 3D OS1 xline 2000-2002: without final statics

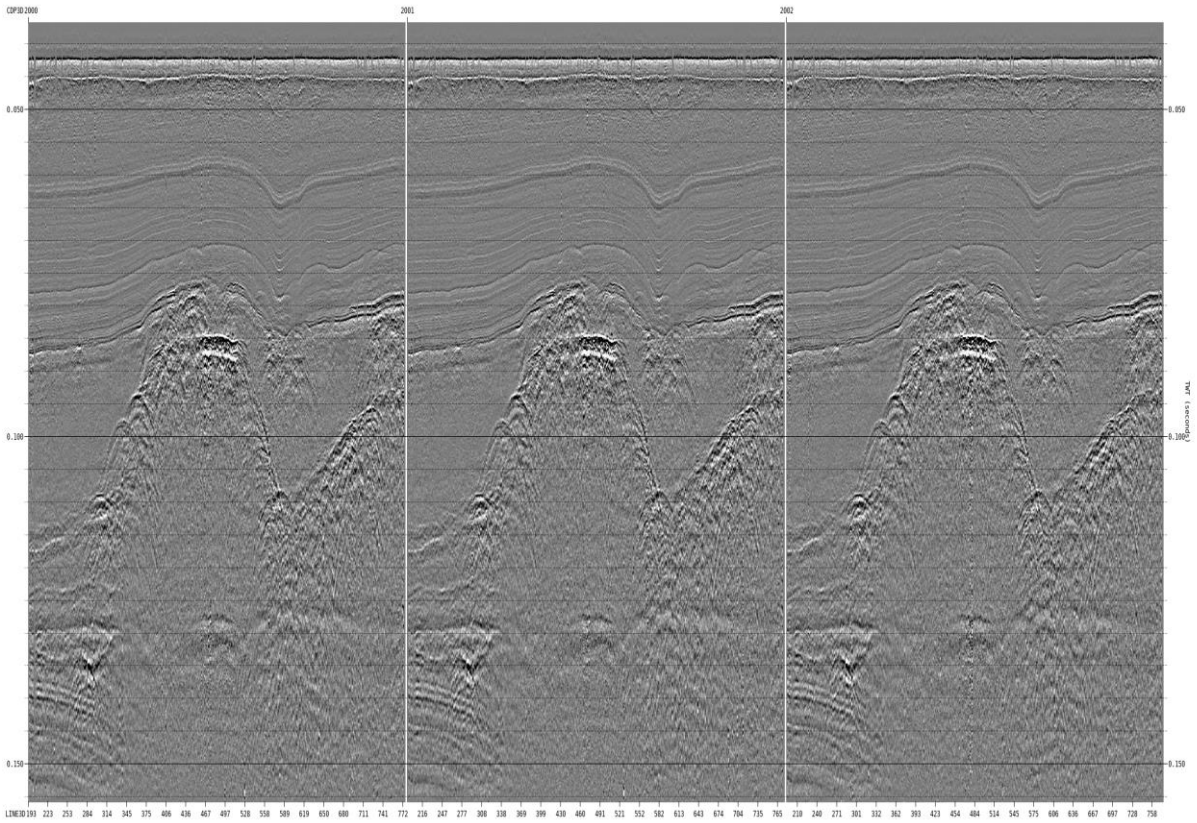

Figure 2.23: 3D OS1 xline 2000-2002: with final statics

2.10 Interpolation and Regularisation

Regularising offset bins involves interpolating traces to bin centre. Empty bins are also interpolated using a 3D anti-leakage Fourier method. Regular offset bins allow the upcoming migration stage to work efficiently while ensuring migration artefacts are restricted to the outer edges of the volume.

Uniseis tool *'FRECON'* was used on each of the 24 offset planes, individually for each OS area. Here, the module works in 3D – selectively transforming data using an anti-leakage Fourier transform. This allows the module to effectively interpolate dipping reflectors while the transform also allows signal to be prioritised over noise.

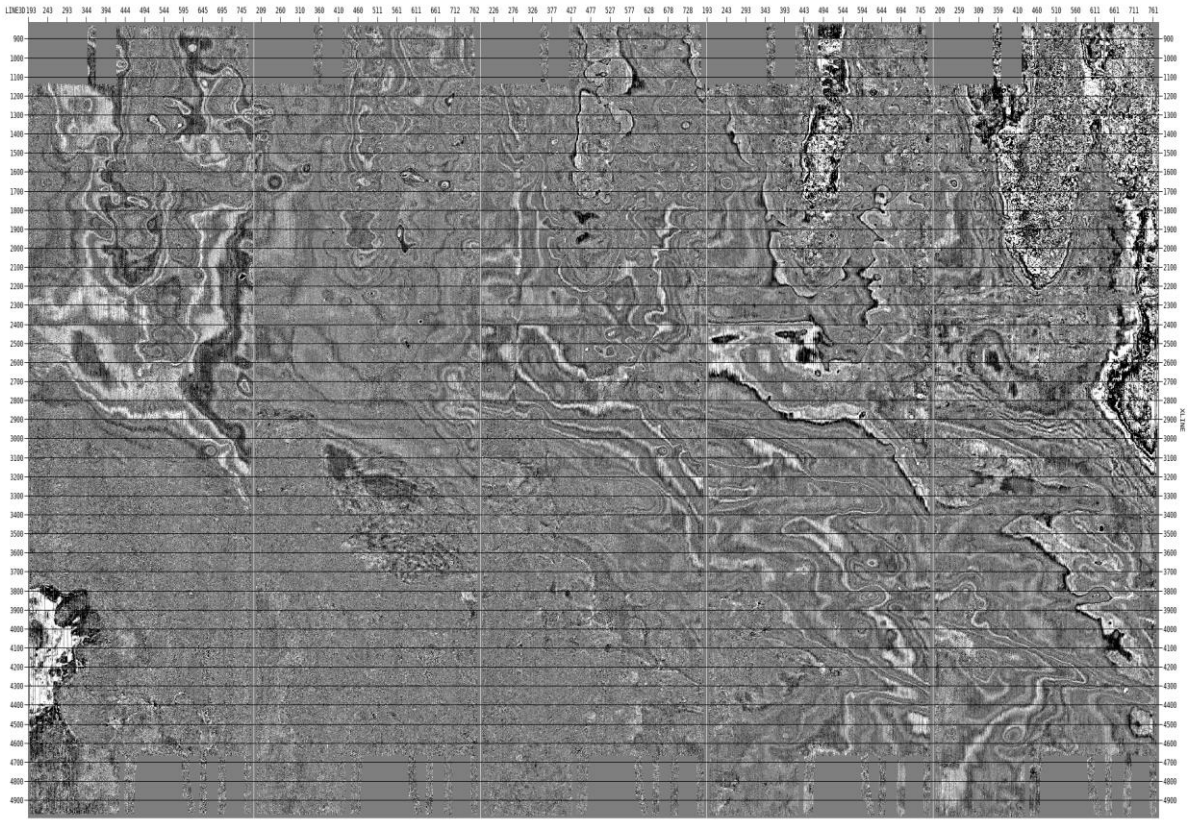

Figure 2.24: 3D OS1 timeslice 60-85 ms: before regularisation

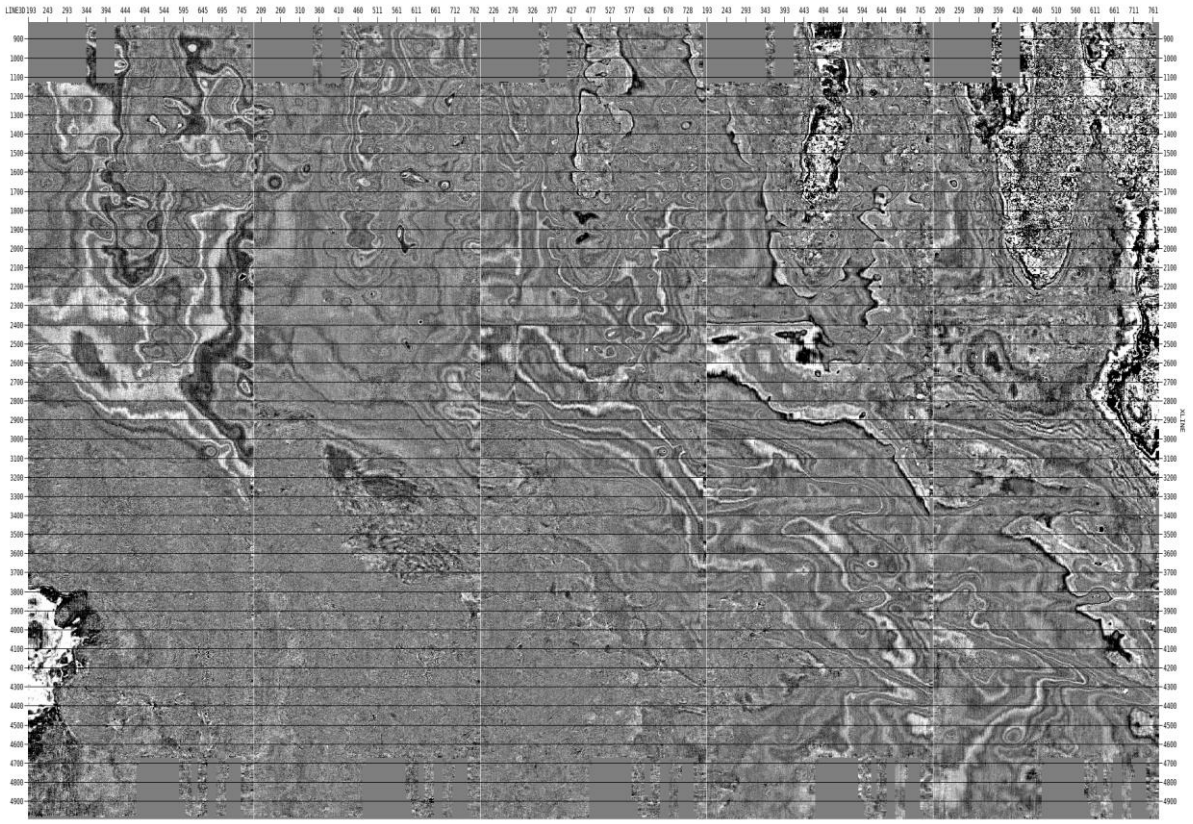

Figure 2.25: 3D OS1 timeslice 60-85 ms: after regularisation

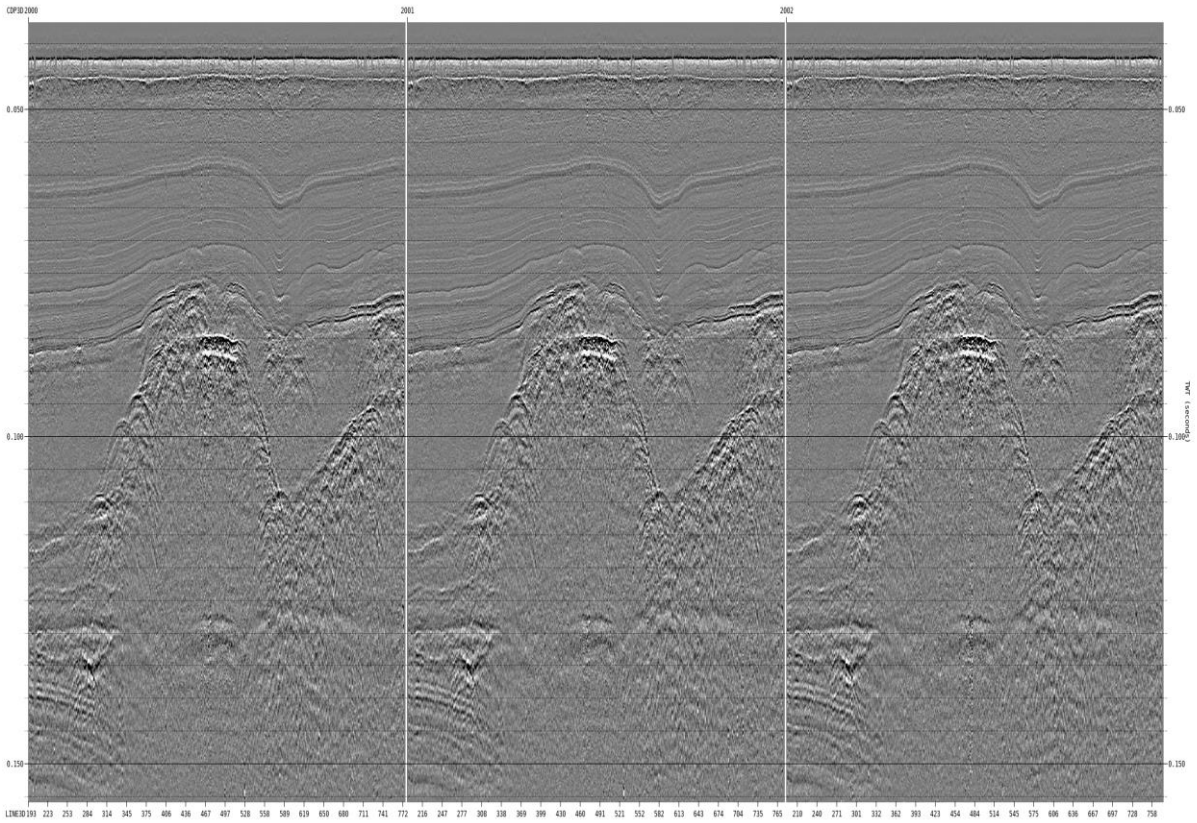

Figure 2.26: 3D OS1 xline 2000-2002: before regularisation

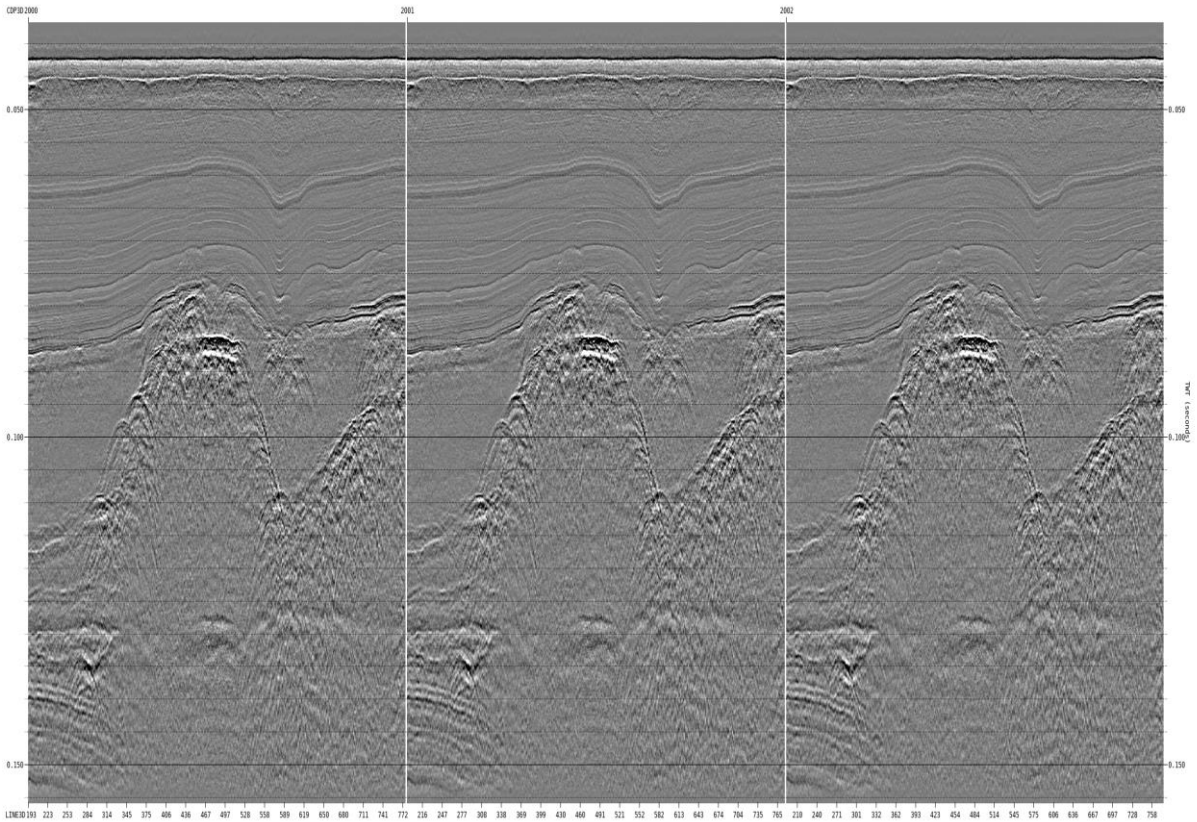

Figure 2.27: 3D OS1 xline 2000-2002: after regularisation

2.11 PASTA Statics, Final Mute and Stack

'PASTA' was applied to NMO corrected CMPs to compensate for any residual receiver side statics. This is achieved in a similar manner, by cross correlating the traces in the 3D CMP with a pilot trace which is a weighted trace mix of the cube.

The data were then ready to be stacked. An outer trace mute was applied to remove NMO stretch on the far offsets. A more open mute would introduce stretch in the shallow regions, a consequence of the rather shallow conditions. Trace normalization of 1/N was used when stacking. See below for an example of the gathers with the final mute overlaid.

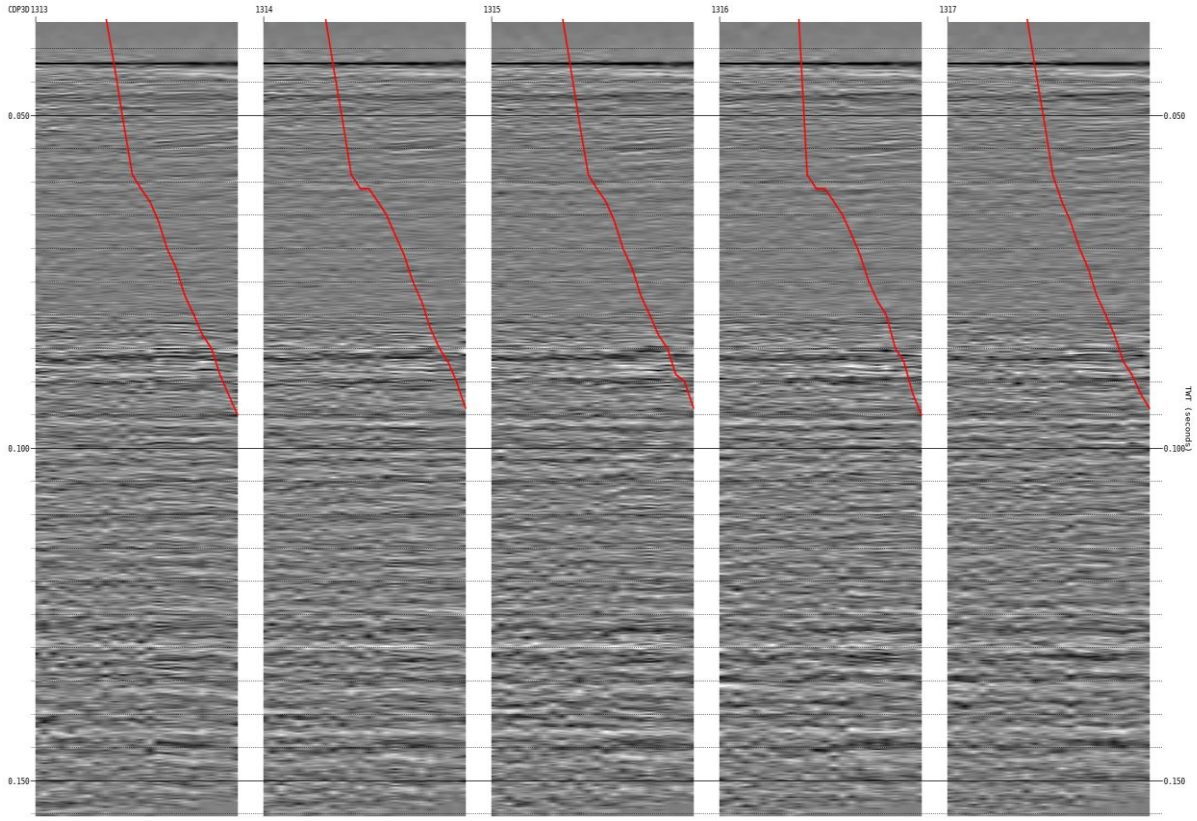

Figure 2.28: 3D OS1: CMP gathers with final stacking mute overlaid

Table 2.1: 3D-UUHR Final mute parameters

Time [ms]	Offset [m]
20	25
60	30
120	65 (full offset range)

2.12 Post Stack Kirchhoff Migration (PoSTM)

As velocity control was good, 3D Post-Stack Kirchhoff Time Migration was performed using 100% of the picked velocity. A migration aperture of radius 60 m was used with a 30% stretch mute to minimise dipping artefacts. Anti-aliasing was applied by pre-filtering the data within the migration scan depending upon the local migration operator dip. Anti-aliasing protection prevents any undesirable data being included.

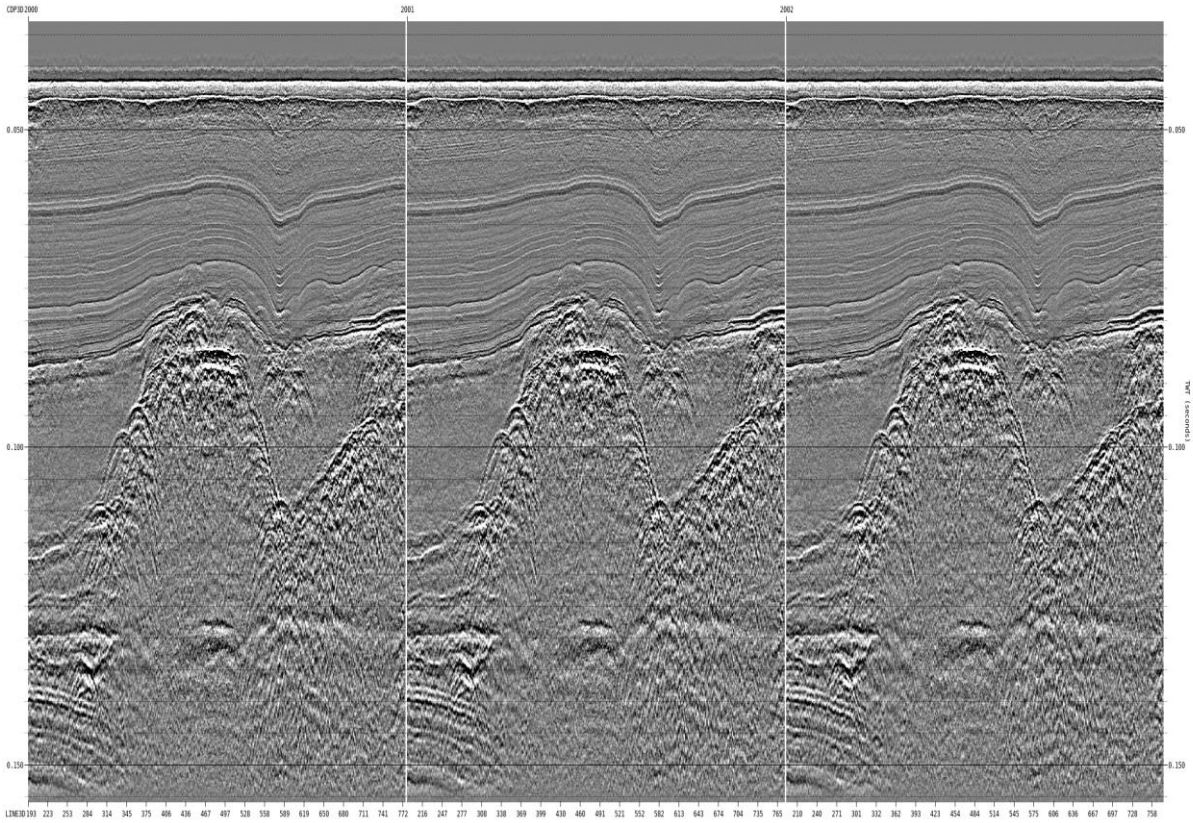

Figure 2.29: 3D OS1 xline 2000-2002: prior to PoSTM

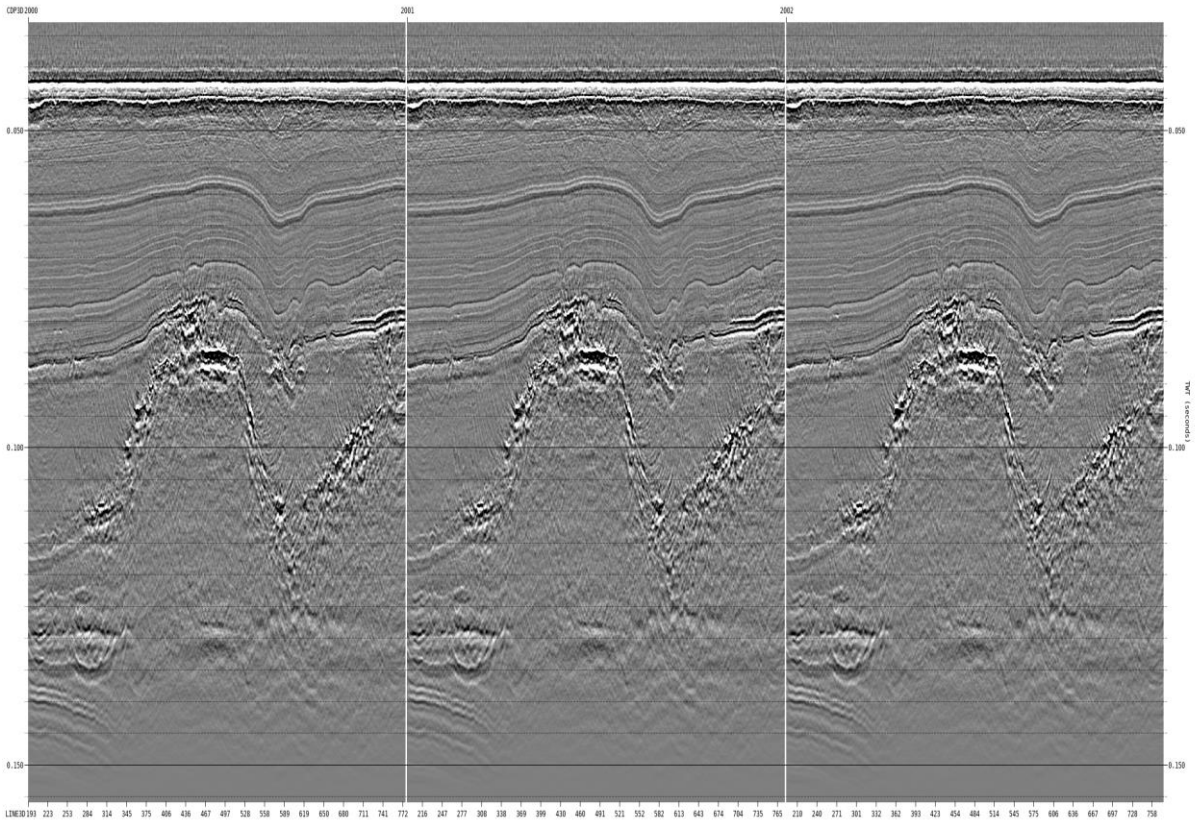

Figure 2.30: 3D OS1 xline 2000-2002: PoSTM

2.13 Acquisition Footprint Filtering

Spatially periodic noise can be viewed on timeslices as regular amplitude modulations or striping. In marine seismic data this is usually related to the streamer/gun configuration where it is commonly known as an acquisition footprint. Stripes in the spatial domain appear as discrete spots of energy in the Kx-Ky domain. Filtering was performed on one transformed time-slice at a time with an example of timeslices below.

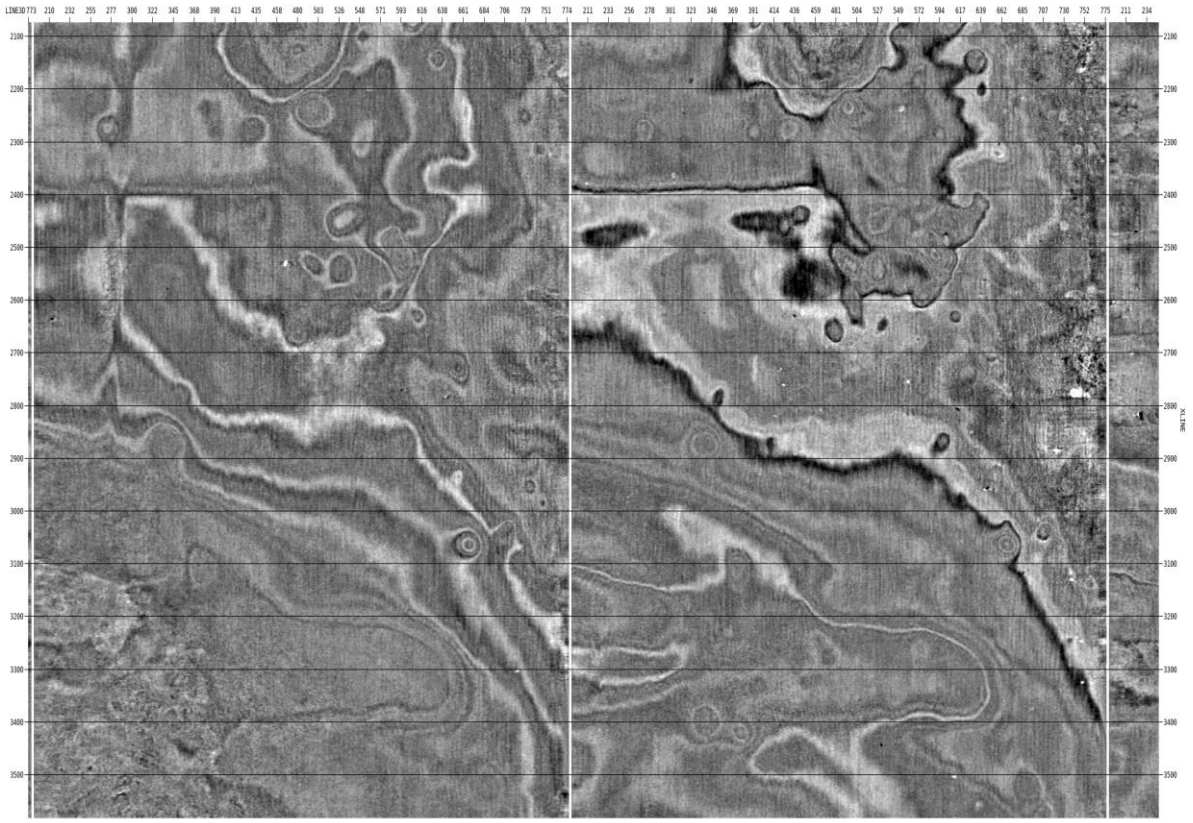

Figure 2.31: 3D OS1 zoomed timeslices: before KxKy footprint filtering

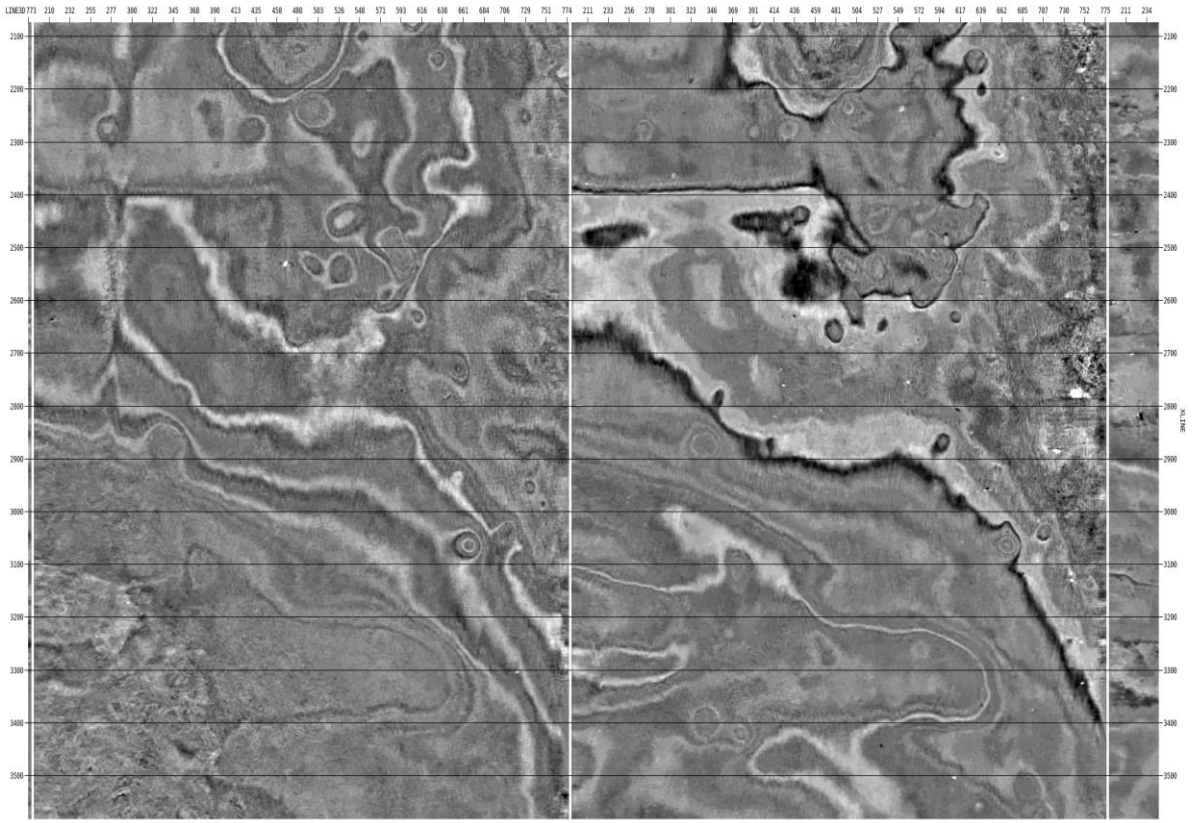

Figure 2.32: 3D OS1 zoomed timeslices: after KxKy footprint filtering

2.14 Post Stack Processing 1

Post stack deconvolution-based shaping was applied to further enhance the resolution. This was averaged over the entire inline with a gap of 0.5 ms at the seabed, increasing linearly to 1.5 ms at a time of 90 ms.

The low frequency noise, mainly boosted by the deghosting process, was attenuated at this stage using the *Uniseis 'WAVDN'* module. This decomposed each seismic trace into separate filter panels, and only the lower frequencies panels were dampened.

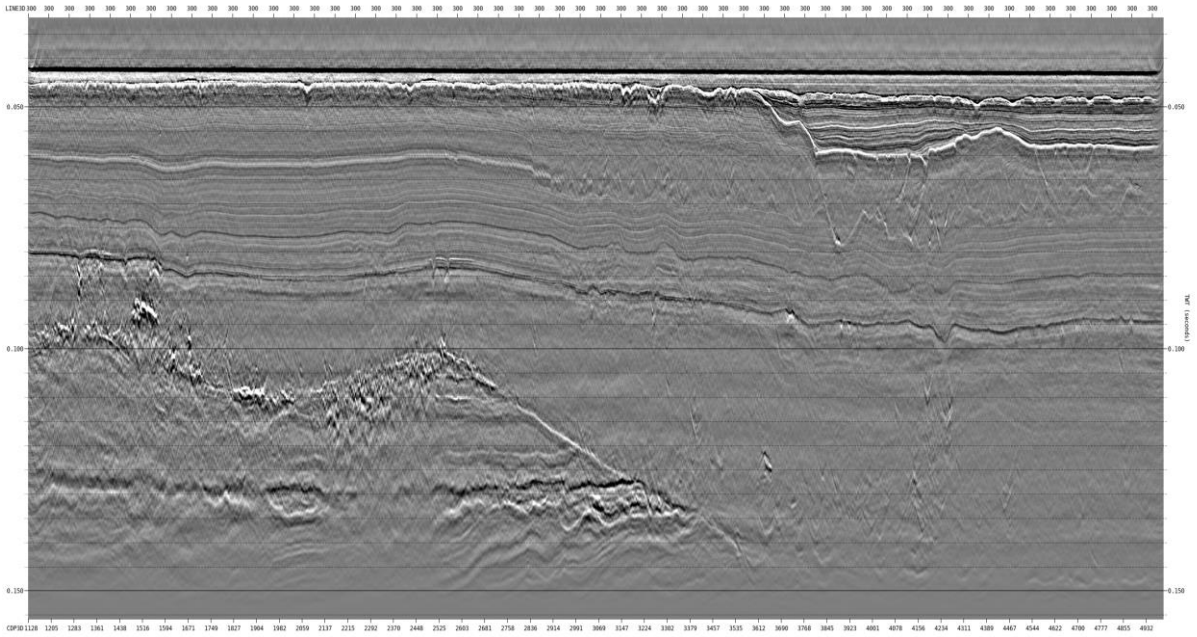

Figure 2.33: 3D OS1 inline 300: before post stack processing 1

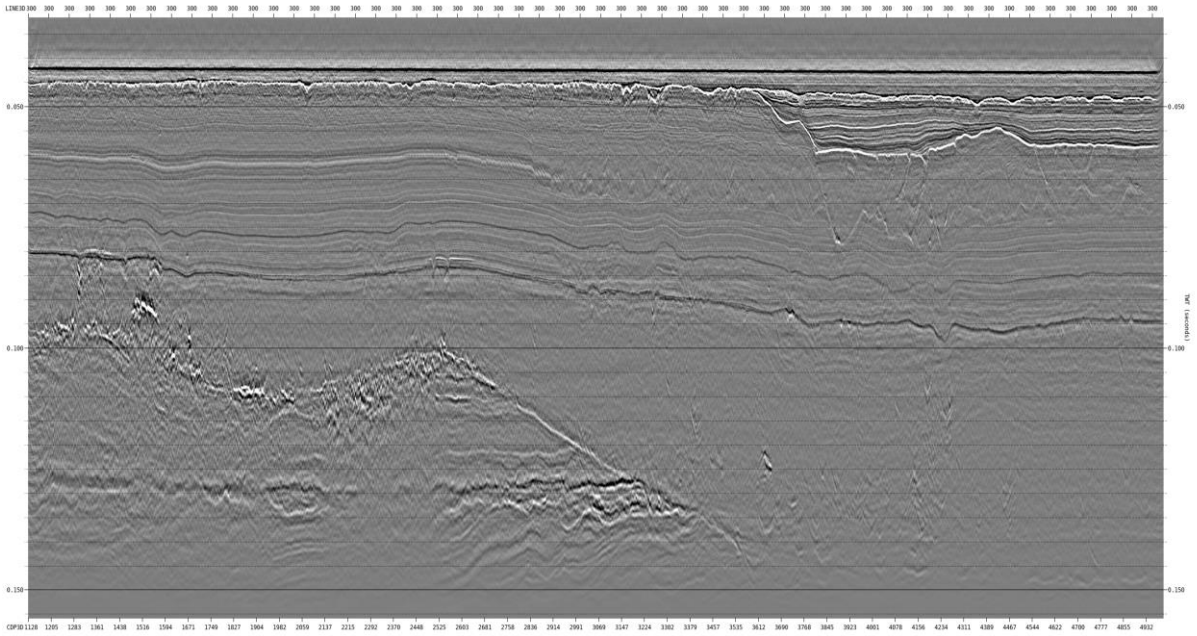

Figure 2.34: 3D OS1 inline 300: after post stack processing 1

2.15 Zero Phase

A zero-phase filter was designed using a data derived source signature wavelet, itself obtained by super stacking central inlines of each cube independently. The water bottom was flattened, and traces shifted to 30 ms prior to the CMPs being super stacked. The onset of the super stacked wavelet was then shifted to 0 ms and the filter calculated. See below for an example of the zero-phase filter applied to the stack.

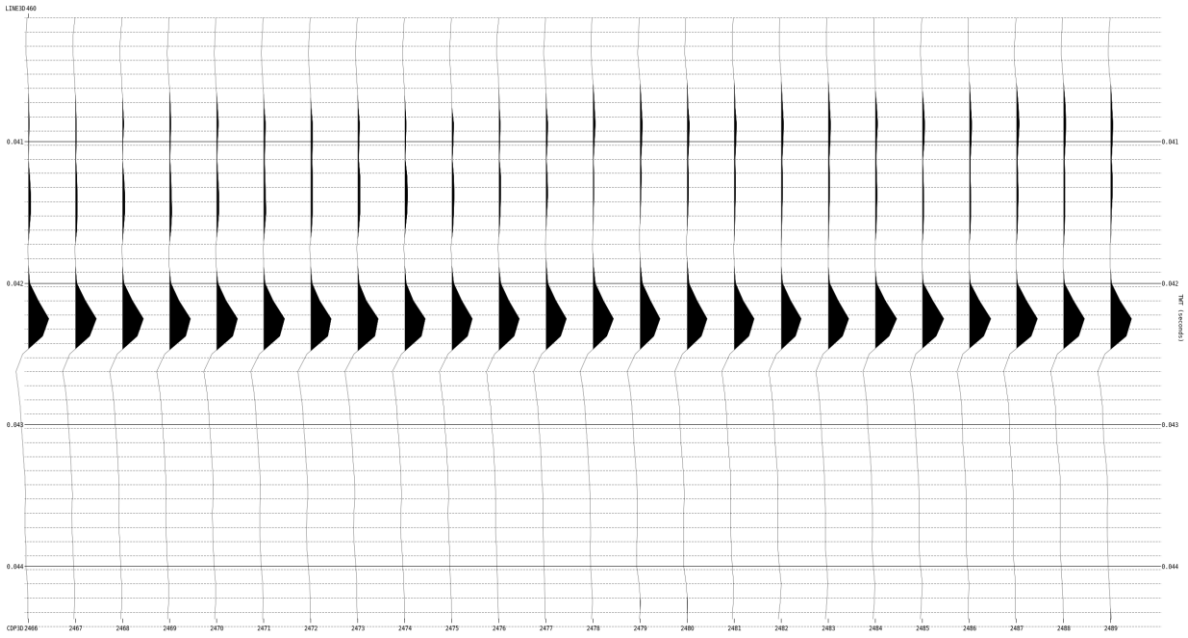

Figure 2.35: Zero phase: zoomed seabed before

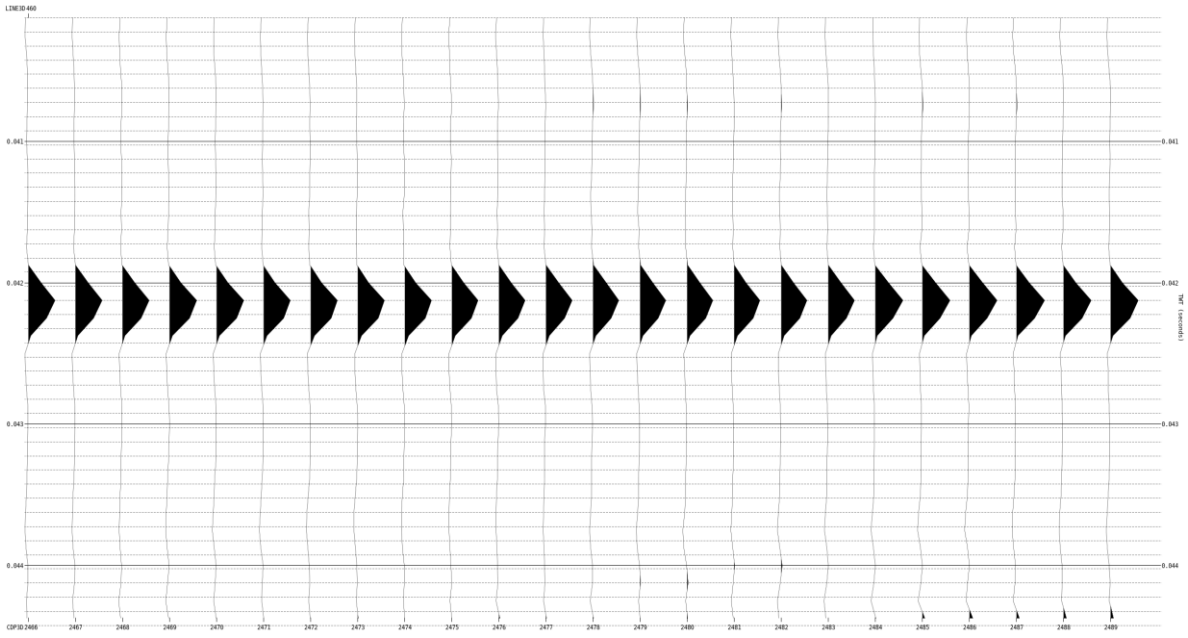

Figure 2.36: Zero phase: zoomed seabed after

2.16 Post Stack Processing 2

A post stack deconvolution followed this to remove further multiple, hitting the remnant second seabed bounce rather effectively. This was a very mild application with averaging of the deconvolution operator over a large 311 traces in both the inline and xline direction, computed with a gap 5 ms shorter than the seabed, and operator 5 ms longer than the seabed.

The final few processing steps were then to further filter the stack before being output as a final product. Various filters were tested with the aim of enhancing signal, preserving resolution and reducing noise. The following set of processes were arrived at:

- Decon remnant demultiple
- Surface wave noise attenuation up to 80 Hz
- Time varying bandpass filter – ref. Table 2.2
- FK filter > 0.55 ms / trace in xline domain
- dB gain of 52 dB/sec from seabed
- SWELL up to 100 Hz
- Apply source / receiver static shift
- Mute above seabed with 1 ms taper
- NLMEAN timeslice image denoise
- Trim data output to take off lower fold edges

Table 2.2: 3D-UUHR Time varying bandpass filter

Start Time	Low Cut [Hz]	Slope [dB Oct]	High Cut [Hz]	Slope [dB Oct]
40 ms	80	18	3300	32
95	60	18	2600	32
115	40	18	2100	32

Data deliverables were also requested in depth. This was done using the *Uniseis 'DTCONV'* tool. The RMS stacking velocities were converted to intervals with a DIX transformation prior to depth conversion. This was applied to both the final migrated time cube and the final non-migrated time cube.

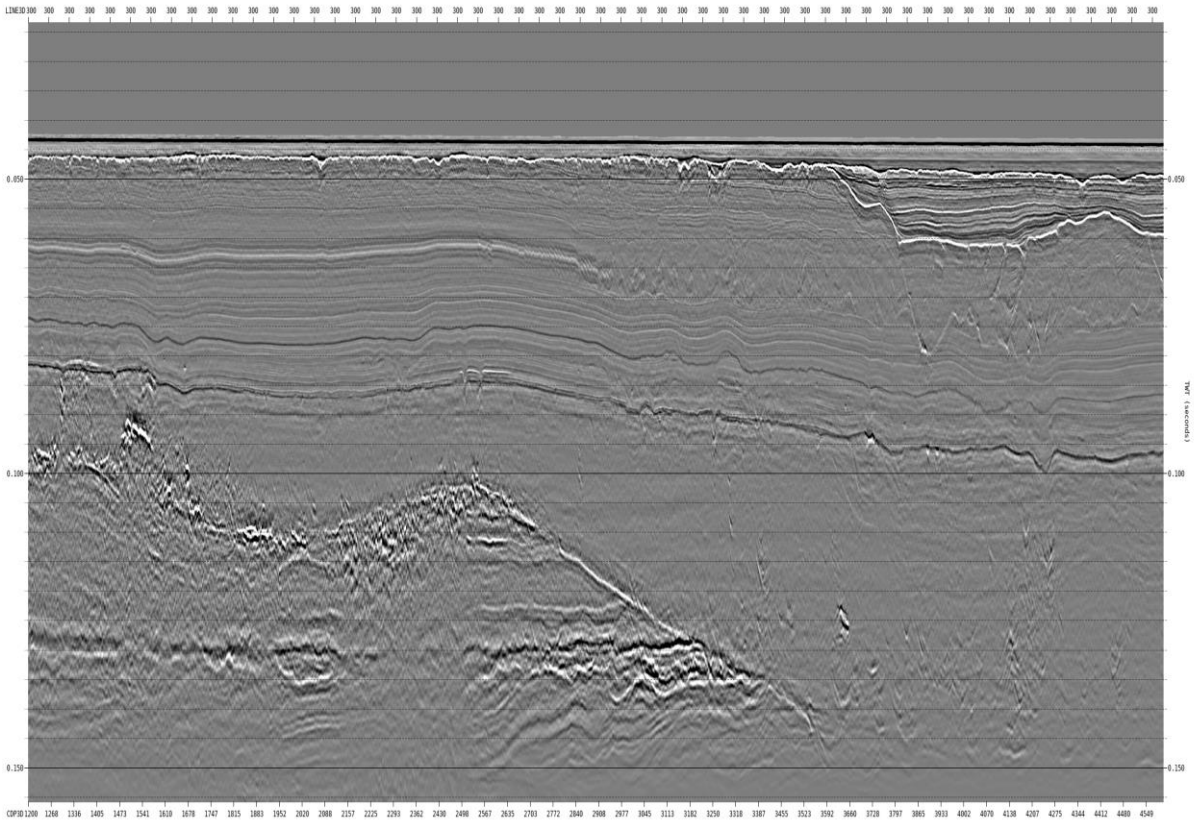

Figure 2.37: 3D OS1 inline 300: final time cube

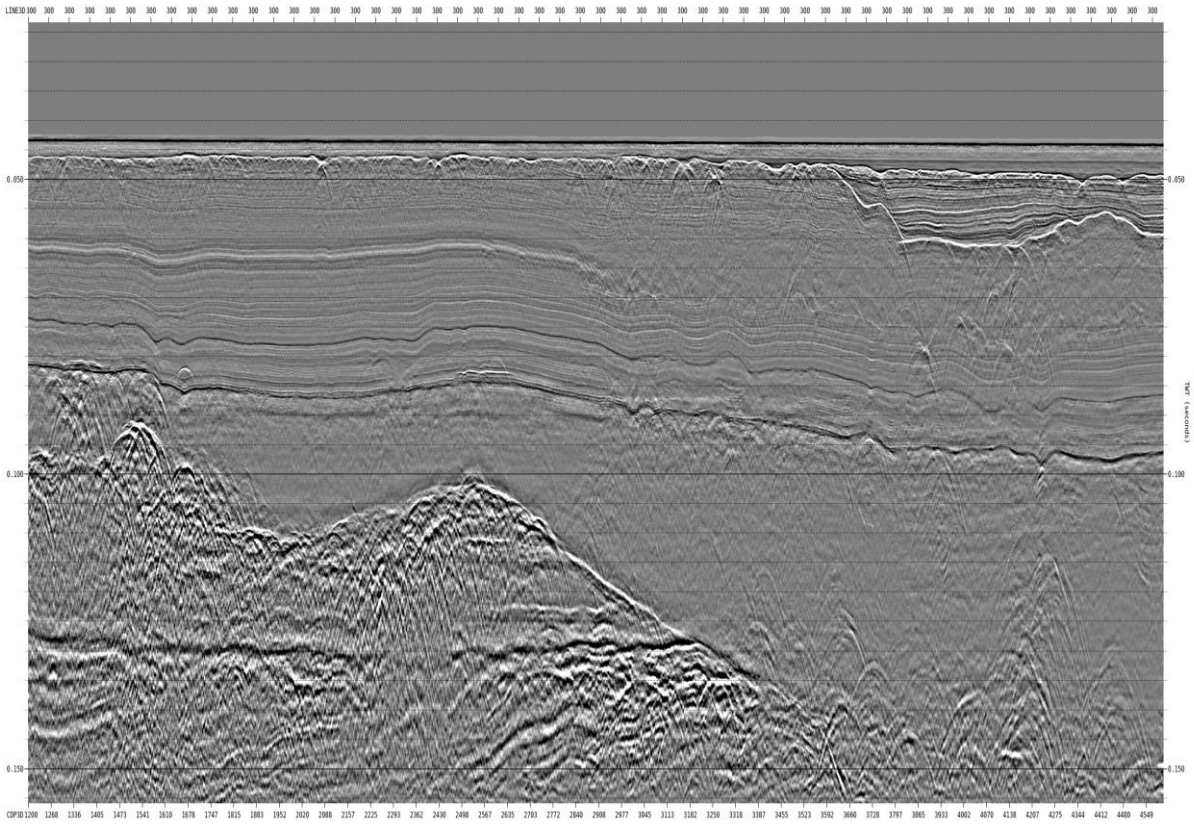

Figure 2.38: 3D OS1 inline 300: final non migrated time cube

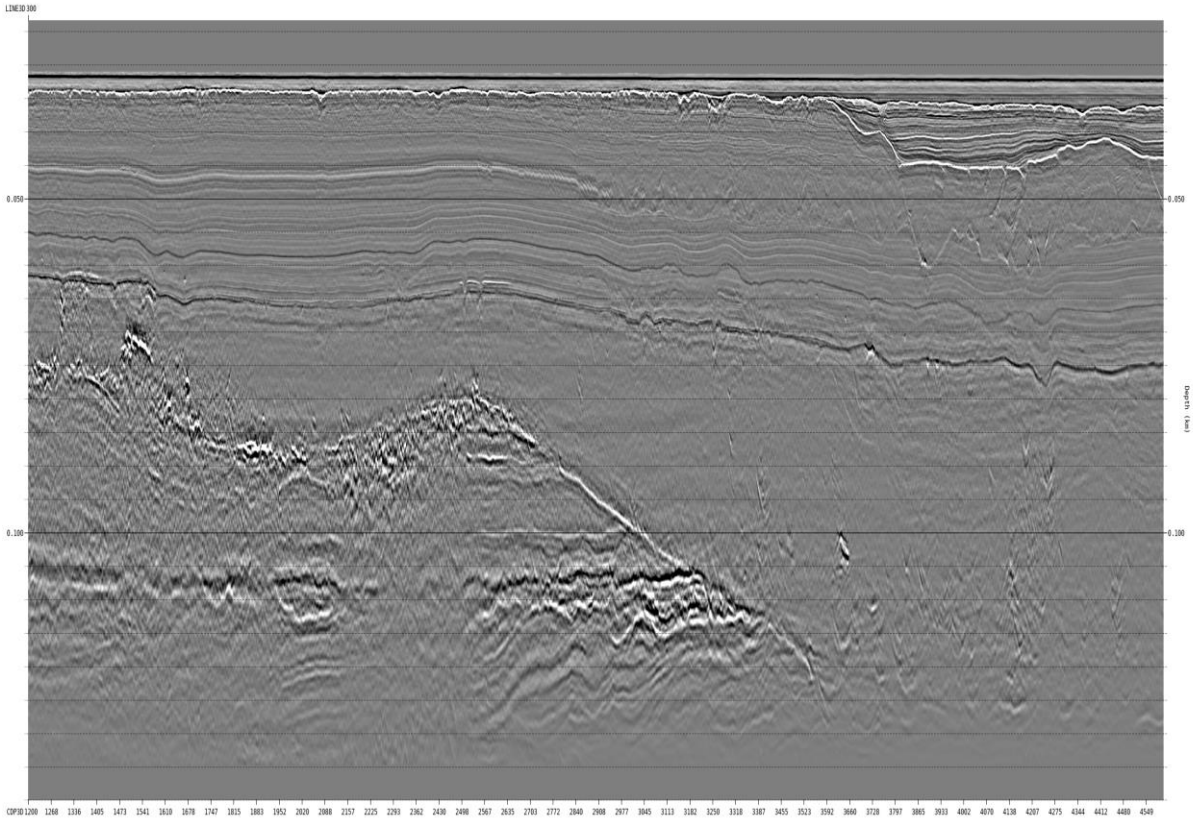

Figure 2.39: 3D OS1 inline 300: final depth cube

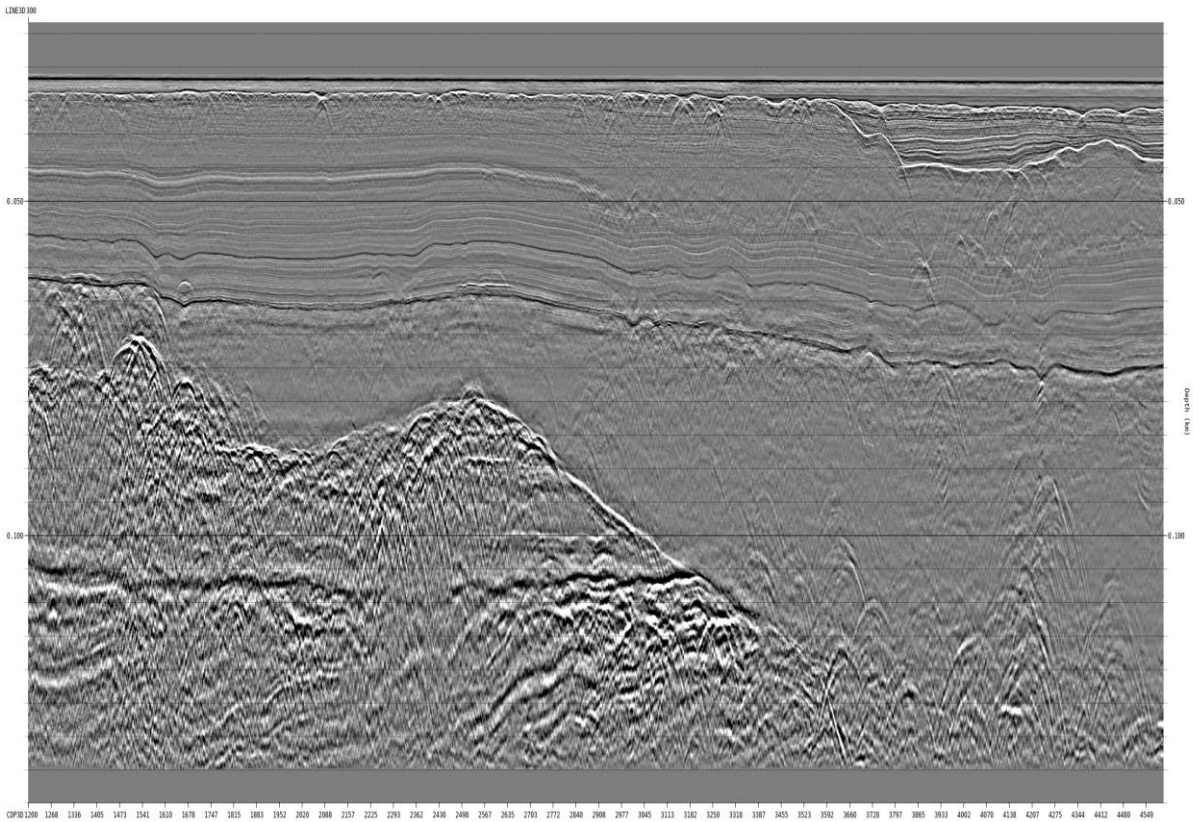

Figure 2.40: 3D OS1 inline 300: final non migrated depth cube

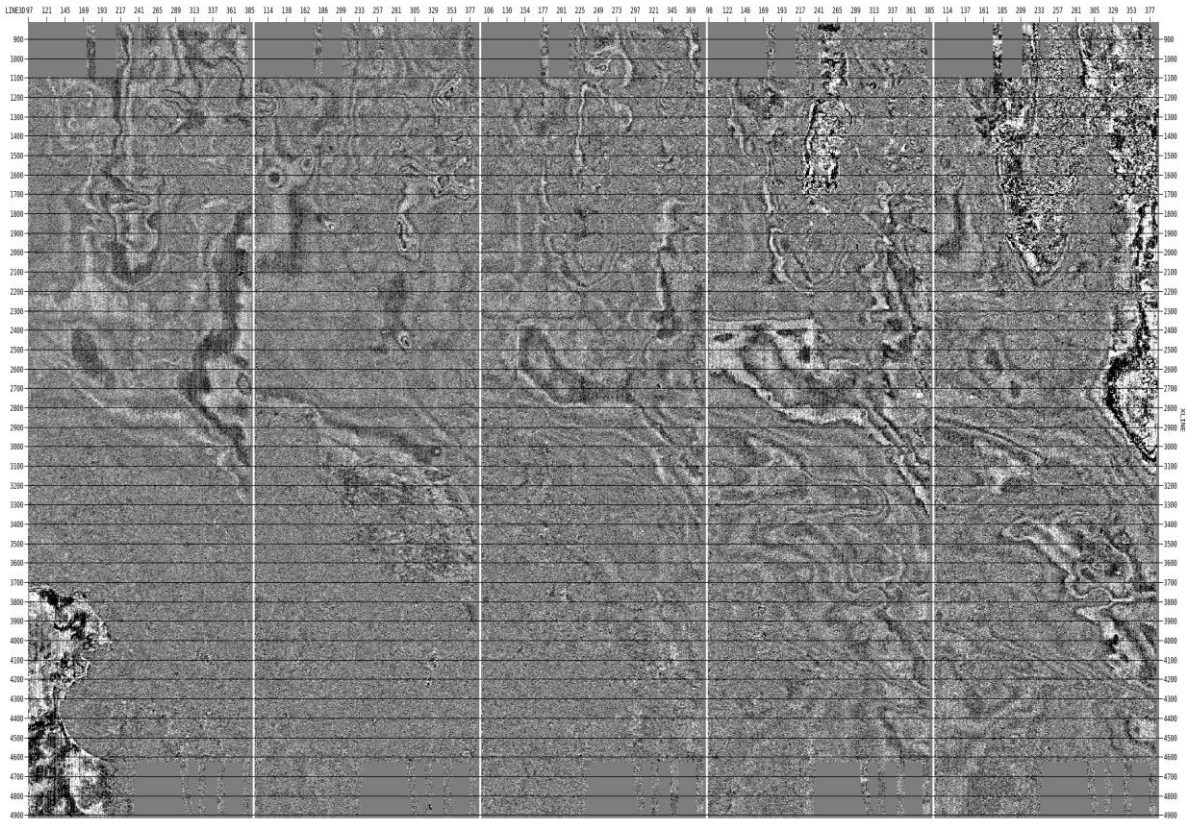

Figure 2.41: 3D summary OS1 timeslice 60-85 ms: raw cube

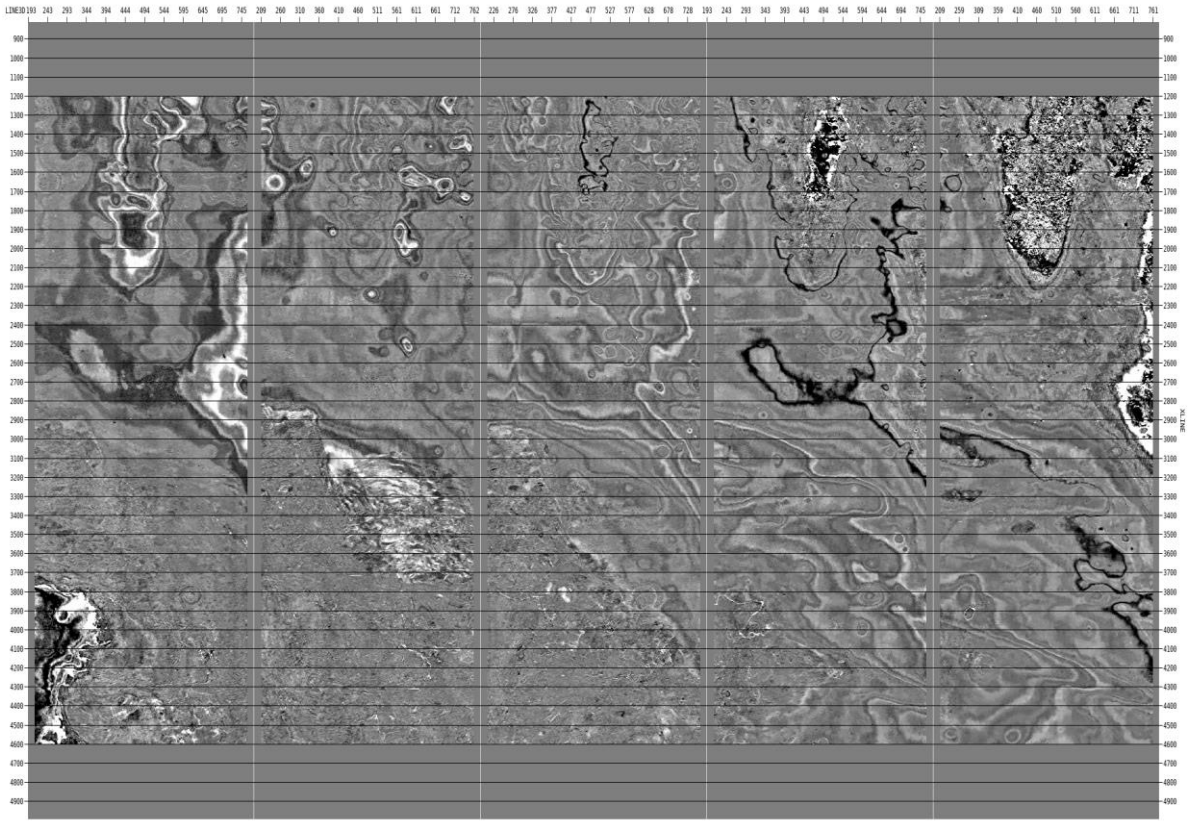

Figure 2.42: 3D summary OS1 timeslice 60-85 ms: final migrated time cube

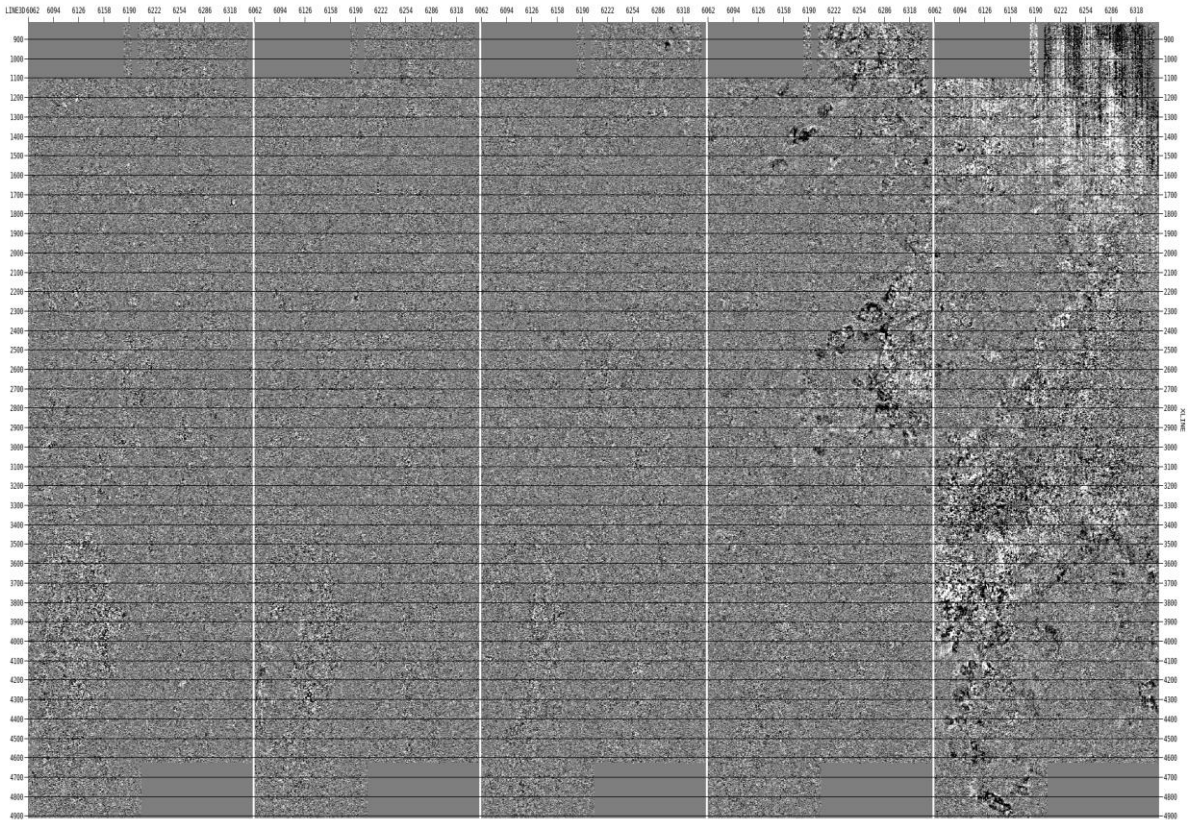

Figure 2.43: 3D summary OS2 timeslice 60-85 ms: raw cube

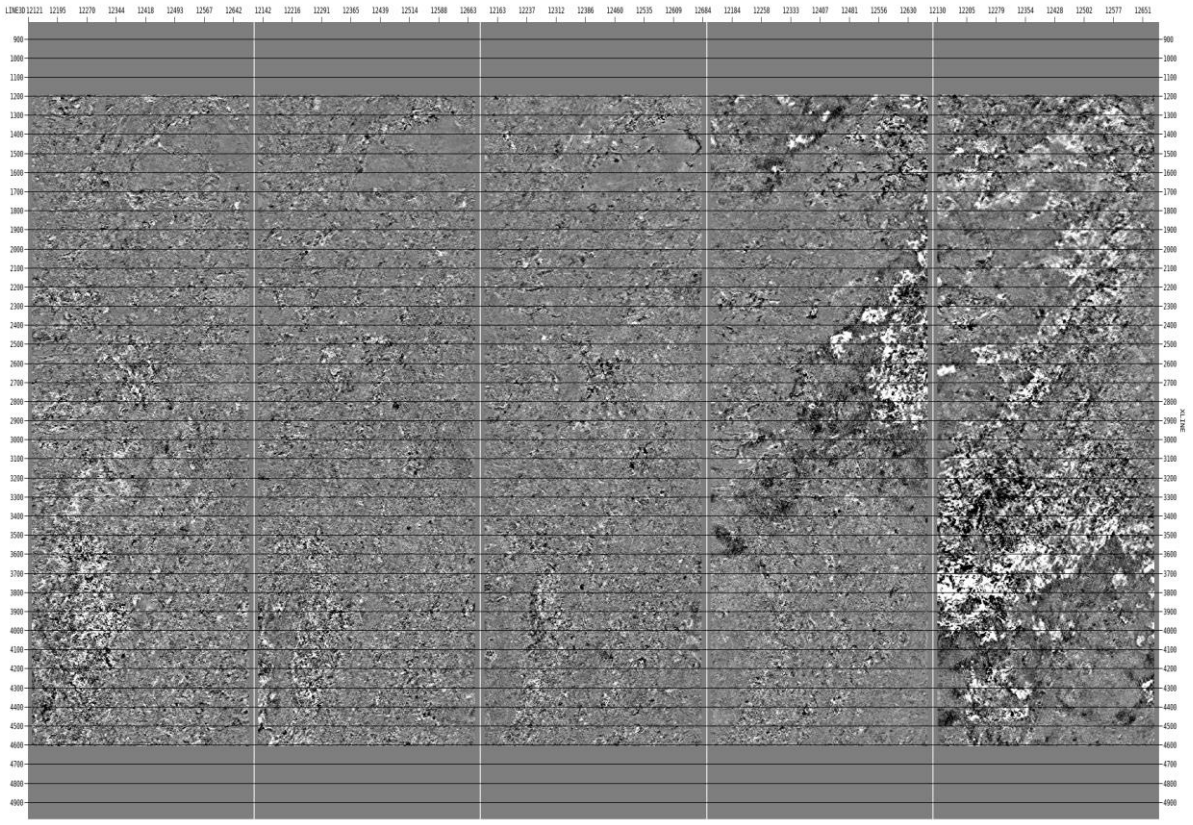

Figure 2.44: 3D summary OS2 timeslice 60-85 ms: final migrated time cube

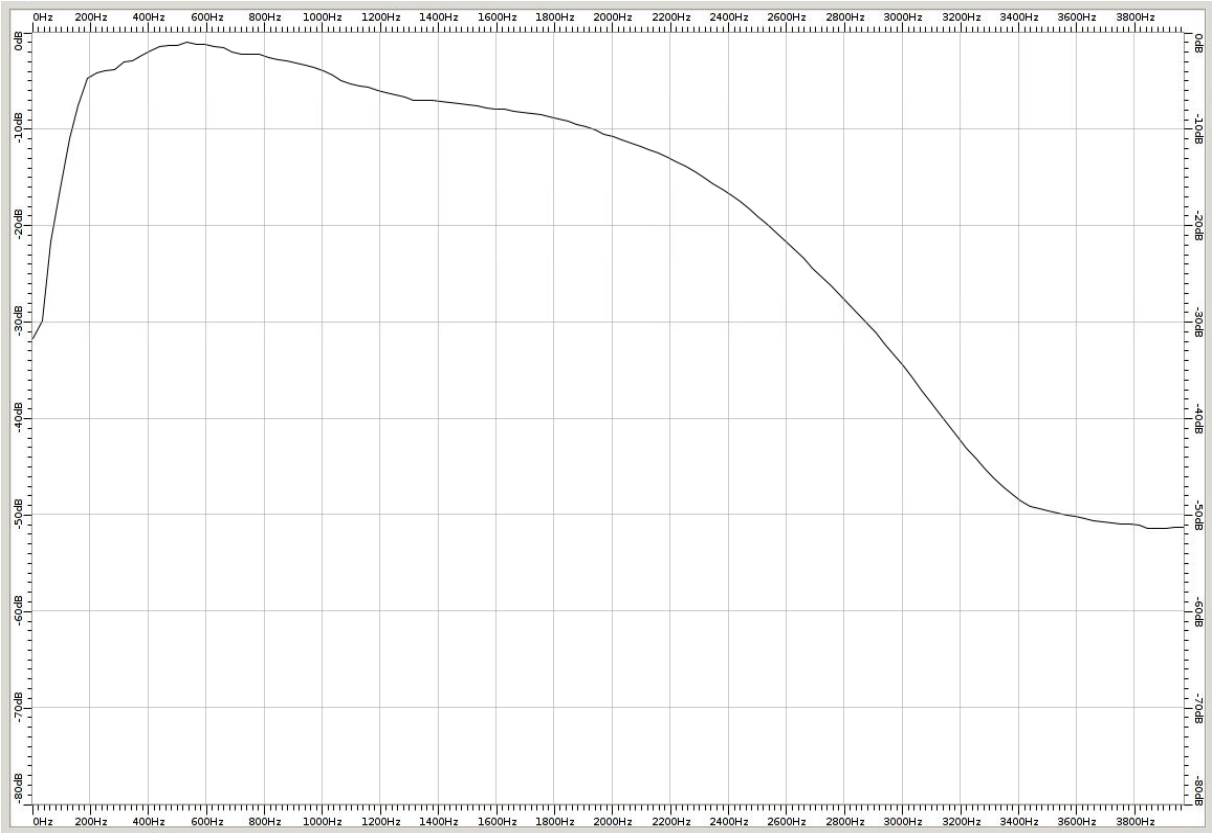

Figure 2.45: Final spectrum for previous 2D acquisition

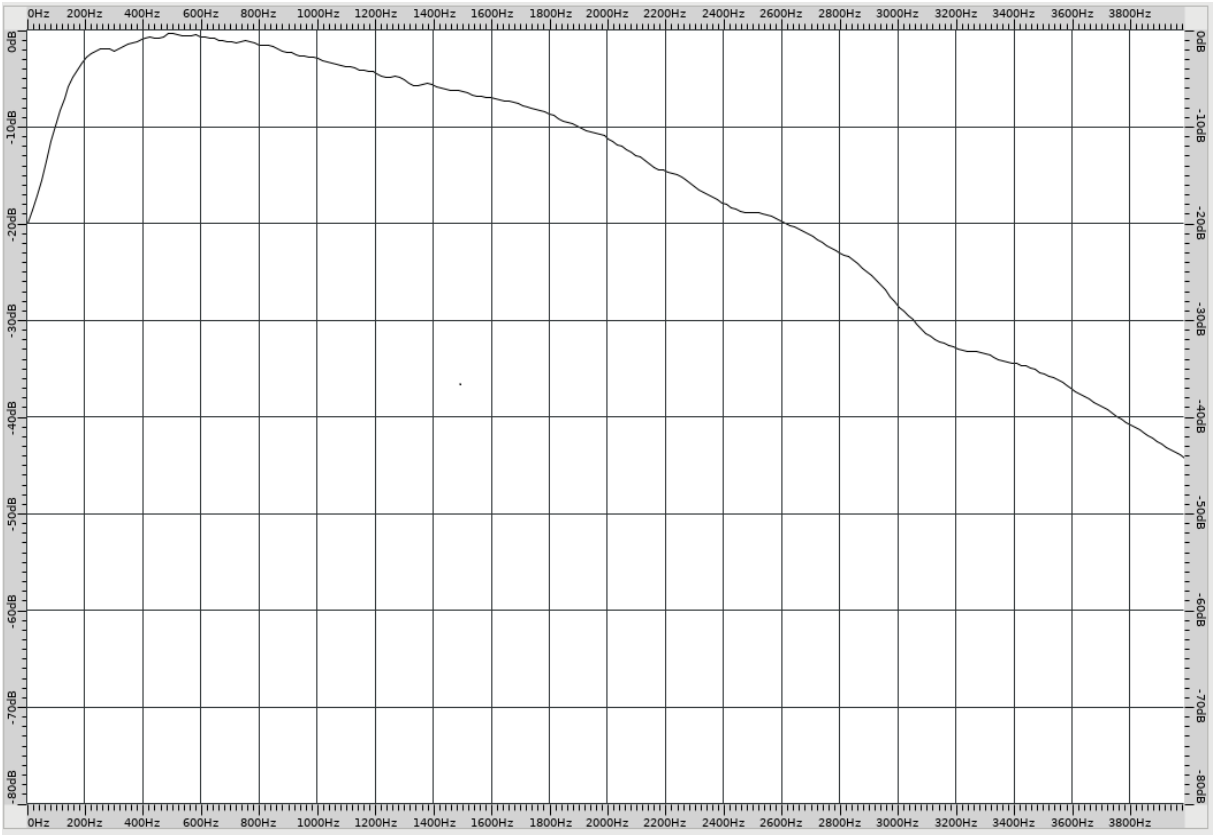

Figure 2.46: Final spectrum for 3D

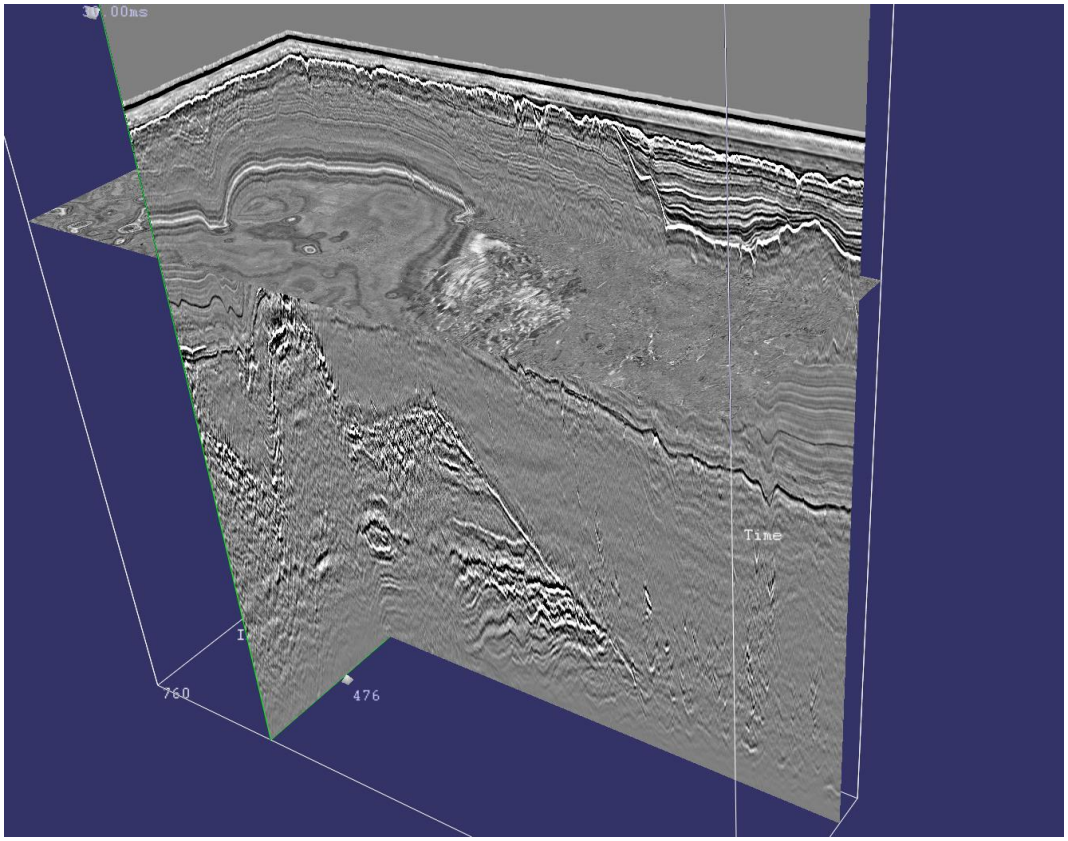

Figure 2.47: 3D view OS1: final migrated time cube

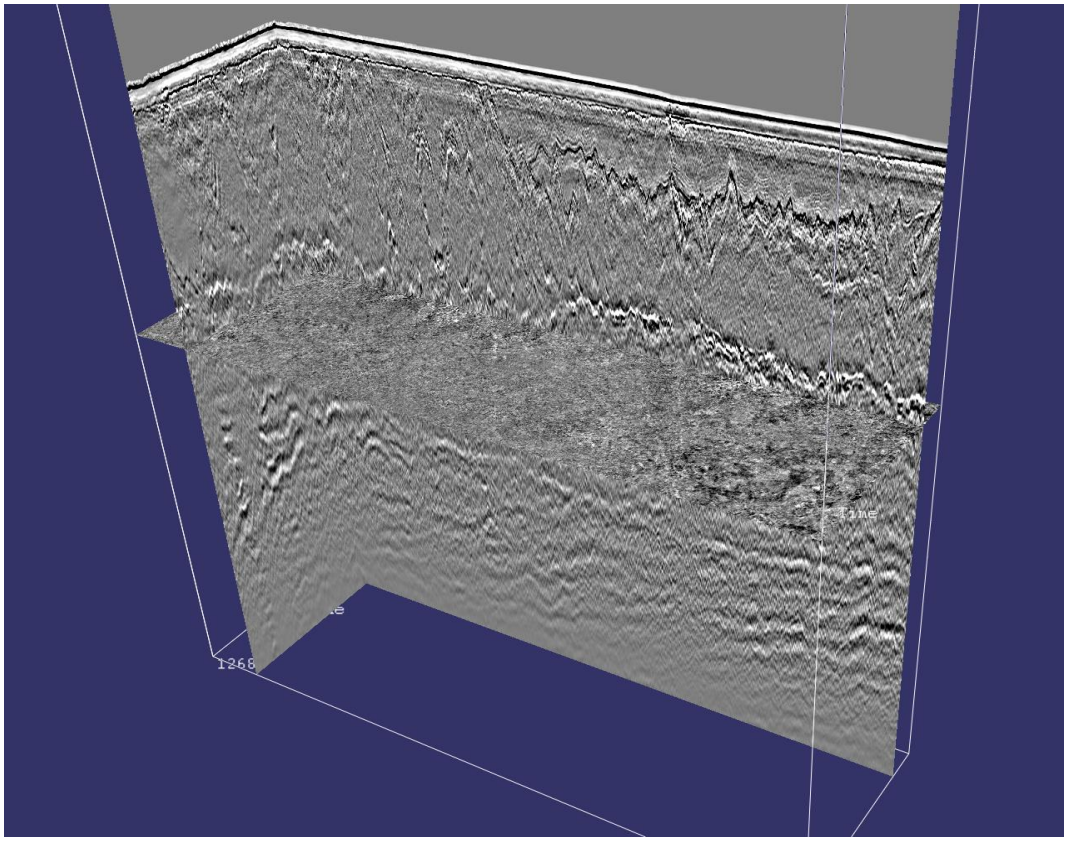

Figure 2.48: 3D view OS2: final migrated time cube

2.17 Output to SEG-Y

The final stacks were output in SEG-Y format with the bin centred positions. These files were electronically transferred internally to the geophysicists for interpretation via *Fugro Shares*. An example of the approved EBCDIC header is displayed below.

```
C01 CLIENT: ENERGINET ELTRANSMISSION A/S        RECORDED BY: FUGRO
C02 LINE: OS1                                   PROJECT: HESSELO 3D
C03 AREA: HESSELO                               SITE SURVEY: WINDFARM UUHR
C04 RECORDING PARAMETERS ========================================================
C05 VESSEL: FUGRO PIONEER                       DATE: APR-2021
C06 FORMAT: SEGY
C07 REC LENGTH: 155.875 MS                      SAMPLE RATE: 0.125 MS
C08 FILTERS LOW CUT: N/A                        HIGH CUT: N/A
C09 SOURCE: 2*SPARKER                           SOURCE DEPTH: 0.52 M
C10 LEVEL: 700J                                 SP INTERVAL: 0.5 M
C11 CABLE TYPE: 4*TELEDYNE                      CABLE DEPTH: 1.4 M
C12 NUM CHANNELS: 4*48                          GP INTERVAL: 1 M
C13 NAVIGATION PRIMARY: STARFIX NG
C14 PROCESSING BY: FUGRO
C15 PROCESSING SYSTEM: UNISEIS
C16 PROCESSING SEQUENCE =========================================================
C17 1)TRANSCRIPTION TO 155.875 MS AT 0.125 MS NO. CHANNELS: 48
C18 2)MERGE SRC/REC NAV 3)APPLY GEOMETRY 4)EDIT BAD TRACES
C19 5)SHOT / CHANNEL / RECEIVER DOMAIN DENOISE 6)LNA
C20 7)2D SRME 8)DEGHOSTING 9)PRELIM 3D STATICS
C21 10)3D VELOCITY PICKS 11)FINAL 3D STATICS 12)REGRID 1M X 0.5M
C22 13)3D FOURIER REG 14)SORT TO 3D CMPS 15)NMO
C23 16)PASTA STATICS 17)MUTE 18)STACK 19)POST STACK MIGRATION
C24 20)DECON SHAPING 21)ZERO PHASE 22)TVF 23)DB GAIN
C25 24)FINAL ZERO SEA LEVEL STATIC 25)OUTPUT TO SEGY
C26 TRACE HEADER BYTE INFORMATION ===============================================
C27 IL   (189-192); XL   (193-196)
C28 CDPX (181-184); CDPY (185-188)
C29 PROCESSING GRID INFORMATION (IL, XL, X, Y) ==================================
C30 1.0000 M INLINE SPACING INC. -1 || 0.5000 M CROSSLINE SPACING INC. 1
C31 210,1200,673389.26,6266305.31
C32 210,4600,675064.96,6266018.93
C33 760,1200,673296.60,6265763.17
C34 760,4600,674972.31,6265476.79
C35 DATA INFORMATION ============================================================
C36 OS NUMBER   : 1                             DATA: MIG TIME CUBE
C37 ILINE RANGE : 210-760
C38 XLINE RANGE : 1200-4600
C39 POLARITY ====================================================================
C40 INCREASE IN ACOUSTIC IMPEDANCE = POSITIVE NUMBER
```

Figure 2.49: Final migrated time stack OS1 EBCDIC example

Appendix A

Line Listings

A.1 3D-UUHR Lines

Table A.1: 3D-UUHR Accepted lines processed

Line Name	Sequence	First SP	Last SP	Length [km]
OS1D4561P01	1	10004	13800	1.90
OS1D4547P01	2	13796	10002	1.90
OS1D4267P01	3	10006	13799	1.90
OS1D4547R01	4	13976	10003	1.99
OS1D4253P01	5	10006	13799	1.90
OS1D4505P01	6	13792	10003	1.89
OS1D4495P01	7	10006	13799	1.90
OS1D4485P01	9	13795	10003	1.90
OS1D4223P01	14	10004	13800	1.90
OS1D4455P01	15	13797	10002	1.90
OS1D4213P01	16	10004	13800	1.90
OS1D4435P01	17	13798	10002	1.90
OS1D4193P01	18	10003	13800	1.90
OS1D4415P01	19	13797	10002	1.90
OS1D4209P01	20	10002	13800	1.90
OS1D4449P01	21	13799	10003	1.90
OS1D4183P01	22	10004	13799	1.90
OS1D4425P01	23	13793	10004	1.89
OS1D4173P01	24	10004	13799	1.90
OS1D4405P01	25	13606	10003	1.80
OS1D4163P01	26	10006	13799	1.90
OS1D4393P01	27	13796	10002	1.90
OS1D4153P01	28	10006	13799	1.90
OS1D4383P01	29	13796	10003	1.90
OS1D4145P01	30	10006	13799	1.90
OS1D4374P01	31	13796	10003	1.90
OS1D4137P01	32	10006	13799	1.90
OS1D4360P01	33	13796	10003	1.90
OS1D4127P01	34	10006	13799	1.90
OS1D4350P01	35	13796	10003	1.90
OS1D4117P01	36	10006	13799	1.90
OS1D4340P01	37	13795	10003	1.90
OS1D4107P01	38	10006	13799	1.90
OS1D4330P01	39	13795	10003	1.90
OS1D4097P01	40	10006	13799	1.90
OS1D4320P01	41	13795	10003	1.90
OS1D4087P01	42	10006	13799	1.90
OS1D4310P01	43	13795	10004	1.90
OS1D4077P01	44	10006	13799	1.90
OS1D4300P01	45	13795	10003	1.90
OS1D4067P01	46	10006	13798	1.90
OS1D4287P01	47	13795	10003	1.90

Line Name	Sequence	First SP	Last SP	Length [km]
OS1D4057P01	48	10006	13798	1.90
OS1D4279P01	49	13652	10003	1.82
OS1D4047P01	50	10006	13798	1.90
OS1D4515P01	51	13795	10003	1.90
OS1D4037P01	52	10006	13798	1.90
OS1D4525P01	53	13795	10003	1.90
OS1D4025P01	54	10006	13799	1.90
OS2D4385P01	56	13795	10003	1.90
OS2D4105P01	57	10006	13798	1.90
OS2D4395P01	58	13795	10003	1.90
OS2D4115P01	59	10010	13798	1.89
OS2D4405P01	60	13795	10003	1.90
OS2D4125P01	61	10006	13798	1.90
OS2D4415P01	62	13796	10003	1.90
OS2D4135P01	63	10006	13799	1.90
OS2D4425P01	64	13796	10003	1.90
OS2D4145P01	65	10006	13799	1.90
OS2D4435P01	66	13796	10003	1.90
OS2D4165P01	67	10006	13799	1.90
OS2D4455P01	68	13793	10003	1.90
OS2D4185P01	69	10006	13799	1.90
OS2D4475P01	70	13796	10003	1.90
OS2D4205P01	71	10006	13798	1.90
OS2D4495P01	72	13795	10003	1.90
OS2D4225P01	73	10006	13798	1.90
OS2D4515P01	74	13795	10003	1.90
OS2D4245P01	75	10006	13798	1.90
OS2D4535P01	76	13795	10003	1.90
OS2D4265P01	77	10006	13798	1.90
OS2D4555P01	78	13796	10004	1.90
OS2D4285P01	79	10006	13799	1.90
OS2D4575P01	80	13796	10003	1.90
OS2D4305P01	81	10006	13799	1.90
OS2D4595P01	82	13796	10005	1.90
OS2D4325P01	83	10006	13799	1.90
OS2D4615P01	84	13796	10003	1.90
OS2D4345P01	85	10006	13798	1.90
OS2D4635P01	86	13795	10003	1.90
OS2D4365P01	87	10006	13798	1.90
OS2D4655P01	88	13400	10003	1.70
OS2D4645P01	89	13795	10003	1.90
OS2D4375P01	90	10006	13798	1.90
OS2D4625P01	91	13795	10003	1.90
OS2D4355P01	92	10006	13798	1.90

Line Name	Sequence	First SP	Last SP	Length [km]
OS2D4605P01	93	13796	10003	1.90
OS2D4335P01	94	10006	13799	1.90
OS2D4585P01	95	13796	10003	1.90
OS2D4315P01	96	10006	13799	1.90
OS2D4295P01	98	10006	13799	1.90
OS2D4528P01	99	13795	10003	1.90
OS2D4274P01	100	10006	13799	1.90
OS2D4519P01	101	13795	10003	1.90
OS2D4255P01	102	10006	13798	1.90
OS2D4509P01	103	13796	10003	1.90
OS2D4237P01	104	10006	13799	1.90
OS2D4463P01	105	13795	10003	1.90
OS2D4215P01	106	10004	13798	1.90
OS2D4445P01	107	13796	10003	1.90
OS1D4008R01	108	10006	13799	1.90
OS1D4233R01	109	13796	10003	1.90
OS1D4021J01	110	10006	13799	1.90
OS1D4247J01	111	13796	10003	1.90
OS1D4057J01	112	10006	13807	1.90
OS1D4355P01	113	13795	10003	1.90
OS1D4111J01	114	10006	13798	1.90
OS1D4379J01	115	13795	10003	1.90
OS1D4147J01	116	10006	13798	1.90
OS1D4471J01	117	13795	10003	1.90
OS1D4167J01	118	10006	13798	1.90
OS1D4491J02	119	13795	10003	1.90
OS1D4189J01	120	10006	13799	1.90
OS1D4537J01	121	13796	10003	1.90
OS1D4205J01	122	10006	13798	1.90
OS1D4555J01	123	13754	10003	1.88
OS1D4219J01	124	10006	13799	1.90
OS1D4459J01	125	13789	10003	1.89
OS1D4476J01	126	13796	10003	1.90
OS1D4105J01	127	10007	12807	1.40
OS1D4467J01	128	13683	10343	1.67
OS1D4141J01	129	10006	13799	1.90
OS1D4392J01	130	13795	10073	1.86
OS1D4200J01	131	10162	11218	0.53
OS1D4235J01	132	11957	10003	0.98
OS1D4405J01	133	10091	11498	0.70
OS1D4255J01	135	13795	10003	1.90
OS1D4451J01	136	10007	13799	1.90
OS1D4161J01	137	13796	11890	0.95
OS1D4427J01	139	10006	12976	1.49

Line Name	Sequence	First SP	Last SP	Length [km]
OS1D4261J01	140	13796	10003	1.90
OS1D4497J01	141	10006	13799	1.90
OS1D4161J02	142	13796	12385	0.71
OS2D4135J01	143	10006	11074	0.53
OS2D4474J01	144	13795	10003	1.90
OS2D4155R01	145	10006	13799	1.90
OS2D4485R01	146	13795	10003	1.90
OS2D4174R01	147	10006	13798	1.90
OS2D4495J01	148	13795	10003	1.90
OS2D4195R01	149	10006	13799	1.90
OS2D4540J01	150	13796	10003	1.90
OS2D4226J01	151	10006	13799	1.90
OS2D4565R01	152	13796	10003	1.90
OS2D4371J01	153	10126	13076	1.48
OS2D4570R01	154	13795	10003	1.90
OS2D4196J01	155	10006	12685	1.34
OS2D4615J01	156	13796	10003	1.90
OS2D4286J01	157	10006	11608	0.80
OS2D4444J01	158	10344	11312	0.48
OS2D4549J01	159	13795	10003	1.90
OS2D4143J01	160	10006	13261	1.63
OS2D4414P01	161	13796	12829	0.48
OS2D4346J01	162	13796	11066	1.37
OS2D4264J01	163	10006	11632	0.81
			Total	**276.82 km**

Appendix B

Deliverables

B.1 3D-UUHR Deliverables

- Offshore
  - Seg-Y : Raw navigation merged shot gathers
  - PDF : End of line QC

- Onshore
  - Seg-Y : Migrated time cubes
  - Seg-Y : Migrated time cubes converted to depth
  - Seg-Y : Non-Migrated time cubes
  - Seg-Y : Non-Migrated time cubes converted to depth
  - Seg-Y : 3D picked 160m RMS velocities

Appendix D

Digital Deliverables

Deliverable Type	Sensor	Deliverable ID	Deliverable Content	Format
Final Deliverable	ALL	FD_001	Electronic database of deliverables	XLSX
Final Deliverable	3DUHR	FD_002	TSG_Geodatabase	
Final Deliverable	3DUHR	FD_003	Raw Data	SEGY
Final Deliverable	3DUHR	FD_004	EOL QC Reports	PDF
Final Deliverable	3DUHR	FD_005	QC Logsheets	XLSX
Final Deliverable	3DUHR	FD_006	Final non-migrated cube MSL TWT	SEGY
Final Deliverable	3DUHR	FD_007	Final non-migrated cube MSL DEPTH	SEGY
Final Deliverable	3DUHR	FD_008	Final migrated cube MSL TWT	SEGY
Final Deliverable	3DUHR	FD_009	Final migrated cube MSL DEPTH	SEGY
Final Deliverable	3DUHR	FD_010	Velocity Model	SEGY
Final Deliverable	3DUHR	FD_011	IHS Kingdom Project	Updated from WP A
Final Deliverable	3DUHR	FD_012	Digitised Horizons	CSV
Final Deliverable	3DUHR	FD_013	Elevation Grids	XYZ
Final Deliverable	3DUHR	FD_014	UHR Depth below Seafloor (BSF) Grids	XYZ
Final Deliverable	3DUHR	FD_015	Isochore (layer thickness) Grids	XYZ